学位論文

Creation of Functional π-Conjugated Systems: Tetraceneimide Disulfide Metal Complexes and Fluorenylideneacridane

(機能性パイ共役系化合物の創製：テトラセンイミドジスルフィド金属錯体と
フルオレニリデンアクリダン)

平成 26 年 12 月博士（理学）申請

東京大学大学院理学系研究科化学専攻

鈴木　毅

Abstract

Organic compounds having large π-conjugated systems have attracted chemists to develop colorful dyes, imaging labels, sensor materials, and organic electronic devices. Such organic compounds often contain fused aromatic rings, which are promising structures to get large π-system and stability. On the other hand, other methods to construct extended π-system have been less developed. For example, metal coordination gives efficient connection between two π-systems in bis(dithiolene) complexes and multi-decker metal complexes. In addition, I also focused on the sterically hindered double bond not only to show large π-conjugation, but also to exhibit characteristic properties like chromic behavior emerged in the analog compounds, bis-tricyclic enes. The general introduction was given in Chapter 1.

The extension of π-system was achieved by dπ–pπ conjugation by using metals and tetraceneimide disulfide ligand (Chapter 2, 3). First, the method started with platinum. It resulted in a mononuclear complex, which clearly displayed longer wavelength light absorption and wider π-systems. The effects of platinum atom were also investigated by transient light absorption measurements (Chapter 2). The other complex using other 10-group metal was provided by using palladium. In comparison to the platinum case, palladium ended in a trinuclear metal complex denoting exceptionally red-shifted light absorption to infrared region. Quantum calculation also showed fully delocalized π-conjugated systems in HOMO and LUMO (Chapter 3).

The second topic about hindered double bond demonstrates the compound displaying two kinds of colors in different conformations (Chapter 4). The origin of color change and conformational change in solid state was examined to conclude the importance of amorphous phase. The substituents played important roles to compare the solid-state behaviors and control the conformations.

On my research, I have established two different ways to expand π-conjugated systems. The overview of my thesis and the perspective were summarized in Chapter 5 to design new organic materials by using the concepts I proposed here.

Acknowledgement

Table of Contents

Chapter 1.

General Introduction

One of the objectives to study organic compounds is to utilize the accomplishments for industrial applications. A lot of chemists have devoted a great deal of time and effort to establishment of organic materials toward achieving higher performances of electronic devices than inorganic ones. To accomplish the goal, organic materials should overcome a lot of issues that are high carrier mobility, stability of molecule, strong light absorption/emission abilities, and so on. Currently, inorganic materials are widely used rather than organic materials. Electrons in inorganic materials form band structures, which provide high carrier mobility. In addition, metallic bonds and ionic bonds result in quite robust materials as elemental metals, alloys, ionic solids, and Werner-type complexes. On the other hand, the inorganic materials are inherently heavy and inflexible. Here, organic chemists have focused on the fact that organic compounds easily solve the inorganic drawbacks.

During the explorations of organic materials, organic materials chemists mainly studied on fused aromatic rings, which are so-called as polycyclic aromatic hydrocarbons (PAHs).[1] PAHs have rigid structures and thermal stability, and therefore the researchers considered PAHs would open the door to creation of practical organic materials (Figure *1*). First, a variety of molecular structures have been designed and synthesized, but the small molecules have small π-orbitals not enough to construct effectively conductive paths. Since organic molecules hardly construct electronic band structures in solid state unlike inorganic materials, charge transporting path should be constructed by very close packing structures and covalent bonds. Accordingly, packing control methods of small molecules and organic polymers composed of small PAHs have been developed.[2] At this stage, organic materials realized conductivity as >1 cm^2/Vs,[3] high performance solar cells with >10% power conversion efficiencies,[4] and absolutely stable electronic devices.[5] In order to improve the device performances, new series of organic materials should be required to widen the variety of organic materials. Organic materials chemists keen to design and create a new molecular structure. The motivation has targeted wide range of molecular structures to find a new family showing prominent properties.[6] The majority of the variation is, however, PAH families composed of carbon, hydrogen, oxygen, nitrogen and sometimes boron, silicon, phosphorus, sulfur, selenium and tellurium atoms.[7] The number of elements allows to form a tremendous kinds of molecular structures, so the situation got me to search an unprecedented concept to design organic materials.
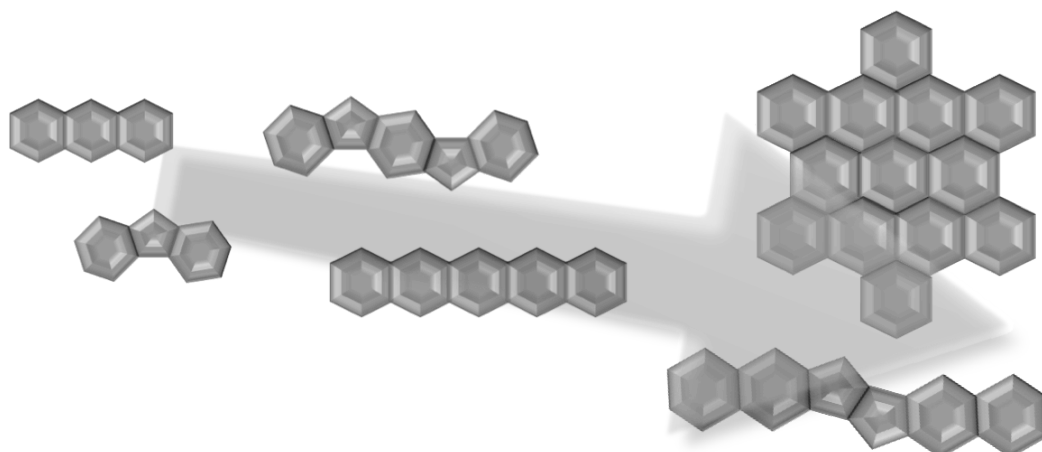
Figure 1. Development of PAH structures.

I decided to change the typical point of view how to construct π-conjugation to other sides that are complexation and utilizing double bond (Figure *2*). The research about a limited number of metal complexes has covered subjects of materials chemistry perhaps because of high reactivity of metal complexes. The high reactivity and unusual instability have attracted chemists, but the characteristic reactivity prevents the metal complexes from applications. Among the situation, some metal complexes were used for electronic devices, however the molecular structures can be categorized into a few types: porphyrinoids,[8] bis(dithiolene) complexes,[9] and hexagonal Werner-type complex with pyridyl groups.[10] These complexes do not have a significant common characteristic but metal atoms obviously work to construct unique π-conjugation and electronic interactions. I estimated that the properties would commonly emerge by making dπ-pπ interactions, which would indicate π-extension at the same time. The feature whether π-system gets extended or not is instantly confirmed by measuring light absorption measurements. I have investigated the π-extension for metal complexes through experimental and computational studies.

In comparison to the field of metal complex materials, double bonds have been unconsciously incorporated to organic materials to link and conjugate two π-systems. One of the examples is poly(*p*-phenylene vinylene).[11] Generally, double bonds can be easily constructed by several synthetic methods, for example McMurry coupling, Knoevenagel condensation, Heck coupling, Wittig reaction, Barton-Kellogg reaction, and so on. The various approaches to get *p*-phenylene vinylene derivatives have helped develop some functional organic materials.[11g,12] In this work, I added an extra property that is steric repulsion (Figure 2). The sterically hindered distortion is sometimes used for packing control, but I thought the distorted double bond would effectively accept charges by releasing the contortion. The schematic molecular structure in Figure *2* is similar to bis-tricyclic aromatic enes (BAEs) that have been studied for over 100 years.[13] It is already known that BAEs exhibit chromic properties between the different

stereoisomers, but the origin of the chromism is not yet clear. In addition, the literatures reported, however, no photophysical properties or electrochemical properties. I thought that the molecular design of BAEs is applicable to organic electronic devices, and hence the electrochemical properties and photophysical properties should be evaluated. I also tried to demonstrate that the distorted double bond can link and extend the π-systems to show long wavelength light absorption. The double bond with contortion would form two stereoisomers possessing different bonding feature at the central bond. I could examine the difference of π-orbital structures.
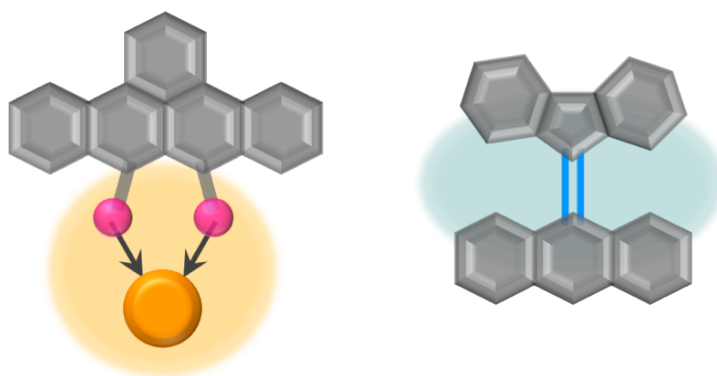
Figure 2. Schematic images of the concepts to build π-conjugated system.

So far, I spent my bachelor and master courses developing organic semiconducting materials, namely tetraceneimide disulfide (TIDS) derivatives. The TIDS derivatives contain unique π-conjugated system to show long wavelength light absorption. We demonstrated that TIDS is applicable to organic electronic devices (Scheme *1*, Figure *3*).[14]

Scheme 1. Synthesis of TIDS derivatives.
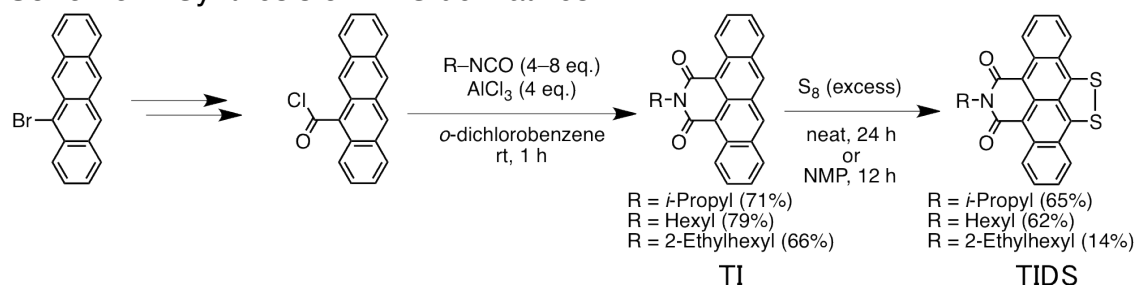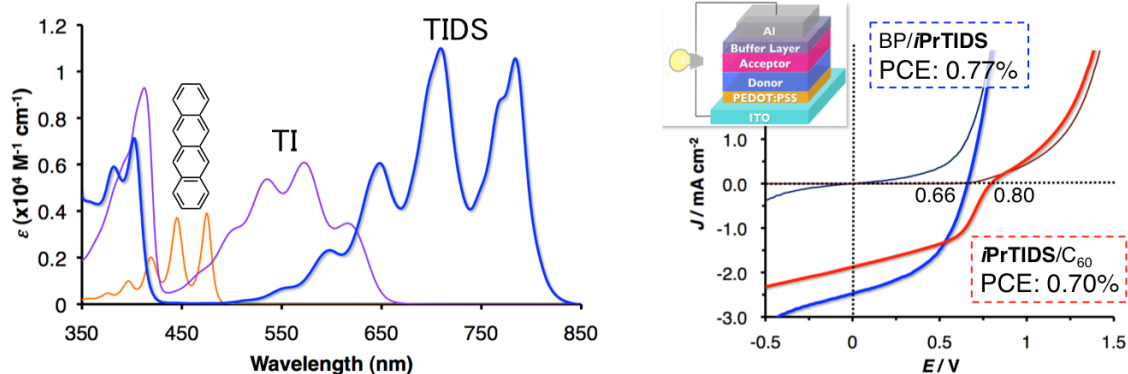
Figure 3. UV-vis absorption spectra of TIDS compared to its precursors and organic thin film solar cell performances using TIDS.

In addition, TIDS derivatives have potential to extend the own π-systems by coordinating metals to the disulfide group. So I decided to use TIDS toward the next theme that is π-extension with metal coordination. In the TIDS studies, we also noticed a drawback of TIDS for application to solar cell devices, that is low mobility of carriers. We considered the issue would come from the rigid structure of π-system of TIDS. The rigidness scarcely accepts a carrier because TIDS cation or anion would weaken double bond features at the π-system to form single bond like characters, which generate steric torsions. I should optimize the molecular structure to improve the carrier transporting properties. At this time, I got thought of the double bond structure. I started to develop the two themes by using two different molecular structures. In the first two chapters, I discussed about the metal complexes. In the next chapter, I summarized the molecules with hindered double bond.

References.

1. (a) Berresheim, A. J.; Müller, M.; Müllen, K. *Chem. Rev.* **1999**, *99*, 1747–1785. (b) Grimsdale, A. C.; Müllen, K. *Angew. Chem. Int. Ed.* **2005**, *44*, 5592–5629. (c) Anthony, J. E. *Angew. Chem. Int. Ed.* **2008**, *47*, 452–483. (d) Chen, Z.; Lohr, A.; Saha-Möller, C. R.; Würthner, F. *Chem. Soc. Rev.* **2009**, *38*, 564–584. (e) Diederich, F.; Kivala, M. *Adv. Mater.* **2010**, *22*, 803–812. (f) Pisula, W.; Feng, X.; Müllen, K. *Chem. Mater.* **2011**, *23*, 554–567. (g) Shen, Y.; Chen, C.-F. *Chem. Rev.* **2012**, *112*, 1463–1535.

2. (a) Nolde, F.; Pisula, W.; Müller, S.; Kohl, C.; Müllen, K. *Chem. Mater.* **2006**, *18*, 3715–3725. (b) Delgado, M. C. R.; Kim, E.-G.; da Silva Filho, D. A.; Bredas, J.-L. *J. Am. Chem. Soc.* **2010**, *132*, 3375–3387. (c) Kim, F. S.; Ren, G.; Jenekhe, S. A. *Chem. Mater.* **2011**, *23*, 682–732. (d) Hinoue, T.; Shigenoi, Y.; Sugino, M.; Mizobe, Y.; Hisaki, I.; Miyata, M.; Tohnai, N. *Chem. Eur. J.* **2012**, *18*, 4634–4643.

3. (a) Ebata, H.; Izawa, T.; Miyazaki, E.; Takimiya, K.; Ikeda, M.; Kuwabara, H.; Yui, T. *J. Am. Chem. Soc.* **2007**, *129*, 15732–15733. (b) Jurchescu, O. D.; Popinciuc, M.; van Wees, B. J.; Palstra, T. T. M. *Adv. Mater.* **2007**, *19*, 688–692. (c) Zhao, Y.; Guo, Y.; Liu, Y. *Adv. Mater.* **2013**, *25*, 5372–5391. (d) Dong, H.; Fu, X.; Liu, J.; Wang, Z.; Hu, W. *Adv. Mater.* **2013**, *25*, 6158–6183. (e) Guo, X.; Facchetti, A.; Marks, T. J. *Chem. Rev.* **2014**, *114*, 8943–9021.

4. (a) Heeger, A. J. *Adv. Mater.* **2014**, *26*, 10–28. (b) Kazim, S.; Nazeeruddin, M. K.; Grätzel, M.; Ahmad, S. *Angew. Chem. Int. Ed.* **2014**, *53*, 2812–2824. (c) Mazzio, K. A.; Luscombe, C. K. *Chem. Soc. Rev.* **2015**, *44*, 78–90.

5. (a) Berntsen, A. J. M.; van de Weijer, P.; Croonen, Y.; Liedenbaum, C. T. H. F.; Vleggaar, J. J. M. *Philips J. Res.* **1998**, *51*, 511–525. (b) Krebs, F. C. *Sol. Energy Mater. Sol. Cells* **2008**, *92*, 715–726. (c) Hau, S. K.; Yip, H.-L.; Baek, N. S.; Zou, J.; O'Mallery, K.; Jen, A. K.-Y. *Appl. Phys. Lett.* **2008**, *92*, 253301. (d) Song, P.-F.; Qin, W.-J.; Ding, G.-J.; Yan, Q.-Q.; Yang, L.-Y.; Yin, S.-G. *Optoelectron. Lett.* **2011**, *7*, 330–333.

6. For example, (a) Blanchard-Desce, M.; Alain, V.; Bedworth, P. V.; Marder, S. R.; Fort, A.; Runser, C.; Barzoukas, M.; Lebus, S.; Wortmann, R. *Chem. Eur. J.* **1997**, *3*, 1091–1104. (b) Innocenzia, P.; Lebeau, B. *J. Mater. Chem.* **2005**, *15*, 3821–3831. (c) Saragi, T. P. I.; Spehr, T.; Siebert, A.; Fuhrmann-Lieker, T.; Salbeck, J. *Chem. Rev.* **2007**, *107*, 1011–1065. (d) Kelly, T. R.; Cai, X.; Damkaci, F.; Panicker, S. B.; Tu, B.; Bushell, S. M.; Cornella, I.; Piggott, M. J.; Salives, R.; Cavero, M.; Zhao, Y.; Jasmin, S. *J. Am. Chem. Soc.* **2007**, *129*, 376–386.

7. For example, (a) Baumgartner, T.; Bergmans, W.; Kárpáti, T.; Neumann, T.; Nieger, M.; Nyulászi, L. *Chem. Eur. J.* **2005**, *11*, 4687–4699. (b) Dienes, Y.; Durben, S.; Kárpáti, T.; Neumann, T.; Englert, U.; Nyulászi, L.; Baumgartner, T. *Chem. Eur. J.* **2007**, *13*, 7487–7500. (c) Fukazawa, A.; Yamaguchi, S. *Chem. Asian J.* **2009**, *4*, 1386–1400. (d) Kronemeijer, A. J.; Gili, E.; Shahid, M. Rivnay, J.; Salleo, A.; Heeney, M.; Sirringhaus, H. *Adv. Mater.* **2012**, *24*, 1558–1565. (e) Kushida, T.; Camacho, C.; Shuto, A.; Irle, S.; Muramatsu, M.; Katayama, T.; Ito, S.; Nagasawa, Y.; Miyasaka, H.; Sakuda,

E.; Kitamura, N.; Zhou, Z.; Wakamiya, A.; Yamaguchi, S. *Chem. Sci.* **2014**, *5*, 1296–1304.

8. Blake, I. M.; Rees, L. H.; Claridge, T. D. W.; Anderson, H. L. *Angew. Chem. Int. Ed.* **2000**, *39*, 1818–1821. (b) Tsuda, A. Osuka, A. *Science* **2001**, *293*, 79–82. (c) Kurotobi, K.; Kim, K. S.; Noh, S. B.; Kim, D.; Osuka, A. *Angew. Chem. Int. Ed.* **2006**, *45*, 3944–3947. (d) Davis, N. K. S.; Thompson, A. L.; Anderson, H. L. *J. Am. Chem. Soc.* **2011**, *133*, 30–31. (e) Sarma, T.; Panda, P. K. *Chem. Eur. J.* **2011**, *17*, 13987–13991.

9. (a) Mueller-Westerhoff, U. T.; Vance, B.; Yoon, D. I. *Tetrahedron* **1991**, *47*, 909–932. (b) Kobayashi, A.; Sasa, M.; Suzuki, W.; Fujiwara, E.; Tanaka, H.; Tokumoto, M.; Okano, Y.; Fujiwara, H.; Kobayashi, H. *J. Am. Chem. Soc.* **2004**, *126*, 426–427. (c) Madhu, V.; Das, S. K. *Inorg. Chem.* **2008**, *47*, 5055–5070. (d) Dalgleish, S.; Matsushita, M. M.; Hu, L.; Li, B.; Yoshikawa, H.; Awaga, K. *J. Am. Chem. Soc.* **2012**, *134*, 12742–12750.

10. (a) Kalyanasundaram, K.; Grätzel, M. *Coord. Chem. Rev.* **1998**, *77*, 347–414. (b) Hagfeldt, A.; Grätzel, M. *Acc. Chem. Res.* **2000**, *33*, 269–277. (c) Kuciauskas, D.; Freund, M. S.; Gray, H. B.; Winkler, J. R.; Lewis, N. S. *J. Phys. Chem. B* **2001**, *105*, 392–403. (d) Wang, P.; Zakeeruddin, S. M.; Moser, J. E.; Humphry-Baker, R.; Comte, P.; Aranyos, V.; Hagfeldt, A.; Nazeeruddin, M. K.; Grätzel, M. *Adv. Mater.* **2004**, *16*, 1806–1811. (e) Polo, A. S.; Itokazu, M. K.; Iha, N. Y. M. *Coord. Chem. Rev.* **2004**, *248*, 1343–1361. (f) Concepcion, J. J.; Jurss, J. W.; Brennaman, M. K.; Hoertz, P. G.; Patrocinio, A. O. T.; Iha, N. Y. M.; Templeton, J. L.; Meyer, T. J. *Acc. Chem. Res.* **2009**, *42*, 1954–1965.

11. (a) Gustafsson, G.; Cao, Y.; Treacy, G. M.; Klavetter, F.; Colaneri, N.; Heeger, A. J. *Nature* **1992**, *357*, 477–479. (b) Greenham, N. C.; Moratti, S. C.; Bradley, D. D. C.; Friend, R. H.; Holmes, A. B. *Nature* **1993**, *365*, 628–630. (c) Yu, G.; Gao, J.; Hummelen, J. C.; Wudl, F.; Heeger, A. J. *Science* **1995**, *270*, 1789–1791. (d) Kraft, A.; Grimsdale, A. C.; Holmes, A. B. *Angew. Chem. Int. Ed.* **1998**, *37*, 402–428. (e) Friend, R. H.; Gymer, R. W.; Holmes, A. B.; Burroughes, J. H.; Marks, R. N.; Taliani, C.; Bradley, D. D. C.; Dos Santos, D. A.; Brédas, J. L.; Lögdlund, M.; Salaneck, W. R. *Nature* **1999**, *397*, 121–128. (f) Thompson, B. C.; Fréchet, J. M. J. *Angew. Chem. Int. Ed.* **2008**, *47*, 58–77. (g) Cheng, Y.-J.; Yang, S.-H.; Hsu, C.-S. *Chem. Rev.* **2009**, *109*, 5856–5923.

12. (a) Grimsdale, A. C.; Chan, K. L.; Martin, R. E.; Jokisz, P. G.; Holmes, A. B. *Chem. Rev.* **2009**, *109*, 897–1091. (b) Xie, Z. Yoon, S.-J.; Park, S. Y. *Adv. Funct. Mater.* **2010**, *20*, 1638–1644. (c) Park, J. H.; Park, J.-I.; Kim, D. H.; Kim, J.-H.; Kim, J. S.; Lee, J. H.; Sim, M.; Lee S. Y.; Cho, K. *J. Mater. Chem.* **2010**, *20*, 5860–5865. (d) Egbe, D. A. M.; Neugebauer, H.; Sariciftci, N. S. *J. Mater. Chem.* **2011**, *21*, 1338–1349. (e) Vijayakumar, C.; Praveen, V. K.; Kartha, K. K.; Ajayaghosh, A. *Phys. Chem. Chem. Phys.* **2011**, *13*, 4942–4949. (f) Praveen, V. K.; Ranjith, C.; Bandini, E.; Ajayaghosh, A.; Armaroli, N. *Chem. Soc. Rev.* **2014**, *43*, 4222–4242.

13. (a) Meyer, H. *Ber. Dtsch. Chem. Ges. B* **1909**, *42*, 143–145. (b) Meyer, H. *Monatsh. Chem.* **1909**, *30*, 165–177. (c) Wasserman, E.; Davis, R. E. *J. Chem. Phys.* **1959**, *30*, 1367. (d) Fanselow, D. L.; Drickamer, H. G. *J. Chem. Phys.* **1974**, *61*, 4567–4574. (e) Biedermann, P. U.; Stezowski, J. J.; Agranat, I. *Chem. Eur. J.* **2006**, *12*, 3345–3354. (f) Johnstone, R. D. L.; Allan, D.; Lennie, A.; Pidcock, E.; Valiente, R.; Rodríguez, F.; Gonzalez, J.; Warren, J.; Parsons, S. *Acta Cryst.* **2011**, *B67*, 226–237.

14. (a) Okamoto, T.; Suzuki, T.; Kojima, S. Matsuo, Y. *Chem. Lett.* **2011**, *40*, 739–741. (b) Okamoto, T.; Suzuki, T.; Tanaka, H.; Hashizume, D.; Matsuo, Y. *Chem. Asian J.* **2012**, *7*, 105–111. (c) Suzuki, T.; Okamoto, T.; Saeki, A.; Seki, S.; Sato, H.; Matsuo, Y. *ACS Appl. Mater. Interfaces* **2013**, *5*, 1937–1942.

Chapter 2.

Synthesis and Photophysical Properties in the Excited States of Platinum Tetraceneimide Disulfide Complex

2.1. Introduction

Toward organic electronic devices, a variety of organic materials have been developed. The organic materials have gained a number of functional groups, made the π-system wider and contained diverse heteroatoms to grow their own electronic properties, for instance carrier mobility, fluorescent properties, and light absorption properties. On the other hand, metal complexes showing heavy atom effects and nonlinear optical properties have attracted chemists to explore unique physical properties. Especially, platinum complexes have been enthusiastically studied to apply some of them to light-emitting diodes,[1] organic solar cells,[2] and nonlinear optics.[3] Nevertheless, platinum complexes with largely fused polyacenes as ligands have hardly got attention. In fact, pentacene and tetracene derivatives, the simplest polyacenes, recorded some applicability to organic electronic devices.[4] Namely, combining platinum atom and polyacenes would easily give functional metal complexes.

To incorporate the polyacence as a ligand to platinum atom, disulfide group effectively works because the reactions between metal atoms and disulfide are well-developed.[5] As analogues of platinum polyacene disulfide complexes, naphthodithiolene complexes were reported, but other complexes having larger polyacene disulfide ligands were drastically less reported.[6] Moreover, the researchers have not deeply investigated the photophysical properties of the naphthodithiolene complexes.

Tetraceneimide disulfide (TIDS) derivatives that we previously reported have wholly delocalized π-orbitals to show long wavelength light absorption and contain coordinative disulfide group,[7] and thus I expected TIDS derivatives would effectively demonstrate the benefits of platinum atom for the photophysical properties. In this work, I chose hexyl chain substituted TIDS as a ligand because it has better solubility than TIDS having smaller aliphatic chains and still keeps crystallinity compared to bulkier aliphatic chains. I guessed hexyl chain substituted TIDS would be suitable to smoothly examine the properties of the products. Here, I describe TIDS as hexyl chain substituted TIDS unless otherwise specified.

2.2. Results and Discussion

Platinum atom was inserted to TIDS through oxidative addition of zero-valent platinum complex precursor, tris(triphenylphosphine)platinum, $Pt(PPh_3)_3$ (Scheme **1**). $Pt(PPh_3)_3$ was prepared by using the reported procedure.[8] The mononuclear platinum TIDS complex, named as Pt-TIDS, was obtained as deep green solids in 70% yield after purification by recrystallization from THF/hexane. Instead of $Pt(PPh_3)_3$, the reaction with (ethylene)bis(triphenylphosphine)platinum, $Pt(C_2H_4)(PPh_3)_2$, also gave Pt-TIDS in 92% yield after recrystallization from THF/hexane. In this reaction condition, only a gas by-product was generated in contrast to the condition with $Pt(PPh_3)_3$. The reaction mixture contained small amount of by-products to result in higher yield after

purification. Pt-TIDS was characterized by ^{1}H, ^{13}C, ^{31}P NMR, high-resolution mass spectrometry, and X-ray single crystal analysis. THF, CH$_2$Cl$_2$, and toluene were good solvents for Pt-TIDS. Surprisingly Pt-TIDS was so soluble and stable even in CHCl$_3$ that NMR data were collected in CDCl$_3$. Pt-TIDS was stable in air for one day, but its solution was relatively unstable to show decomposition in two hours. No further reaction was observed even if excess amount of Pt(PPh$_3$)$_3$ or tris(dibenzylideneacetone)dipalladium, Pd$_2$dba$_3$, was added to the solution of Pt-TIDS.

Scheme 1. Synthesis of Pt-TIDS.

(a) Pt(PPh$_3$)$_3$ (1.0 equiv.)
THF, rt, 4 h

(b) Pt(C$_2$H$_4$)(PPh$_3$)$_2$ (1.3 equiv.)
THF, rt, 1 h

HexylTIDS (1)

Pt-TIDS (2) (a: 70%, b: 92%)
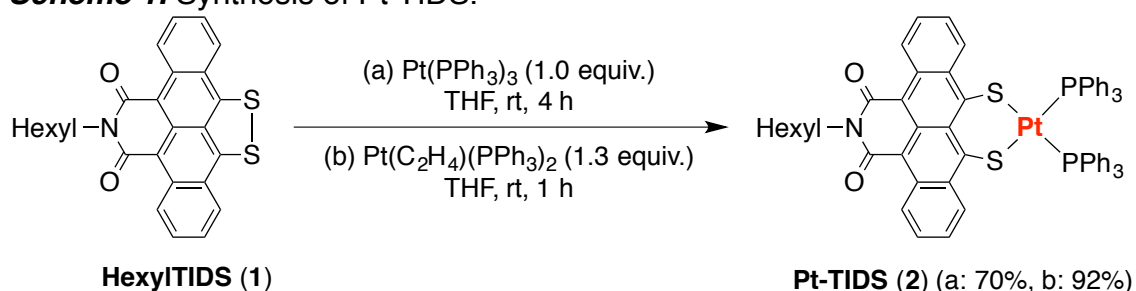
The coordination manner and the distortion of TIDS ligand were investigated by X-ray single crystal analysis. It was crystallographically compared with the napththodithiolne platinum complexes, which have been studied by Woollins and his coworkers.[6b,9]

The crystal structure of Pt-TIDS is shown with selected bond lengths, angles, a dihedral angle, and torsion angles (Figure **1**). The distances of S–Pt bonds around the platinum coordination plane were 2.286(1) and 2.316(1) Å. The bond lengths of S–Pt are slightly shorter than those of [Pt(AcepnaphtheneS$_2$)(PPh$_3$)$_2$] (2.323(3) and 2.336(2) Å) and [Pt(Naphtho(SO)S)(PPh$_3$)$_2$] (2.344(2) and 2.338 (2) Å).[9a, c] In contrast, [Pt(Naphtho(SO$_2$)S)(PPh$_3$)$_2$] and [Pt(Naphtho(SO$_2$)(SO))(PPh$_3$)$_2$] have similar S–Pt bond lengths: 2.310(5) (O$_2$S–Pt), 2.308(5) (S–Pt), 2.291(5) (O$_2$S–Pt), 2.332(5) (S–Pt), 2.306(2) (O$_2$S–Pt) and 2.327(2) (OS–Pt). The bond lengths would represent electron population around the atoms. Pt-TIDS includes TIDS ligand, which contains highly electron-negative substituents that is imide part, and therefore sulfur atoms in TIDS is as electron-deficient as SO$_2$. P–Pt bond lengths of Pt-TIDS (2.293(1) and 2.311(1) Å) are quite similar to those of [Pt(AcepnaphtheneS$_2$)(PPh$_3$)$_2$] (2.301(2) and 2.295(2) Å). The P–Pt bond lengths in [Pt(Naphtho(SO)S)(PPh$_3$)$_2$], [Pt(Naphtho(SO$_2$)S)(PPh$_3$)$_2$] and [Pt(Naphtho(SO$_2$)(SO))(PPh$_3$)$_2$] vary from 2.295(5) to 2.338(2), but the average is near to Pt-TIDS. Pt-TIDS possesses shorter C–S bond lengths (1.729(4) and 1.746(5) Å) than [Pt(Naphtho(SO)S)(PPh$_3$)$_2$], [Pt(Naphtho(SO$_2$)S)(PPh$_3$)$_2$] and [Pt(Naphtho(SO$_2$)(SO))(PPh$_3$)$_2$] (1.752(8) – 1.829(8) Å). As is discussed above, electron deficiency of sulfur atoms in Pt-TIDS is similar to [Pt(Naphtho(SO$_2$)S)(PPh$_3$)$_2$] and [Pt(Naphtho(SO$_2$)(SO))(PPh$_3$)$_2$], thus the short bond lengths would come from

other characters. Different from naphthodithiole ligands, TIDS ligand has larger π-conjugated system, which spreads to disulfide part. The C–S bonds in Pt-TIDS are shorter than typical C–S single bond length (1.82 Å), implying the aromaticity of Pt-TIDS is higher than the other naphthodithiolene platinum complexes. The degree of torsion in Pt-TIDS is evaluated by comparing the S···S distances. The distance of Pt-TIDS is 3.270(2) Å, which is larger than those of [Pt(Naphtho(SO)S)(PPh$_3$)$_2$], [Pt(Naphtho(SO$_2$)S)(PPh$_3$)$_2$] and [Pt(Naphtho(SO$_2$)(SO))(PPh$_3$)$_2$] (2.94(1) – 3.19(1) Å). The S···S distance in Pt-TIDS is, however, almost identical to that of [Pt(AcepnaphtheneS$_2$)(PPh$_3$)$_2$] (3.267(4) Å). The angles around the platinum coordination centers are 85.38(5) – 96.44(5)º for Pt-TIDS, 86.53(8) – 97.51(8)º for [Pt(AcepnaphtheneS$_2$)(PPh$_3$)$_2$], 77.87(8) – 97.86(6)º for [Pt(AcepnaphtheneS$_2$)(PPh$_3$)$_2$], 86.54(18) – 96.53(18)º for [Pt(Naphtho(SO)S)(PPh$_3$)$_2$], and 81.69(6) – 103.64(6) for [Pt(Naphtho(SO$_2$)S)(PPh$_3$)$_2$]. There is high variability among the angles, but the tendencies are comparable with each complex, suggesting those complexes have similar torsion in platinum coordination planes. The characteristic torsion properties appear at the angles around disulfide parts. The angles at bay positions, which are the positions surrounded by sulfur atoms and acene rings, vary with small differences (122.1(5) – 131.8(15)º) among the platinum complexes, however clear differences were found in torsion angles at S–C···C–S. In Pt-TIDS, the value is –41.9(3)º, which is much larger than others, 1.2(5)º for [Pt(AcepnaphtheneS$_2$)(PPh$_3$)$_2$], 3.2(5)º for [Pt(Naphtho(SO)S)(PPh$_3$)$_2$], 14(1), –24(1)º for [Pt(Naphtho(SO)S)(PPh$_3$)$_2$], 9.3(4)º for [Pt(Naphtho(SO$_2$)S)(PPh$_3$)$_2$], –24.3(2)º for [Pt(Naphtho(SO$_2$)(SO))(PPh$_3$)$_2$]. The angle reflects twisting angle between acene ligand and platinum coordination plane. According to the torsion angles, [Pt(AcepnaphtheneS$_2$)(PPh$_3$)$_2$], [Pt(Naphtho(SO)S)(PPh$_3$)$_2$] and [Pt(Naphtho(SO$_2$)S)(PPh$_3$)$_2$] form envelope-like conformations. In contrast, Pt-TIDS shapes a twisted structure.

The most characteristic differences between the reported platinum complexes and Pt-TIDS are found in the ligation manner of platinum coordination planes to the acene ligands. In contrast to the envelope-like ligations of the reported naphthodithiolene complexes, the platinum coordination plane in Pt-TIDS is twisted to tetraceneimide moiety. In the twisted manner, coordinative lone pairs in sulfur atoms are sterically protected by the tetracene moiety not to form multi-nuclear complex. Accordingly, a multinuclear metal complex was not obtained by using Pt-TIDS.
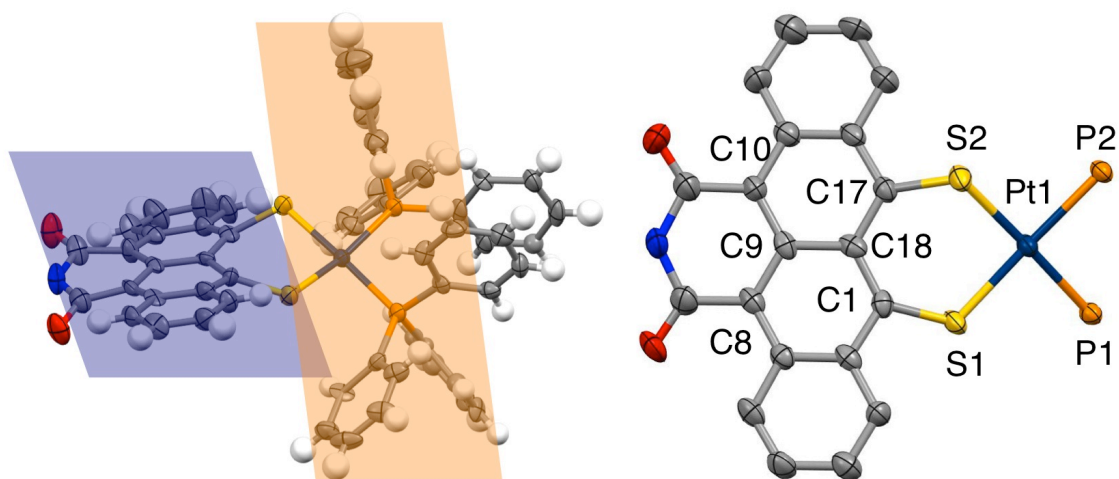
Figure 1. Crystal structure of Pt-TIDS. Selected bond length [Å], angles [º], dihedral angles [º], and torsion angles [º]: C1–S1 1.729(4), C17–S2 1.746(5), S1–Pt1 2.286(1), S2–Pt1 2.316(1), P1–Pt1 2.293(1), P2–Pt1 2.311(1), S1···S2 3.270(2), P1–Pt1–P2 96.44(5), P2–Pt1–S2 85.38(5), S2–Pt1–S1 90.55(5), S1–Pt1–P1 87.87(5), Pt1–S1–C1 118.0(2), S1–C1–C18 126.3(4), C1–C18–C17 123.0(5), C18–C17–S2 124.2(4), C17–S2–Pt1 110.5(2), torsion angles of tetracene ring S1–C1–C17–S2 –41.9(3).

Introduction of platinum atom into TIDS should change the electronic structure compared to the TIDS ligand itself. Electrochemical properties, light absorption properties and light emitting properties were measured to identify the differences. Moreover, photophysical properties were compared by using femtosecond transient measurements.

The electrochemical properties of Pt-TIDS was measured by cyclic voltammetry (CV) and differential pulse voltammetry (DPV). The CV chart showed reversible oxidation and reduction waves at 0.04 V and –1.45 V (Figure *2*). The both potentials were highly negative-shifted compared to those of TIDS (0.44 V and –1.15 V). The shift would represent the effect of inserting electron-rich platinum atom and phosphine ligands to TIDS. Both of the oxidation and reduction steps appeared as reversible to suggest Pt-TIDS is electrochemically stable. The results roughly determined HOMO level, LUMO level and HOMO–LUMO gap as –4.84, –3.35 and 1.49 eV.[10]
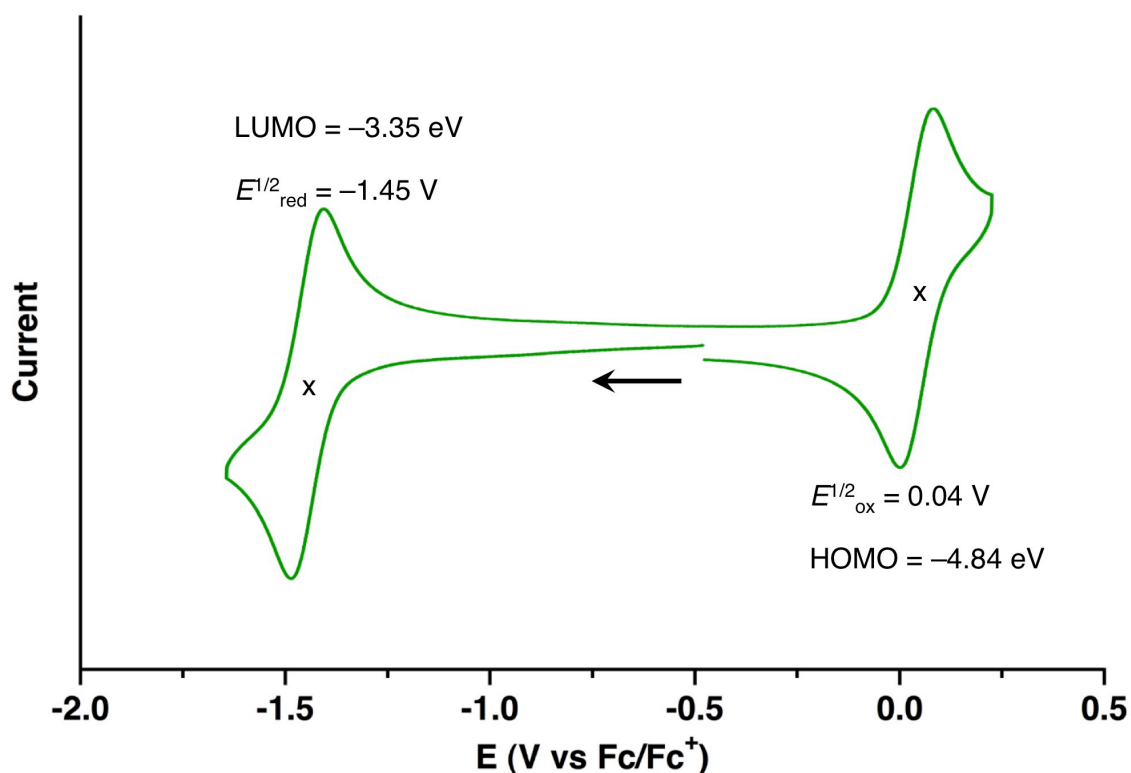
Figure 2. Cyclic voltammogram of Pt-TIDS in CH_2Cl_2.

The electronic structure of Pt-TIDS was evaluated by light absorption measurements as well. The light absorption spectrum of Pt-TIDS showed slightly red-shifted light absorption spectrum with maxima at 699 and 843 nm compared to free TIDS (Figure *3*). The molar absorption coefficient of TIDS also increased from 1.6 $\times 10^4$ M^{-1} cm^{-1} into 2.2 $\times$ 10^4 M^{-1} cm^{-1} at the highest points. These extensions would be derived from the expansion of π-system, which should be composed of pπ orbital of TIDS and dπ orbital of platinum atom.
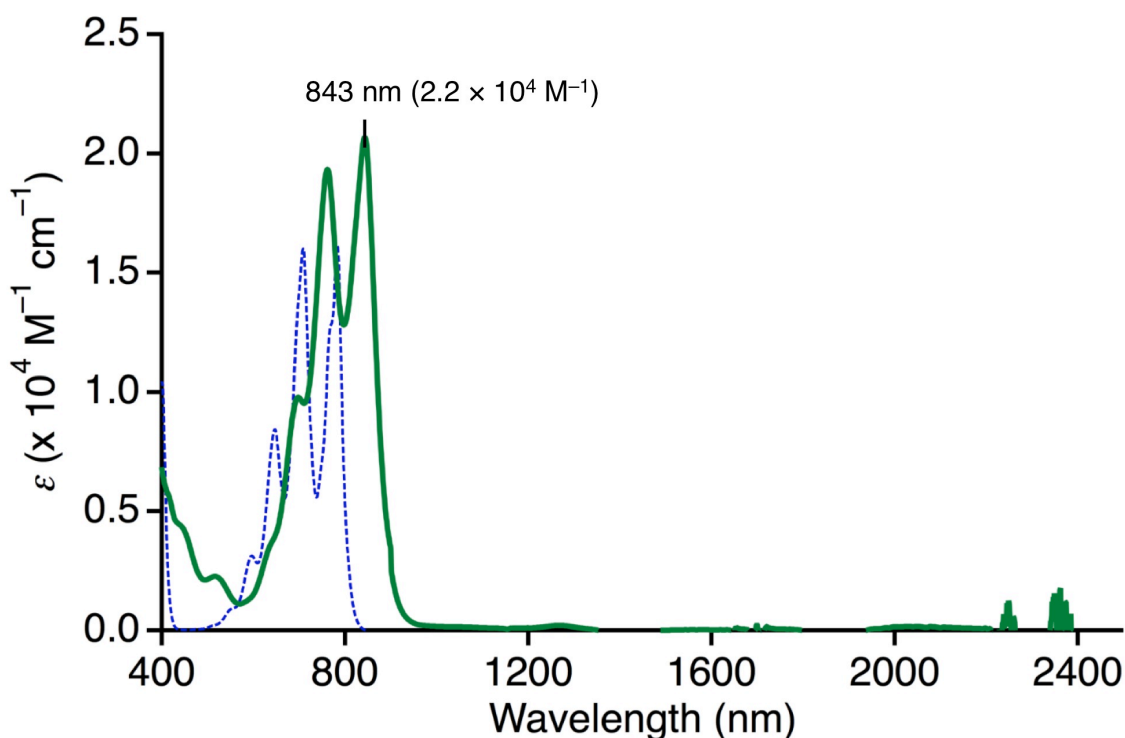
Figure 3. Light absorption spectra of TIDS (blue dot) and Pt-TIDS (green) in CH_2Cl_2.

DFT studies directly illustrated the electronic structures of a model complex that is an analogue of Pt-TIDS having methyl group (**3**) (Figure **4**). The HOMO and LUMO delocalize whole of molecule **3**. It is noteworthy that HOMO and LUMO are obviously constituted of pπ of TIDS and dπ of platinum atom to form fully delocalized π-systems. The conjugation also led decrease of HOMO–LUMO gap into 2.10 eV compared to 2.21 eV of TIDS. Accordingly, the calculation evidenced that insertion of platinum to disulfide unit can enlarge the π-system. The HOMO and LUMO are constructed from molecular orbitals of TIDS ligand and platinum atom (Figure **5**). HOMOs of TIDS ligand and platinum atom interact to form HOMO of **3**. The LUMO of **3** comes from the interaction between LUMOs of TIDS ligand and platinum atom. Consequently, the HOMO–LUMO gap of **3** should be reduced compared to TIDS. Additionally, electron-rich phosphine ligands would make the levels negatively shifted to exhibit the CV waves as displayed in Figure **2**.
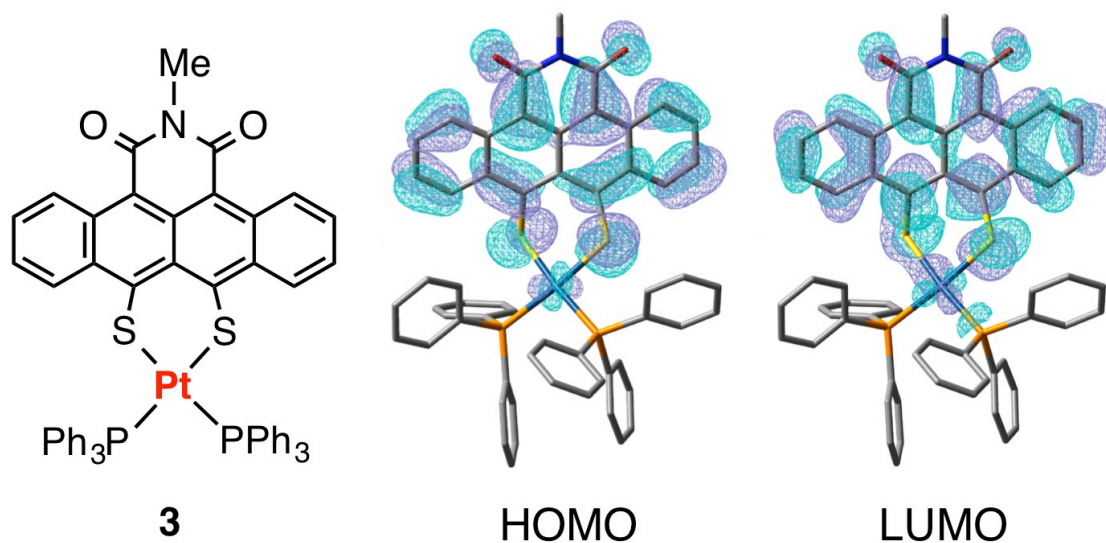
Figure 4. Model complex (**3**) of Pt-TIDS for DFT calculations and HOMO and LUMO structures of the model complex.
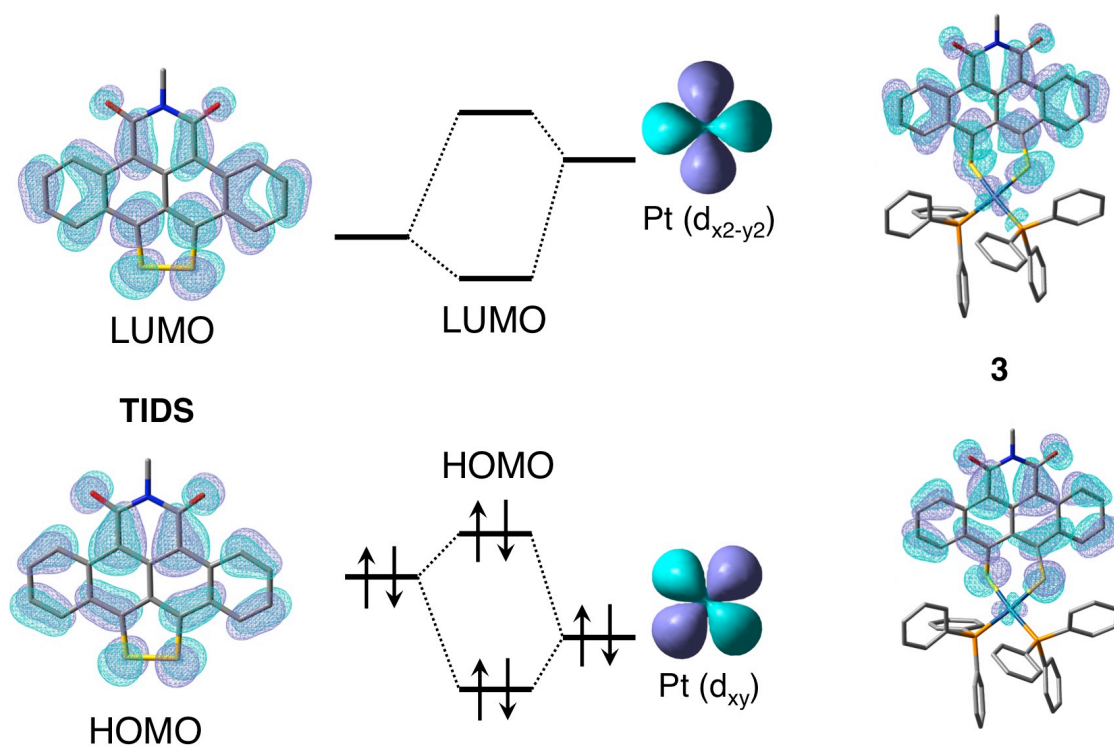
Figure 5. Molecular orbital analysis for HOMO and LUMO of **3**.

The photophysical properties of Pt-TIDS were investigated by fluorescence and transient light absorption measurements. The fluorescence of TIDS from S_1 state was detected as a mirror image of the light absorption spectrum with peaks at 788, 905, and 990 nm (Figure *6*). The fluorescence quantum yields were also obtained as 2×10^{-2} in toluene, 3.4×10^{-2} in THF, and 7×10^{-2} in DMF. In contrast to TIDS, the fluorescent spectrum of Pt-TIDS appeared as a broad shape at room temperature with a maximum at 964 nm (Figure *7*). The quantum yields were 2–3×10^{-2} in toluene, THF, and DMF. The vibrational structure of Pt-TIDS was observed to clearly resolve the peaks at 867, 945, and 1078 nm when the solution was cooled to 77 K, probably because solvent reorganization was suppressed in the frozen system. Additionally, Pt-TIDS gave fluorescence from S_2 state by exciting at 387 nm to result in a quantum yield of *ca.* 10^{-4}. Such emission from S_2 state was absent for TIDS.
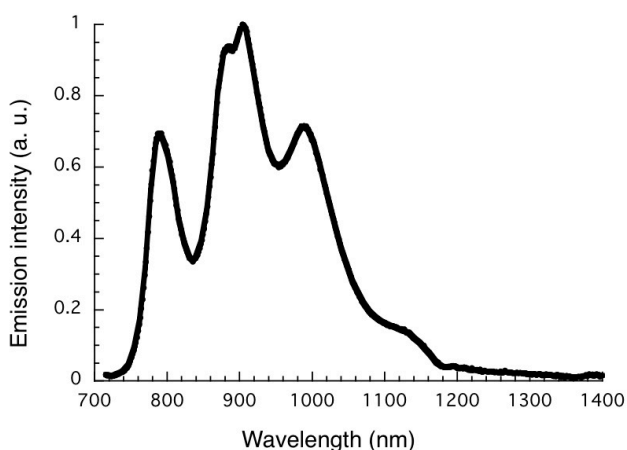
Figure 6. Fluorescence spectrum of TIDS excited at 692 nm at room temperature in THF.
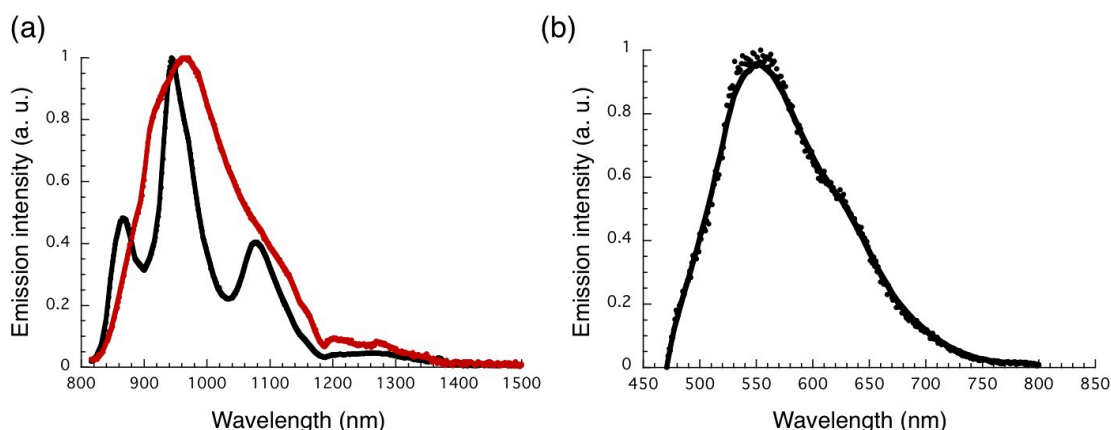
Figure 7. Fluorescence spectra of Pt-TIDS excited at (a) 692 and (b) 387 nm. In the left figure, spectra measured at room temperature (red) and at 77K (black) are shown.

In transient light absorption measurements, TIDS was excited at 387 and 656 nm. S_2 excitation state of TIDS was instantaneously formed when excited at 387 nm (Figure *8*). In 1–3 ps, the state transformed into a different state that was more stable radical ion pair. This state indicated some characteristic markers in 800–950 nm. It relaxed into S_1 state bearing maxima at 484, and 564 nm as well as minima at 645, 705, and 780 nm. The ground state followed S_1 state with diverse kinetics, which depended on solvents (60 ps in toluene, 110 ps in THF, 200 ps in DMF). When 656 nm irradiation excited TIDS, S_1 state directly emerged without generating S_2 and radical ion pair states. It exponentially converted into the ground state with similar kinetics depending on solvents.
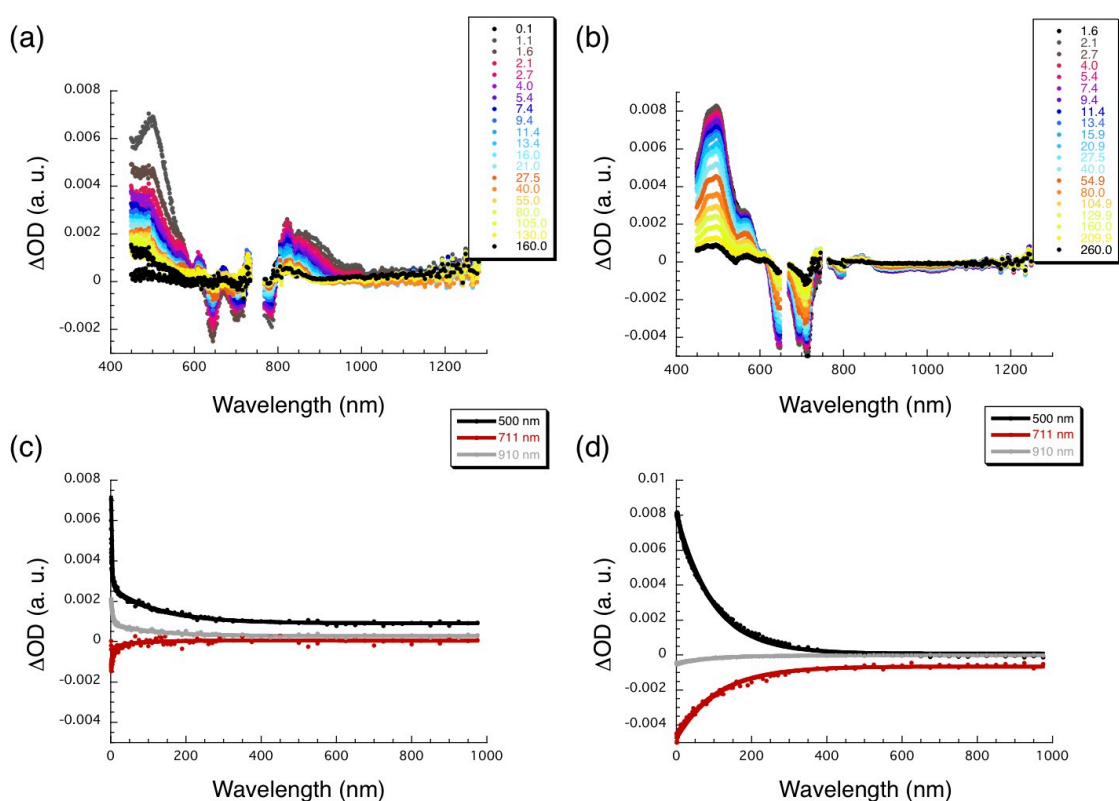
Figure 8. Transient light absorption spectra of TIDS excited at (a, c) 387 nm and at (b, d) 656 nm in THF.

Excitation at 387 nm for Pt-TIDS rapidly induced S_2 excited state within 0.5 ps (Figure *9*). Instant relaxation of the state to S_1 state followed maxima at 480, 550, and 650 nm as well as minima at 750 and 840 nm. Different from TIDS, the platinum promoted an intersystem crossing into a triplet state with high rate constants, which were independent from solvents (*e.g.* 70 ps in THF). The intersystem crossing should be triggered by heavy atom effect of the platinum atom. The triplet state displayed transient light absorption maxima at 465, 555, 650, and 966 nm as well as minima at

760 and 840 nm. To generate lower excited state directly, a laser at 670 nm was irradiated to Pt-TIDS to generate S_1 state with emission at 900–1200 nm. Additional nanosecond transient light absorption measurement and quenching experiment further evidenced the triplet state (Figure *10*). The nanosecond transient light absorption measurement excited at 355 nm exhibited the characteristics of the triplet state. The multiwavelength analysis determined the lifetime of the triplet state as 0.18 μs (toluene), 0.27 μs (THF) and 0.28 μs (DMF), which were relatively short compared to other platinum complexes.[11] These short lifetimes of triplet state would be derived from the large dπ–pπ conjugated system.[12] The quenching experiment obviously depicted the emission of singlet oxygen at 1275 nm, which was produced by quenching the excited molecule with triplet oxygen. Note that TIDS showed no triplet properties or emission from singlet oxygen at the quenching experiment. The triplet excitation state contributes to bring effective charge separation in solid state because of the forbidden transition to ground state. Namely, generation of triplet state is desirable for organic solar cells.[13] The energy diagrams of TIDS and Pt-TIDS obtained on the transient light absorption measurements are summarized in Figure *11*.
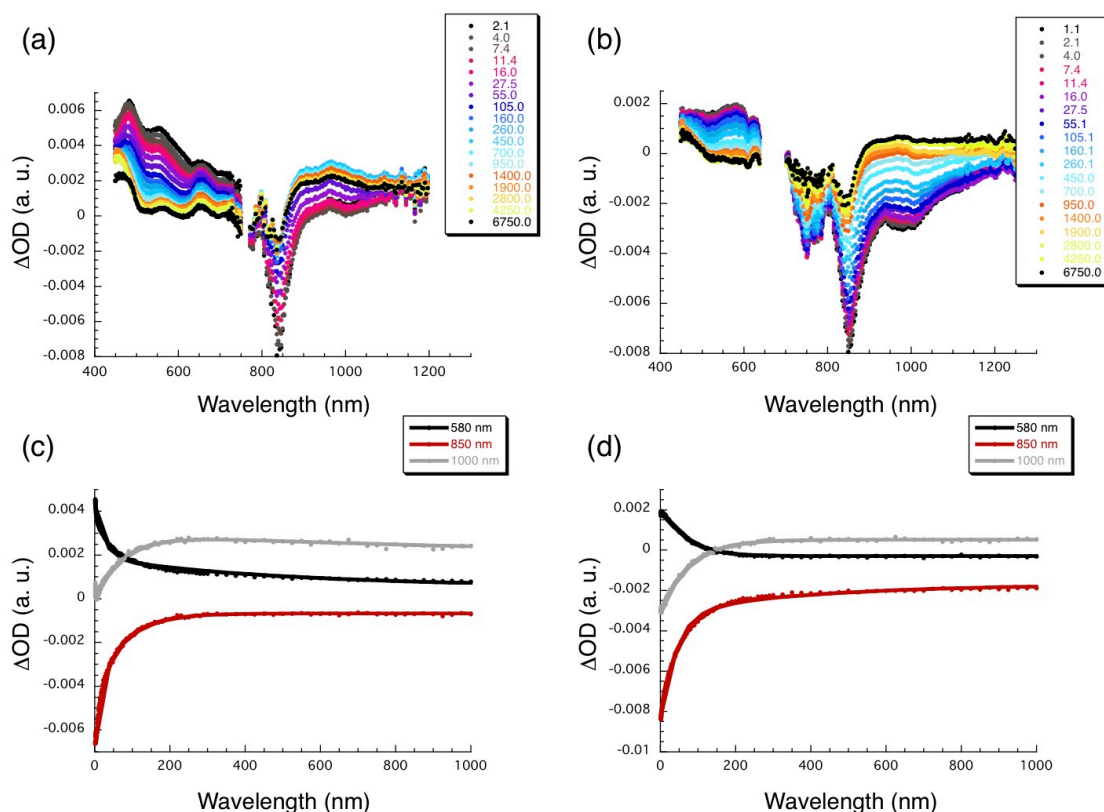
Figure 9. Transient light absorption spectra of Pt-TIDS excited at (a, c) 387 nm and at (b, d) 670 nm in THF.
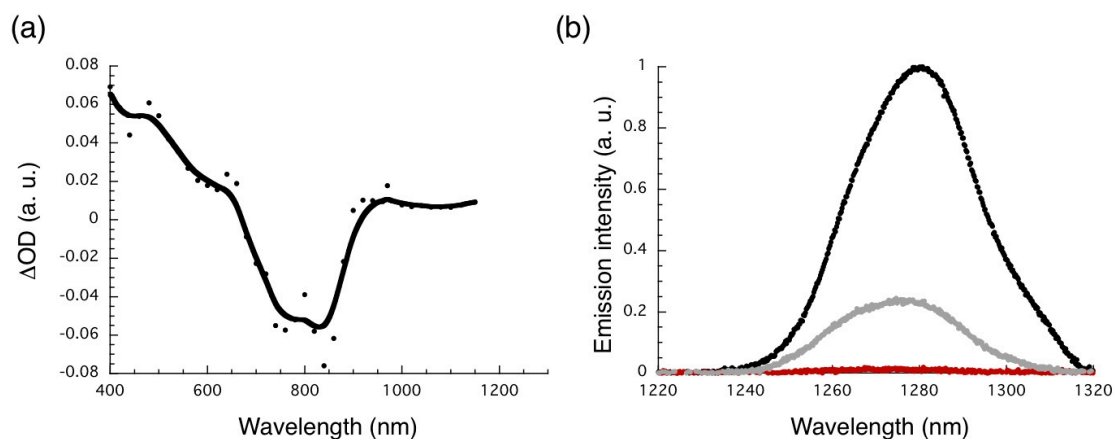
Figure 10. (a) Nanosecond transient light absorption measurement excited at 355 nm. The time delay was 110 ns. (b) Quenching experiment by detecting singlet oxygen. Excitation wavelength was 692 nm. TIDS (red), Pt-TIDS (grey), and a reference (zinc phthalocyanine, black) are shown. Both experiments were carried out in THF at room temperature.
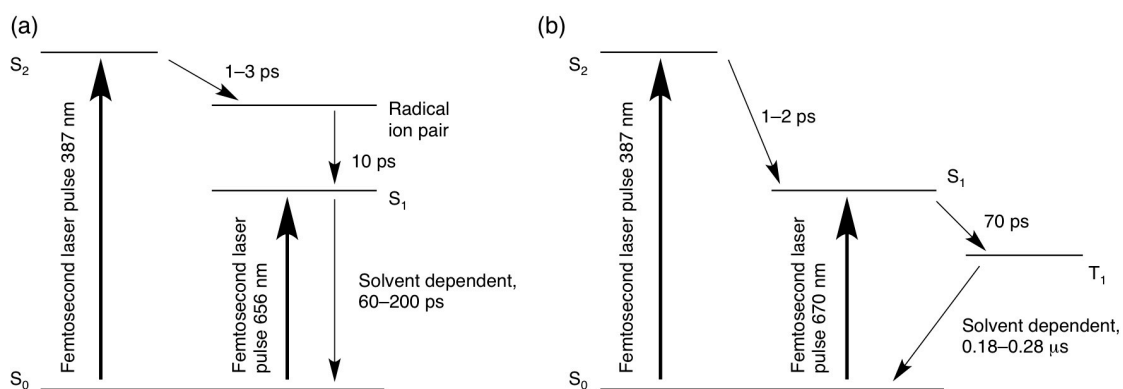
Figure 11. Energy diagrams of (a) TIDS and (b) Pt-TIDS obtained at transient light absorption measurements.

2.3. Summary

I have synthesized platinum complex with TIDS ligand. The crystal structure of Pt-TIDS showed a number of similarities compared to reported naphthodithiolene platinum complexes, but the most critical difference was observed at the coordination manner between platinum and disulfide group. The platinum coordination plane in Pt-TIDS twisted to tetraceneimide moiety, although naphthodithiolene platinum complexes in the literatures have envelope structures. The characteristic would bring different reactivity that Pt-TIDS did not form multinuclear complex, but reported naphthodithiolene platinum complexes were converted into other complexes containing multi-metal centers. Light absorption measurement and DFT calculations demonstrated larger π-conjugated system than TIDS to show NIR light absorption. The photophysical properties of Pt-TIDS were deeply investigated by transient light absorption measurements. In the results, the presence of platinum atom evoked triplet excited state for Pt-TIDS with lifetime (0.18–0.28 μs) varied by solvent. The achievements demonstrated the potential to use metal atom for π-conjugation that longer wavelength light absorption and heavy atom effects are introduced at the same time. This methodology would bring diversity to organic material chemistry to design metal complex materials.

2.4. Experimental Section

General. All reactions dealing with air or moisture-sensitive compounds were carried out in a dry reaction vessel under argon. Analytical thin-layer chromatography was performed on glass plates coated with 0.25 mm 230–400 mesh silica gel containing a fluorescent indicator (Merck). Flash silica gel column chromatography was performed on silica gel (Wako, Wakogel® C-200). Size exclusion column chromatography was performed on a Japan Analytical Industry LC-9201 (eluent: toluene) with JAIGEL 2H and 3H polystyrene columns. NMR spectra were measured on JEOL ECA-500 and ECX-400 spectrometers and reported in parts per million from tetramethylsilane. High-resolution mass spectra were acquired by atmospheric pressure ionization (APCI) using a time-of-flight mass analyzer on JEOL JMS-T100LC (AccuTOF) spectrometer. UV-vis absorption spectra were recorded on a JASCO V-670 spectrometer.

Materials. TIDS was prepared accorrding to our previous report (ref. 8 in the main text). $Pt(PPh_3)_3$ and $Pt(PPh_3)_2(C_2H_4)$ were synthesized through the reported procedures.[14] The other materials were purchased from Tokyo Kasei Co., Sigma Aldrich Inc. and other commercial suppliers and used after appropriate purification. Solvents were purchased from Kanto Chemical Co., Inc and purified by solvent purification system (GlassContour) equipped with columns of activated alumina and supported copper catalyst (Q-5) prior to use.

Synthesis of $Pt(TIDS)(PPh_3)_2$. Method A) A mixture of TIDS (450 mg, 1.02 mmol) and $Pt(PPh_3)_3$ (1.00 g, 1.02 mmol) in THF (30 mL) was stirred at room temperature for 4 h under argon gas atmosphere. Proceeding of the reaction was monitored by ^1H and ^{31}P NMR measurements. To the reaction mixture was added hexane to precipitate the product, which was washed with hexane to obtain $Pt(TIDS)(PPh_3)_2$ as green crystals (820 mg, 70% isolated yield).
Method B) A mixture of TIDS (44.4 mg, 0.100 mmol) and $Pt(PPh_3)_2(C_2H_4)$ (100.1 mg, 0.134 mmol) in THF (3.0 mL) was stirred at room temperature for 1 h under argon gas atmosphere. Proceeding of the reaction was monitored by ^1H and ^{31}P NMR measurements. To the reaction mixture was added hexane to precipitate the product, which was washed with hexane to obtain $Pt(TIDS)(PPh_3)_2 \cdot 2THF$ as green crystals (119.8 mg, 92% isolated yield).
^1H NMR (400 MHz, $CDCl_3$): δ = 0.88 (t, J = 6.9 Hz, 3H, Me in hexyl), 1.30–1.38 (m, 4H, CH_2 in hexyl), 1.46–1.52 (m, 2H, CH_2 in hexyl), 1.79–1.85 (m, 2H, CH_2 in hexyl), 4.34 (t, J = 7.6 Hz, 2H, CH_2 in hexyl), 7.07 (ddd, J = 1.4, 6.6, 8.9 Hz, 2H, 2- and 9-tetracene), 7.22 (t, J = 7.6 Hz, 12H, o-Ph), 7.37 (t, J = 7.3 Hz, 6H, p-Ph), 7.52-7.58 (m, 14H, m-Ph overlapping with 3- and 8-tetracene), 8.45 (dd, J = 0.85, 8.9 Hz, 2H, 1- and 10-tetracene), and 9.83 (dd, J = 0.60, 8.4 Hz, 2H, 4- and 7-tetracene). $^{13}C\{^1H\}$ NMR (100 MHz, $CDCl_3$): δ = 14.1, 22.7, 27.2, 28.2, 31.8, 40.8, 108.3, 123.7, 126.4, 128.1, 128.5, 128.8, 129.1, 129.5, 130.4, 131.0, 132.3, 134.0, 135.0, 153.0, and 164.5.

$^{31}P\{^1H\}$ NMR (161 MHz, CDCl$_3$): δ = 21.1 (s, with ^{195}Pt satellites, J_{Pt-P} = 3040 Hz). IR (ZnSe): 1646, 1605 cm^{-1}. HR-MS (APCI$^+$): Calcd. for C$_{62}$H$_{52}$NO$_2$P$_2$S$_2$Pt (M+H)$^+$ = 1163.2567, found 1163.2616.

X-ray Crystallographic Analysis. X-ray crystallographic analysis was performed using a RIGAKU R-AXIS RAPID II (imaging plate detector) with monochromic CuKα (λ = 1.5406 Å) radiation. The positional and thermal parameters were refined by a full-matrix least-squares method using the SHELXL97 program on the Yadokari-software.

Computational studies.
All calculations were carried out by Gaussian09 package at the B3LYP level.[15] Platinum atom was represented by the LANL2DZ basis set, a 6-31G+(d) basis set was used for phosphine and sulfur atoms, and others were described by 6-31G(d) (C, H, N, and O). The calculation levels are described as "B3LYP/LANL2DZ/6-31G+(d)/6-31G(d)".

Electrochemical Studies. Cyclic voltammetry (CV) was performed using HOKUTO DENKO HZ-5000 voltammetric analyzer. All CV measurements were carried out in a one-compartment cell under argon gas, equipped with a glassy-carbon working electrode, a platinum wire counter electrode, and an Ag/Ag$^+$ reference electrode. The supporting electrolyte was a 0.1 mol/L dichloromethane solution of tetrabutylammonium hexafluorophosphate (TBAPF$_6$).

Photophysical Studies. All solvents used were spectroscopic grade and were purchased from Sigma-Aldrich. UV/vis spectra were recorded with a Perkin Elmer Lambda 2 instrument. For emission, a FluoroMax 3 fluorometer by HORIBA JobinYvon was used to detect in the visible region (< 800 nm), whereas a HORIBA JobinYvon Fluorolog instrument was applied to detect emission in the NIR region. All UV/vis absorption and emission studies were carried out in argon saturated solutions in a 10 × 10 mm quartz cell. For singlet oxygen detection, the samples were instead purged with oxygen. Femtosecond transient absorption studies were performed in argon-saturated solutions with 387 nm, 656 nm and 670 nm excitation laser pulses (1 kHz, 150 fs pulse width) from an amplified Ti:Sapphire laser system (Clark-MXR Inc.) with a laser energy of 200 nJ. Nanosecond laser flash photolysis experiments were carried out with argon or oxygen purged samples using a 355 nm laser pulse from a Quanta-Ray CDR Nd:Yag system (6 ns pulse width) in a front face excitation geometry.

Crystal Data Collection Parameters for Pt-TIDS.

Formula	$C_{62}H_{51}NO_2P_2PtS_2$
Formula Weight	1163.19
Crystal System	triclinic
Space Group	$P\bar{1}$
R, R_w ($I>2\sigma(I)$)	0.0461, 0.0993
$R1, wR2$ (all data)	0.0514, 0.1047
GOF on F^2	1.151
a (Å)	13.6201(3)
b (Å)	13.7861(3)
c (Å)	13.8277(3)
α (º)	85.265(2)
β (º)	79.447(2)
γ (º)	78.335(1)
V (Å^3)	2496.97(9)
Z	2
T (K)	293(2)
Crystal Size (mm)	0.10, 0.10, 0.10
D_{calcd} (g·cm^{-3})	1.547
$2\theta_{min}, 2\theta_{max}$ (º)	3.25, 68.24
no. refl. measured (unique)	8969
no. refl. measured ($I>2\sigma(I)$)	7799
no. parameters	631
μ (CuKα)	1.54178

Coordinates of Pt-TIDS Analogue (3) Calculated at B3LYP/LNAL2DZ/6-31G+(d)/6-31G(d).

106

C	-2.706000	1.203101	-0.726093
C	-3.573600	2.220040	-1.225207
C	-3.055586	3.359008	-1.917900
H	-1.986617	3.418864	-2.083171
C	-3.883672	4.328585	-2.422280
H	-3.470351	5.165678	-2.978425
C	-5.282255	4.210977	-2.240746
H	-5.945496	4.967823	-2.652478
C	-5.820105	3.140601	-1.568475
H	-6.887560	3.062967	-1.435632
C	-4.996186	2.102007	-1.029407
C	-5.508492	0.980342	-0.309453
C	-4.672489	-0.145106	-0.059852
C	-5.196738	-1.346959	0.498748
C	-4.392245	-2.521936	0.570798
C	-4.867811	-3.768145	1.098503
H	-5.861291	-3.790704	1.516441
C	-4.104153	-4.907435	1.062346
H	-4.509305	-5.832393	1.465940
C	-2.803691	-4.891199	0.503751
H	-2.205347	-5.798142	0.474561
C	-2.297867	-3.717465	0.010380
H	-1.300511	-3.693356	-0.407277
C	-3.047628	-2.497099	0.039933
C	-2.485940	-1.270214	-0.421099
C	-3.254924	-0.077346	-0.393043
C	-6.899979	0.977749	0.159829
C	-6.593512	-1.356850	0.978821
C	-8.720932	-0.240547	1.281920
H	-8.715664	-0.404098	2.362886
H	-9.188426	0.709943	1.038693
C	1.299278	3.479430	0.907114
C	1.592494	4.590954	0.105483
H	2.301660	4.507809	-0.710741
C	0.975474	5.820158	0.352520
H	1.215607	6.674633	-0.274319

25

C	0.059146	5.950501	1.396045
H	-0.421093	6.906640	1.584652
C	-0.243423	4.844964	2.195258
H	-0.963607	4.934488	3.003438
C	0.368678	3.616993	1.951959
H	0.114968	2.762065	2.571455
C	2.724980	1.482255	2.322363
C	2.338987	0.313079	2.992134
H	1.694802	-0.401618	2.490126
C	2.759906	0.072120	4.302954
H	2.445046	-0.836408	4.808695
C	3.571019	0.999090	4.957761
H	3.897843	0.814357	5.977422
C	3.945326	2.178065	4.306097
H	4.558752	2.913710	4.819144
C	3.515663	2.425786	3.002608
H	3.776938	3.365597	2.525145
C	3.457624	2.159754	-0.513204
C	3.135290	2.264429	-1.878744
H	2.111907	2.093448	-2.203842
C	4.117301	2.586683	-2.815851
H	3.850896	2.672986	-3.865774
C	5.436735	2.792009	-2.405020
H	6.202986	3.039927	-3.134475
C	5.767614	2.668807	-1.055351
H	6.794229	2.812675	-0.729916
C	4.785023	2.357636	-0.112074
H	5.064017	2.256545	0.930385
C	4.036819	-1.346096	-0.349735
C	4.810294	-1.229764	-1.515064
H	4.342919	-1.316049	-2.489735
C	6.189178	-1.023160	-1.435465
H	6.770446	-0.942715	-2.349842
C	6.817767	-0.932268	-0.193426
H	7.892568	-0.783555	-0.133337
C	6.056795	-1.038978	0.972804
H	6.534673	-0.974118	1.946706
C	4.678275	-1.240391	0.896587
H	4.108897	-1.332200	1.814424
C	2.009320	-2.463193	-2.078498
C	2.080499	-3.853252	-2.244183

H	2.217332	-4.500999	-1.385180
C	1.951639	-4.419357	-3.514037
H	1.996261	-5.499228	-3.626130
C	1.755994	-3.605937	-4.631508
H	1.651847	-4.049753	-5.617717
C	1.679355	-2.220728	-4.474636
H	1.509000	-1.580968	-5.336021
C	1.797574	-1.652040	-3.205841
H	1.698412	-0.576798	-3.086471
C	1.963420	-2.951363	0.840340
C	0.794231	-2.954840	1.616115
H	0.041961	-2.190406	1.453962
C	0.587444	-3.941899	2.583003
H	-0.328970	-3.933924	3.165626
C	1.544268	-4.936737	2.785370
H	1.381995	-5.705478	3.536079
C	2.713443	-4.942004	2.019758
H	3.464289	-5.712376	2.173642
C	2.924945	-3.955489	1.056333
H	3.845460	-3.962994	0.480830
N	-7.345989	-0.199723	0.776224
O	-7.680611	1.929045	0.064759
O	-7.148008	-2.293139	1.562434
P	2.060559	1.818201	0.637029
P	2.207526	-1.641343	-0.437250
S	-1.089821	1.762565	-0.338340
S	-0.921731	-1.370800	-1.268658
Pt	0.625199	0.142752	-0.261323
H	-9.259980	-1.070739	0.818927

2.5. References

1. (a) Kwong, R. C.; Sibley, S.; Dubovoy, T.; Baldo, M.; Forrest, S. R. Thompson, M. E. *Chem. Mater.* **1999**, *11*, 3709–3713. (b) Hudson, Z. M.; Wang, S. *Dalton Trans.* **2011**, *40*, 7805–7816. (c) Druet, S.; Paul-Roth, C. O.; Fattori, V.; Cocchi, M.; Williams, J. A. G. *New J. Chem.* **2011**, *35*, 438–444. (d) Graham, K. R.; Yang, Y.; Sommer, J. R.; Shelton, A. H.; Schanze, K. S.; Xue, J.; Reynolds, J. R. *Chem. Mater.* **2011**, *23*, 5305–5312. (e) Hang, X.-C.; Fleetham, T.; Turner, E.; Brooks, J.; Li, J. *Angew. Chem. Int. Ed.* **2013**, *52*, 6753–6756.

2. (a) Shao, Y. Yang, Y. *Adv. Mater.* **2005**, *17*, 2841–2844. (b) Wong, W.-Y.; Wang, X.-Z.; He, Z.; Djurišić, A. B.; Yip, C.-T.; Cheung, K.-Y.; Wang, H.; Mak, C. S. K.; Chan, W.-K. *Nat. Mater.* **2007**, *6*, 521–527. (c) Baek, N. S.; Hau, S. K.; Yip, H.-L.; Acton, O.; Chen, K.-S.; Jen, A. K.-Y. *Chem. Mater.* **2008**, *20*, 5734–5736.

3. (a) Powell, C. E.; Humphrey, M. G. *Coord. Chem. Rev.* **2004**, *248*, 725–756. (b) Batema, G. D.; Lutz, M.; Spek, A. L.; van Walree, C. A.; de Mello Donegá, C.; Meijerink, A.; Havenith, R. W. A.; Perez-Moreno, J.; Clays, K.; Büchel, M.; van Dijken, A.; Bryce, D. L.; van Klink, G. P. M.; van Koten, G. *Organometallics* **2008**, *27*, 1690–1701.

4. (a) Wilson, M. W. B.; Rao, A.; Ehrler, B.; Friend, R. H. *Acc. Chem. Res.* **2013**, *46*, 1330–1338. (b) Moon, H.; Zeis, R.; Borkent, E.-J.; Besnard, C.; Lovinger, A. J.; Siegrist, T.; Kloc, C.; Bao, Z. *J. Am. Chem. Soc.* **2004**, *126*, 15322–15323. (c) Bertolazzi, S.; Wünsche, J.; Cicoira, F. Santato, C. *Appl. Phys. Lett.* **2011**, *99*, 013301.

5. (a) Bosman, W. P.; van der Linden, H. G. M. *J. Chem. Soc., Chem. Commun.* **1977**, 714–715. (b) Tesmer, M.; Vahrenkamp, H. *Eur. J. Inorg. Chem.* **2001**, 1183–1188. (c) Xu, H. Yip, J. H. K. *Inorg. Chem.* **2003**, *42*, 4492–4494. (d) Wright, R. J.; Lim, C.; D. Tilley, T. *Chem. Eur. J.* **2009**, *15*, 8518–8525. (e) Samuel, A. P. S.; Co, D. T.; Stern, C. L.; Wasielewski, M. R. *J. Am. Chem. Soc.* **2010**, *132*, 8813–8815.

6. (a) Teo, B.-K. Snyder-Robinson, P. A. *Inorg. Chem.* **1979**, *18*, 1490–1495. (b) Benson, C. G. M.; Schofield, C. M.; Randall, R. A. M.; Wakefield, L.; Knight, F. R.; Slawin, A. M. Z.; Woollins, J. D. *Eur. J. Inorg. Chem.* **2013**, 427–437.

7. (a) Okamoto, T.; Suzuki, T.; Tanaka, H.; Hashizume, D.; Matsuo, Y. *Chem. Asian J.* **2012**, *7*, 105–111. (b) Suzuki, T.; Okamoto, T.; Saeki, A.; Seki, S.; Sato, H.; Matsuo, Y. *ACS Appl. Mater. Interfaces* **2013**, *5*, 1937–1942.

8. (a) Ugo, R.; Cariati, F.; La Monica, G. *Inorg. Synth.* **1968**, *11*, 105–108. (b) Blake, D. M.; Roundhill, D. M.; Ambridge, C.; Dwight S.; Clark, H. C. *Inorg. Synth.* **1978**, *18*, 120–124.

9. (a) Aucott, S. M.; Milton, H. L.; Robertson, S. D.; Slawin, A. M. Z.; Walker, G. D.; Woollins, J. D. *Chem. Eur. J.* **2004**, *10*, 1666–1676. (b) Robertson, S. D.; Slawin, A. M. Z.; Woollins, J. D. *Eur. J. Inorg. Chem.* **2007**, 247–253.

10. HOMO and LUMO levels were determined from the first oxidation and reduction potentials in our investigation with the following equation:

HOMO or LUMO level = $-(4.8 + E^{1/2})$ eV.

11. (a) Ji, Z.; Li, S.; Li, Y.; Sun, W. *Inorg. Chem.* **2010**, *49*, 1337–1346. (b) Archer, S.; Weinstein, J. A. *Coord. Chem. Rev.* **2012**, *256*, 2530–2561. (c) Liu, L.; Guo, S.; Ma, J.; Xu, K.; Zhao, J.; Zhang, T. *Chem. Eur. J.* **2014**, *20*, 14282–14295. (d) Yang, J.; Kersi, D. K.; Giles, L. J.; Stein, B. W.; Feng, C.; Tichnell, C. R.; Shultz, D. A.; Kirk, M. L. *Inorg. Chem.* **2014**, *53*, 4791–4793.

12. Wilson, J. S.; Chawdhury, N.; Al-Mandhary, M. R. A.; Younus, M.; Khan, M. S.; Raithby, P. R.; Kohler A.; Friend, R. H. *J. Am. Chem. Soc.* **2001**, *123*, 9412–9417.

13. (a) Guo, F.; Kim, Y.-G.; Reynolds, J. R.; Schanze, K. S. *Chem. Commun.* **2006**, 1887–1889. (b) Guo, F.; Ogawa, K.; Kim, Y.-G.; Danilov, E. O.; Castellano, F. N.; Reynolds, J. R.; Schanze, K. S. *Phys. Chem. Chem. Phys.* **2007**, *9*, 2724–2734. (c) Mei, J.; Ogawa, K.; Kim, Y.-G.; Heston, N. C.; Arenas, D. J.; Nasrollahi, Z.; McCarley, T. D.; Tanner, D. B.; Reynolds, J. R.; Schanze, K. S. *ACS Appl. Mater. Interfaces* **2009**, *1*, 150–161.

14. (a) Ugo, R.; Cariati, F.; La Monica, G. *Inorg. Synth.* **1968**, *11*, 105–108. (b) Blake, D. M.; Roundhill, D. M.; Ambridge, C.; Dwight S.; Clark, H. C. *Inorg. Synth.* **1978**, *18*, 120–124.

15. *Gaussian 09*, Revision A.02, Frisch, M. J.; Trucks, G. W.; Schlegel, H. B.; Scuseria, G. E.; Robb, M. A.; Cheeseman, J. R.; Scalmani, G.; Barone, V.; Mennucci, B.; Petersson, G. A.; Nakatsuji, H.; Caricato, M.; Li, X.; Hratchian, H. P.; Izmaylov, A. F.; Bloino, J.; Zheng, G.; Sonnenberg, J. L.; Hada, M.; Ehara, M.; Toyota, K.; Fukuda, R.; Hasegawa, J.; Ishida, M.; Nakajima, T.; Honda, Y.; Kitao, O.; Nakai, H.; Vreven, T.; Montgomery, Jr., J. A.; Peralta, J. E.; Ogliaro, F.; Bearpark, M.; Heyd, J. J.; Brothers, E.; Kudin, K. N.; Staroverov, V. N.; Kobayashi, R.; Normand, J.; Raghavachari, K.; Rendell, A.; Burant, J. C.; Iyengar, S. S.; Tomasi, J.; Cossi, M.; Rega, N.; Millam, J. M.; Klene, M.; Knox, J. E.; Cross, J. B.; Bakken, V.; Adamo, C.; Jaramillo, J.; Gomperts, R.; Stratmann, R. E.; Yazev, O.; Austin, A. J.; Cammi, R.; Pomelli, C.; Ochterski, J. W.; Martin, R. L.; Morokuma, K.; Zakrzewski, V. G.; Voth, G. A.; Salvador, P.; Dannenberg, J. J.; Dapprich, S.; Daniels, A. D.; Farkas, O.; Foresman, J. B.; Ortiz, J. V.; Cioslowski, J.; Fox, D. J. Gaussian, Inc., Wallingford CT, **2009**.

Chapter 3.

Extension of π-Conjugated System throughout Two Tetraceneimide Disulfide Ligands in Tri-palladium Complex

3.1. Introduction

Long wavelength absorption and large molecular absorption coefficient that are the characteristics derived from extended π-conjugated system have attracted chemists, who have established a huge number of organic photo-functional materials. This situation has encouraged researchers to design a variety of π-conjugated backbones such as porphyrinoids,[1] perylene dyes,[2] acene analogues,[3] and so on, which have been applied to organic electronics,[4] bioimaging,[5] and chemosensing.[6] In a different way, long wavelength absorption was achieved in a field of metal complex chemistry. That is dπ-pπ conjugation between metal and organic atoms. Metal bis(dithiolene) complex is a good example having amazingly narrow HOMO–LUMO gap.[7] Although the metal bis(dithiolene) complexes are well-known complexes showing long wavelength absorption and being applied to some electronic devices, other complexes were seldom reported to possess exceptional π-conjugation except for a multiple-decker phthalocyanine structure.[8] In the structure, metal atoms and phthalocyanines alternatively stack in a longitudinal direction. The researches demonstrated the potential of metal-bridging structure to construct light-absorbing materials, however π-extended metal complexes are less developed than organic molecules.[9]

In this work, I have established a trinuclear palladium complex as well as a prototype mononuclear palladium complex with tetraceneimide disulfide (TIDS) ligands, which have been studied in our laboratory previously.[10] The trinuclear one showed exceptionally long wavelength light absorption containing a peak at 1982 nm in solution state. The properties and the origins of its characteristic light absorption were explored by light absorption measurements, DFT calculations, and transient light absorption measurements. Here, I describe TIDS as hexyl chain substituted TIDS unless otherwise specified.

3.2. Results and Discussion

When 1 equiv. of tetrakis(triphenylphosphine)palladium and 1 equiv. of TIDS were mixed in THF at room temperature, the blue suspension turned into dark-red solution to give palladium TIDS complex as black solids. NMR data exhibited the same symmetry to Pt-TIDS, but preliminary X-ray single crystal analysis displayed a trinuclear structure. At that time, the yield based on TIDS was 30%. The other reaction condition with 1.5 equiv. of tetrakis(triphenylphosphine)palladium and 1 equiv. of TIDS improved the yield of the trinuclear palladium TIDS complex (*tri*-Pd-TIDS) as 77% after purification (Scheme *1*). The purification was sequential recrystallization from THF/hexane and then CH$_2$Cl$_2$/hexane. The first recrystallization did not remove triphenylphosphine completely, but the second one could purify the product to give crystallographically acceptable single crystals. Through the modification of the reaction condition, mononuclear TIDS complex (*mono*-Pd-TIDS) was successfully obtained.

The reaction condition required CH_2Cl_2 as a solvent instead of THF to solubilize the reaction precursors. Separately prepared two solutions of tetrakis(triphenylphosphine)palladium and TIDS were mixed by a cannula. The color of reaction mixture turned from blue to black. It is noteworthy that *mono*-Pd-TIDS was not separated from free triphenylphosphine because recrystallization of *mono*-Pd-TIDS decomposed during the crystallization. The instability of solid state would be derived from stabilization of *mono*-Pd-TIDS by triphenylphosphine in solution state. In a similar reaction condition with bis(1,5-cyclooctadiene)nickel (Ni(COD)$_2$), TIDS and Ni(COD)$_2$ reacted, but it gave paramagnetic products. Additionally, it was thermally unstable at room temperature, so the product was neither separated nor determined.

Scheme 1. Synthesis of TIDS palladium complexes.
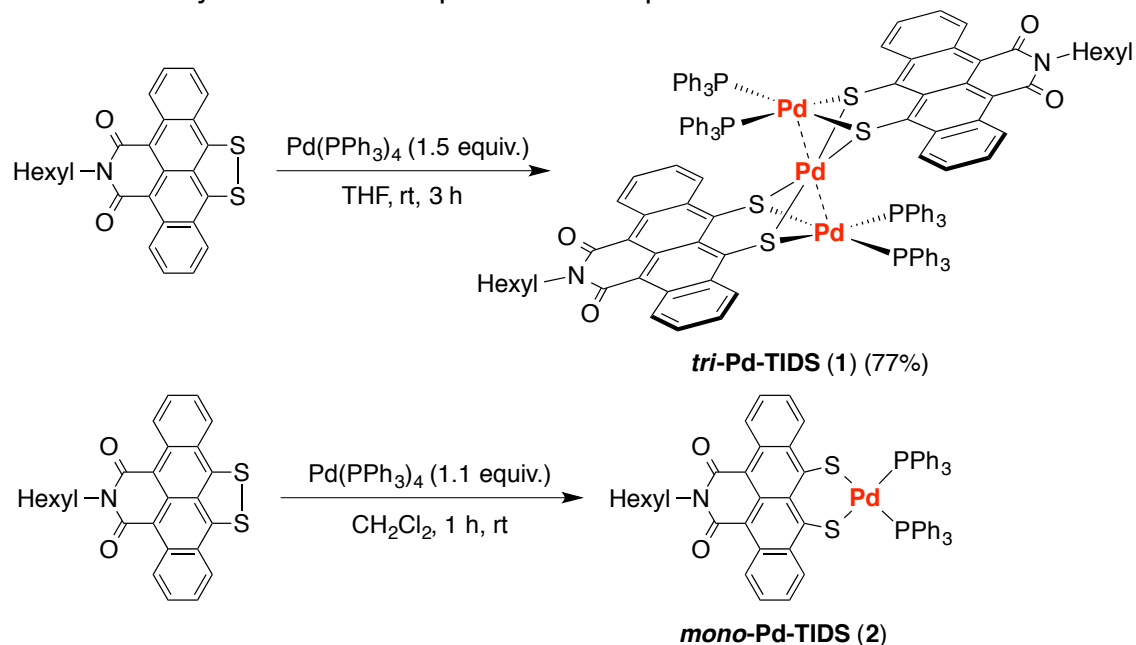
The electrochemical properties of *tri*-Pd-TIDS were collected by cyclic voltammetry (CV) and differential pulse voltammetery (DPV). The CV chart displayed three reversible reduction waves at –0.50, –0.76 and –1.12 V in CH_2Cl_2 (Figure *1*). The reduction potentials were highly positive-shifted compared to TIDS (–1.21 V) and Pt-TIDS (–1.45 V). In DPV chart, the three reductions appeared with similar heights (–0.44, –0.72 and –1.07 V), but the fourth peak was around half of the others (–1.24 V). In the CV measurement, The fourth reduction peak was irreversible. I considered that the forth peak indicated decomposition of the complex. On the other hand, no oxidation peak was detected even if the working electrode and the solvent were changed from glassy carbon/CH_2Cl_2 to gold/CH_2Cl_2, platinum/CH_2Cl_2, and grassy carbon/THF.
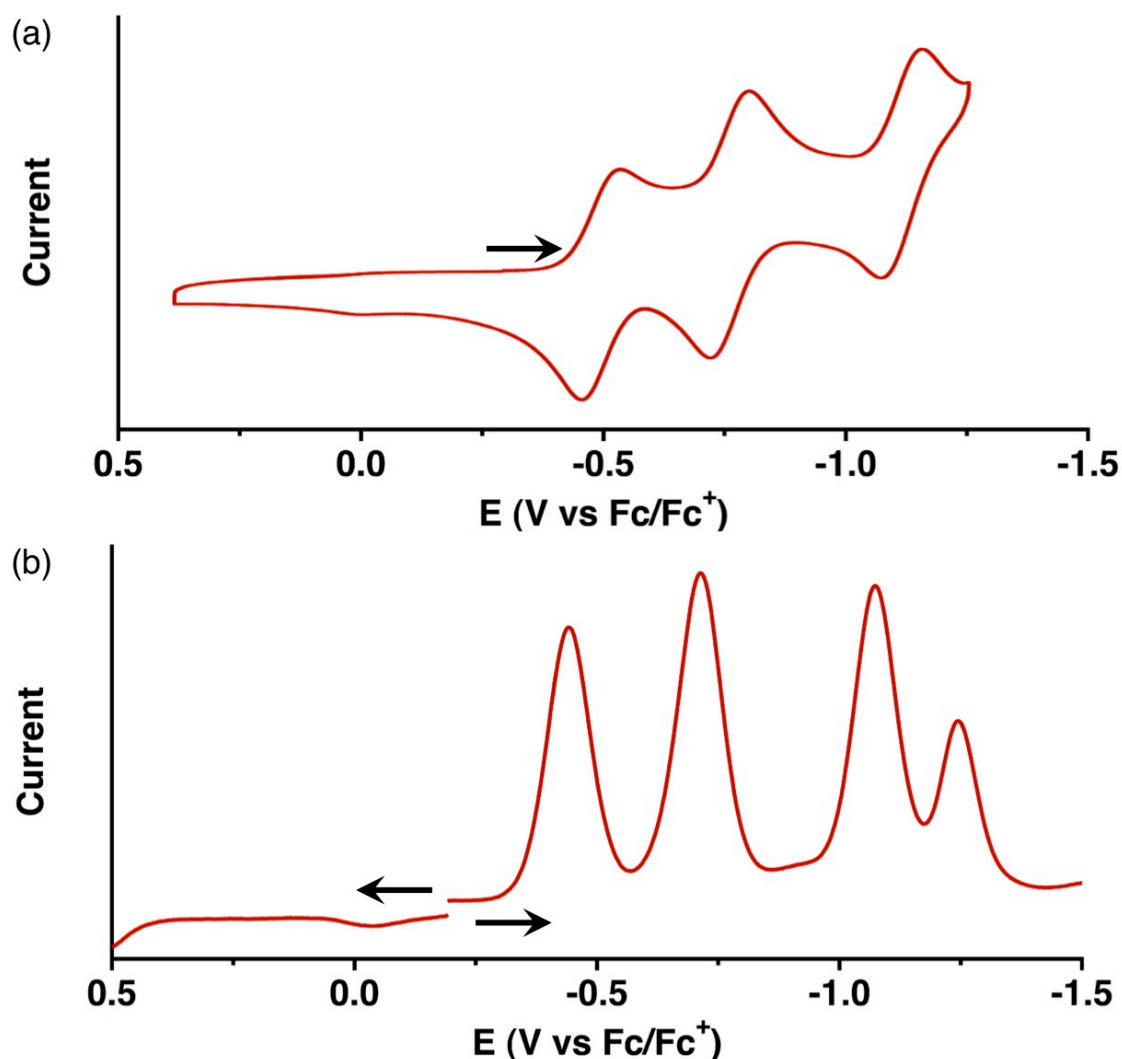
Figure 1. (a) Cyclic voltammogram and (b) differential pulse voltammogram of *tri*-Pd-TIDS measured in CH$_2$Cl$_2$ with a grassy carbon working electrode.

The single crystal of *tri*-Pd-TIDS was obtained by the recrystallization technique from CH$_2$Cl$_2$/hexane. The X-ray structural analysis clearly illustrated the trimetallic structure (Figure **2**). In the structure, each TIDS ligand bridges two palladium atoms in a similar manner to dinuclear naphthodithiolene complexes.[11] Unlike Pt-TIDS, TIDS ligands and palladium coordination planes structured envelope-like conformations to build such multi-nuclear cluster. The three palladiums atoms align almost linearly with the angle of 174.08(2)º. The distances between the palladium atoms are 2.8818(5) and 2.9241(5) Å. The lengths are slightly longer than the Pd–Pd metallic bond length (2.76 Å), but shorter than van der Waals distance of Pd···Pd (3.26 Å). It would imply existence of weak interactions between the palladium atoms. The three palladium coordination planes formed all square planar. The distances are longer than other complexes having linearly aligned palladium atoms.[12] Among the

34

literatures, dithiadiazole palladium complex and tetrahedral palladium cluster involve similar distances between palladium atoms.[12b, 13] In the packing structure, π–π interaction between the TIDS ligands was not observed, but coplanar interaction was found between imide group and tetracene moiety in TIDS ligands (2.416 Å, H···O_{vdW}: 2.72 Å). The similar interactions were also observed in bare TIDS.[10b] The trinuclear structure is isoelectronic to the reported complex composed of Pt(II)–Ag(I)–Pt(II) with two naphthodithiolene lignads.[14] The critical difference between the reported complex and *tri*-Pd-TIDS is distance between the metals. The distances of Pt-Ag are 3.0739(13) and 3.2044(13) Å, which are 0.15–0.32 Å longer than the Pd···Pd distances of *tri*-Pd-TIDS. Although the literature did not mention the light absorption properties and other optical properties of the Pt–Ag–Pt complex, the difference of the metals would deeply effect to the complexes' light absorption properties. The Pt–Ag–Pt complex and *tri*-Pd-TIDS contain trimetallic system and acene disulfide ligands to form the similar structures. I can say that the acene disulfide ligand has a potential to construct the trimetallic system with the ligands placing in parallel. Here, a donor–acceptor structure of TIDS ligand between disulfide and imide groups is not involved in the Pt–Ag–Pt complex. The donor–acceptor structure would be critical for the fully π-conjugated system and infrared light absorption.

(a)

(b)

(c)

2.747 Å

2.416 Å
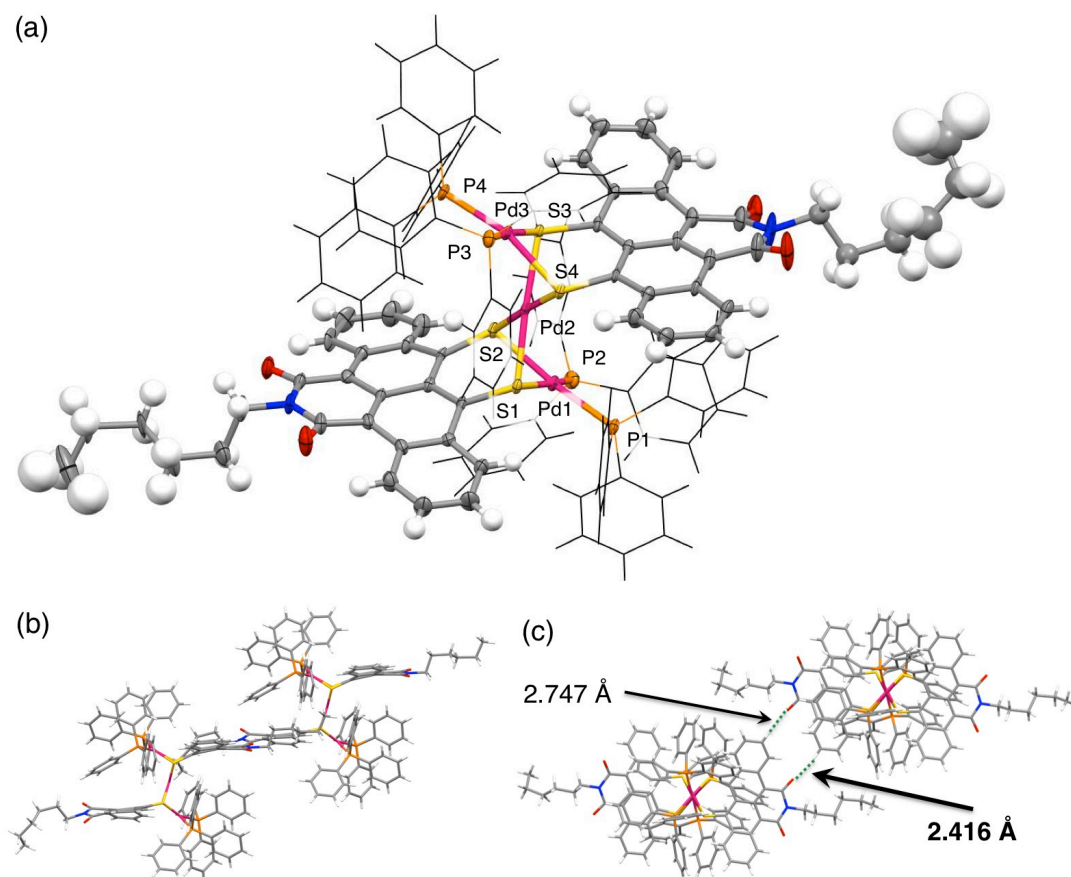
Figure 2. Crystal structure of *tri*-Pd-TIDS and interaction between the peripheral

molecules. (a) Closed view of *tri*-Pd-TIDS drawn with thermal ellipsoids with the 50% probability level. The phenyl groups at the phosphine ligands are shown as wire-frame style. (b), (c) Two peripheral molecules of *tri*-Pd-TIDS are shown in different views. Selected bond lengths [Å], angles [º], and torsion angles [º]: Pd1–P1 2.335(2), Pd1–P2 2.365(1), Pd1–S1 2.355(1), Pd1–S2 2.377(1), Pd1–Pd2 2.8818(5), Pd2–S1 2.315(1), Pd2–S2 2.336(1), Pd2–S3 2.353(1), Pd2–S4 2.351(1), Pd2–Pd3 2.9241(5), Pd3–P3 2.342(1), Pd3–P4 2.320(2), Pd3–S3 2.350(1), Pd3–S4 2.344(1), S1···S2 3.030(1), S3···S4 3.058(1), P1–Pd1–P2 100.59(5), P2–Pd1–S2 89.85(5), S2–Pd1–S1 79.64(4), S1–P1–P1 91.12 (5), Pd1–S1–Pd2 76.21(4), Pd1–S2–Pd2 75.38(4), S2–Pd2–S1 81.31(4), S1–Pd2–S4 96.95(4), S4–Pd2–S3 81.07(4), S3–Pd2–S2 100.53(4), Pd2–S3–Pd3 76.88(4), Pd2–S4–Pd3 77.03(4), P3–Pd3–P4 98.60(5), P4–Pd3–S3 92.27(5), S3–Pd3–S4 81.28(4), S4–Pd3–P3 88.96(5), Pd1–Pd2–Pd3 174.08(2), P2–P1–Pd1–S1 172.49(5), S1–S2–Pd2–S3 176.83(5), P4–Pd3–P3–S4 163.31(5).

The total valence number of TIDS ligands is –4 in *tri*-Pd-TIDS, and therefore the total oxidation number of palladium atoms should be +4. The solution of *tri*-Pd-TIDS was NMR active, but ESR inactive. It means there was no Pd(I) among the palladium atoms. By considering the conditions, the distribution of the oxidation number would be Pd(II)–Pd(0)–Pd(II). In this electronic structure, Pd(II) forms 16-electron configuration, and Pd(0) forms 18-electron configuration.

The light absorbing properties were evaluated by UV-vis-IR absorption measurements. The light absorption spectrum of *tri*-Pd-TIDS was amazingly red-shifted compared to free TIDS ligand and monometallic Pt-TIDS (Figure *3*). The spectrum involved two intense peaks at 922 nm and 1982 nm. The peak at 922 nm appeared at the similar wavelength to TIDS and Pt-TIDS with similar molar absorption coefficient (2.1×10^4 M^{-1} cm^{-1}), but the infrared absorption at 1982 nm indicated much larger molar absorption coefficient as 4.0×10^4 M^{-1} cm^{-1}, which is almost twice as much as those of TIDS and Pt-TIDS in visible region. The height of the infrared absorption peak is reasonably explained that *tri*-Pd-TIDS has two TIDS ligands to show light absorption with a double molar absorption coefficient.
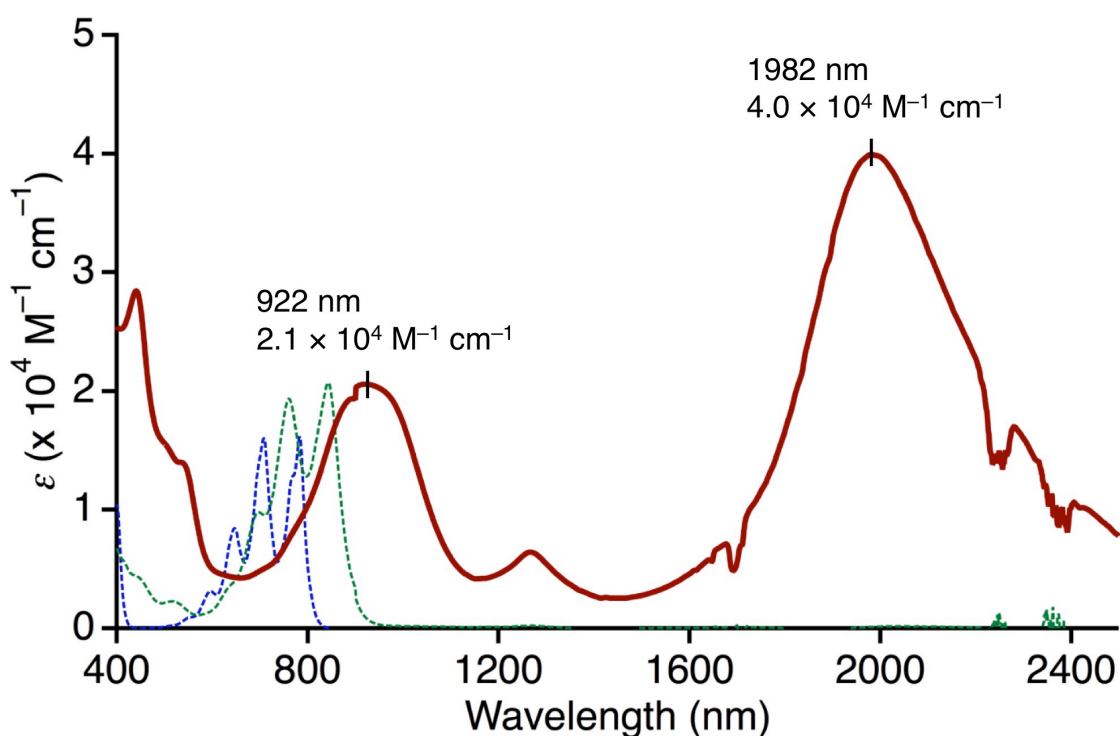
Figure 3. Light absorption spectra of TIDS (blue), Pt-TIDS (green) and *tri*-Pd-TIDS (red) in CH_2Cl_2.

The intense light absorption in infrared region was observed by solid state IR measurements (Figure **4**). The absorption peak appears at around 2500 nm, which is shifted in 500 nm compared to the solution state. The energy shift would be derived from solid-state intermolecular interaction. The energetic difference is calculated as 0.13 eV (13kJ/mol, 3.0 kcal/mol), which is near to the rotation barrier of ethane. Namely, the energetic shift between solution and solid states would be negligibly small.
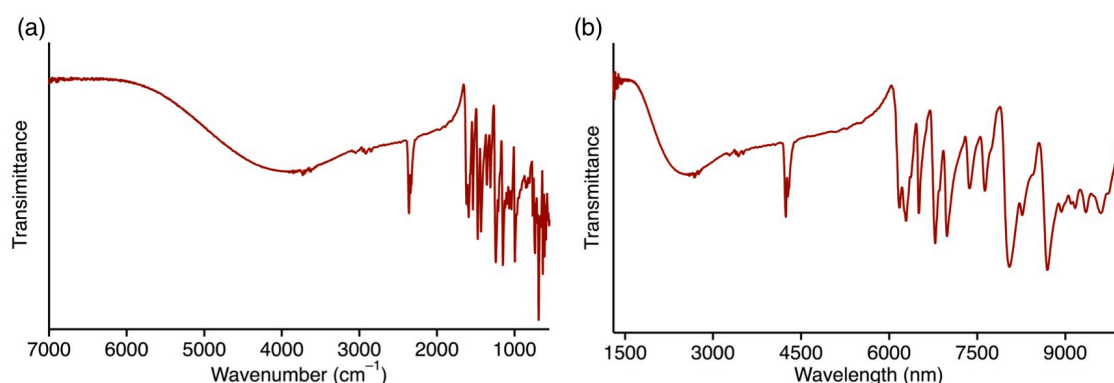
Figure 4. IR spectra of *tri*-Pd-TIDS in solid states. The spectra are plotted in (a) wavenumber, and in (b) wavelength.

The unique light absorption properties of *tri*-Pd-TIDS were deeply investigated by DFT calculations to determine the origin of the intense long wavelength absorption. The DFT calculations were carried out by using a methyl-substituted analogue of *tri*-Pd-TIDS (**3**) with bases of B3LYP/LANL2DZ/6-31G(d) and B3LYP/SDD/6-31G(d). Both of the bases gave the similar optimized structures as shown in Figure **5**. The comparison of bond lengths obtained by calculations and by crystal structure clearly denoted the similarity (Table **1**). The result of B3LYP/SDD/6-31G(d) exhibited slightly better accordance with the crystal data than B3LYP/LANL2DZ/6-31G(d). The differences between B3LYP/SDD/6-31G(d) and experimental data varies 2–3% except for Pd···Pd distances (*ca.* 7%), but B3LYP/LANL2DZ/6-31G(d) showed differences in 3–4% (Pd···Pd: *ca.* 7%). In both cases, all distances were estimated as longer than the experimental data.
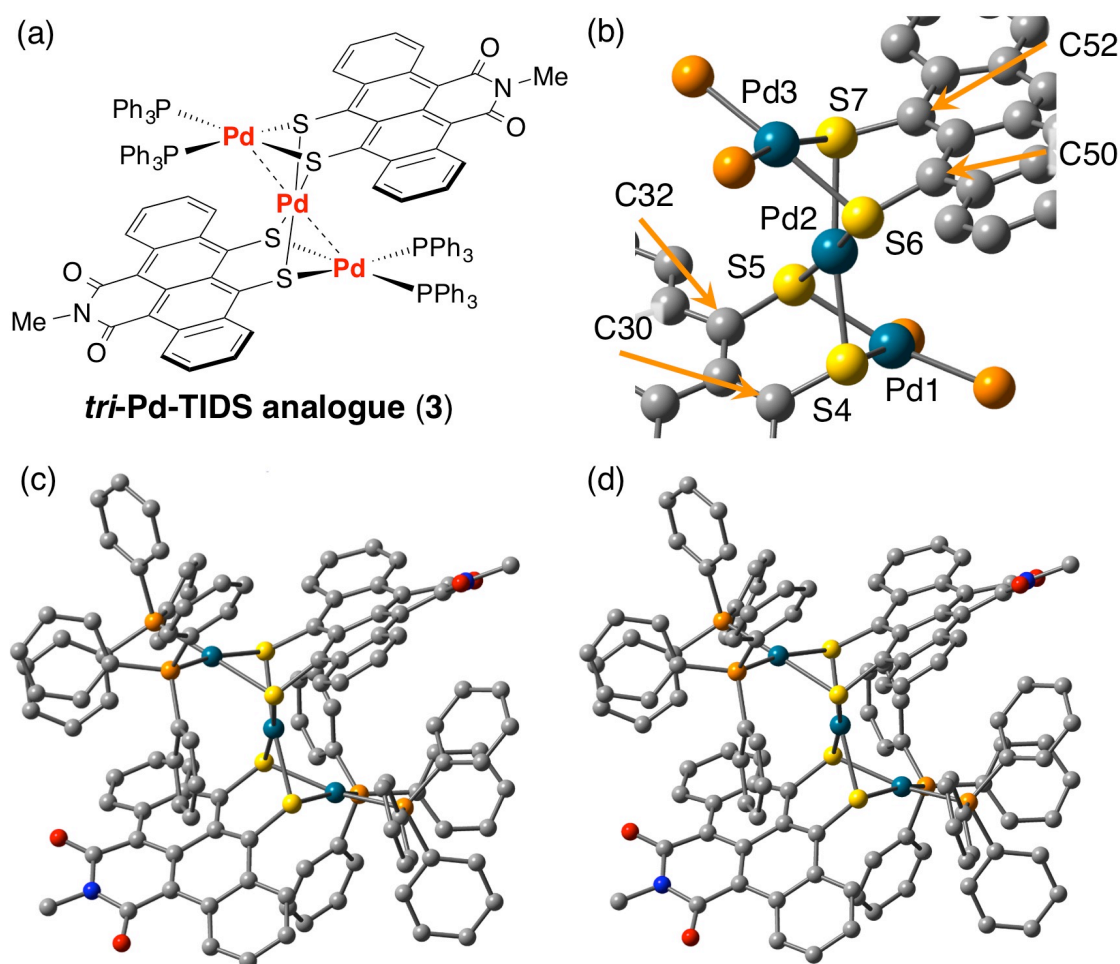
Figure 5. Optimized structure of *tri*-Pd-TIDS analogues (**3**). (a) The structure of model complex and (b) its atomic labels are shown. The calculation conditions were (c) B3LYP/LANL2DZ/6-31G(d) and (d) B3LYP/SDD/6-31G(d).

Table 1. Bond lengths of *tri*-Pd-TIDS analogues obtained by the calculations and the crystal structure.

	Crystal (**1**) (Å)	Calculation (**3**) (Å) [a]	Calculation (**3**) (Å) [b]	Difference (%) [a]	Difference (%) [b]
Pd···Pd	2.8828(5)	3.099	3.100	6.976	7.006
	2.9241(5)	3.150	3.157	7.171	7.377
Pd–P	2.335(2)	2.418	2.439	3.433	4.264
	2.365(1)	2.445	2.469	3.272	4.212
	2.342(1)	2.437	2.460	3.898	4.797
	2.320(2)	2.412	2.435	3.814	4.723
Pd–S	2.355(1)	2.429	2.437	3.047	3.365
	2.377(1)	2.423	2.447	1.898	2.861
	2.315(1)	2.396	2.418	3.381	4.260
	2.336(1)	2.402	2.424	2.748	3.630
	2.353(1)	2.396	2.426	1.795	3.009
	2.351(1)	2.402	2.430	2.123	3.251
	2.350(1)	2.400	2.415	2.083	2.692
	2.344(1)	2.419	2.433	3.100	3.658

[a] Calculated at B3LYP/LANL2DZ/6-31G(d) level.
[b] Calculated at B3LYP/SDD/6-31G(d) level.

By using time-dependent DFT calculations (TD-DFT), a simulation of light absorption assigned each light absorption band of *tri*-Pd-TIDS with molecular orbital transition. Both of the calculation bases depicted similar simulated light absorption bands (Figure **6**). The intense absorption at infrared region was attributed to HOMO–LUMO transition (table **2**). It was found that the absorption around 900 nm was composed of several transitions. The transitions are HOMO–2 –> LUMO, HOMO–1 –> LUMO, HOMO –> LUMO+1 and HOMO –> LUMO+2. The simulated absorption band at 765 nm is not seemed to be coincident with the experimental data. Light absorption should be described as energetic changes, which can be properly illustrated the absorption spectra plotted by wavenumber (Figure **6**c, d). The absorption at 900 nm constituted of four simulated bands is broader than the peak at infrared region. The simulated band of 765 nm would be composed in the peak at 900 nm to display the broadness.
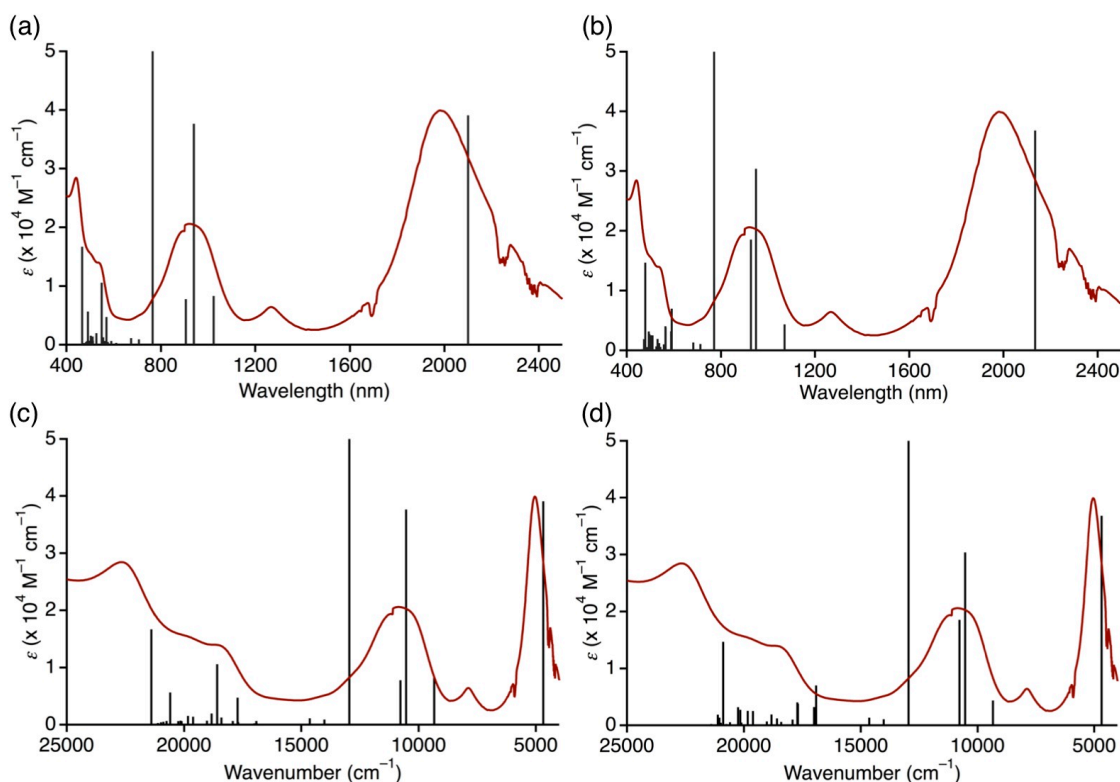
Figure 6. Simulated light absorption bands of *tri*-Pd-TIDS analogue (**3**) by TD-DFT. (a) B3LYP/SDD/6-31G(d) plotted by wavelength, (b) B3LYP/LANL2DZ/6-31G(d) plotted by wavelength, (c) B3LYP/SDD/6-31G(d) plotted by wavenumber and (d) B3LYP/LANL2DZ/6-31G(d) plotted by wavenumber.

Table 2. List of light absorption bands simulated by TD-DFT (B3LYP/SDD/6-31G(d)). The bands with coefficient lower than 0.3 are omitted.

Entry	Wavelength [nm]	Oscillator strength	Transition	The largest coefficient in the CI expansion
1	2099.43	0.1302	HOMO –> LUMO	0.74847
2	1024.05	0.0277	HOMO –> LUMO+1	0.53154
			HOMO –> LUMO+2	0.43898
3	939.57	0.1254	HOMO –> LUMO+1	–0.40969
			HOMO –> LUMO+2	0.45228
4	906.11	0.0259	HOMO–1 –> LUMO	0.60777
5	765.60	0.2014	HOMO–2 –> LUMO	0.67489
6	707.47	0.0030	HOMO –> LUMO+3	0.67517
7	674.27	0.0037	HOMO–3 –> LUMO	0.68077
8	610.78	0.0010	HOMO –> LUMO+4	0.62580
9	590.19	0.0021	HOMO –> LUMO+4	–0.31909
			HOMO –> LUMO+5	0.33865
			HOMO –> LUMO+6	0.39961
			HOMO –> LUMO+8	–0.31359
10	577.96	0.0007	HOMO–4 –> LUMO	0.67921

The DFT calculation also demonstrated the optimized structures of *tri*-Pd-TIDS analogues, **3**. The resulted HOMO and LUMO exhibited wholly delocalized structures (Figure *7*). The orbitals spread to both of TIDS ligand through the central palladium atom. An interesting feature of the orbitals was observed in the pattern of phases. In the LUMO, the orbital at the central palladium atom was absent to be a node of LUMO. The patterns of phase in TIDS ligand at the right side from the central palladium are the same in both of HOMO and LUMO, however the opposite side of TIDS ligand shows inversed phases between HOMO and LUMO. The characteristic resembles π–π* structures like organic aromatics. As is discussed above, the HOMO–LUMO transition contributes to the intense infrared absorption, and hence the entire delocalization should be a key to have extended π-conjugated system and long wavelength absorption for metal complexes. In the structure, TIDS ligands

coordinate in parallel that is identical to the crystal structure. The parallel arrangement would be helpful to effectively delocalize the orbitals to whole of the molecule.
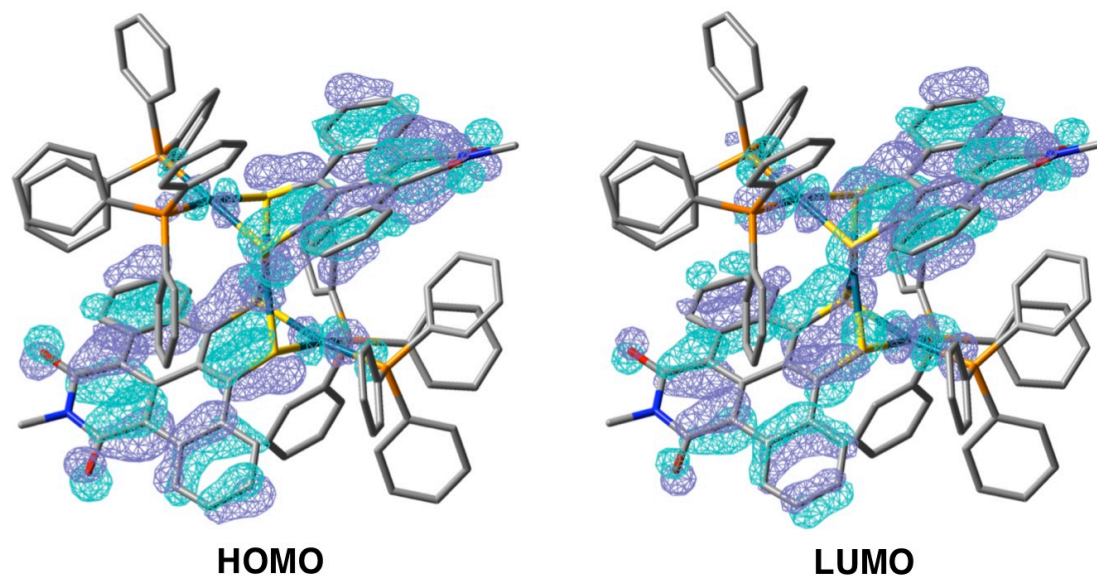
HOMO **LUMO**

Figure 7. HOMO and LUMO orbitals of **3**.

The orbitals energetically deeper than HOMO and shallower than LUMO were also calculated by the DFT (Figure **8**). Unlike HOMO and LUMO, LUMO+1 and LUMO+2 localize to the one sides, especially on the palladium atoms. In comparison, HOMO–1 and HOMO–2 possess delocalized orbitals including the central palladium like HOMO. According to the orbital structures, the electronic transitions corresponding to the light absorption at 900 nm contain LMCT (HOMO –> LUMO+1, LUMO+2).
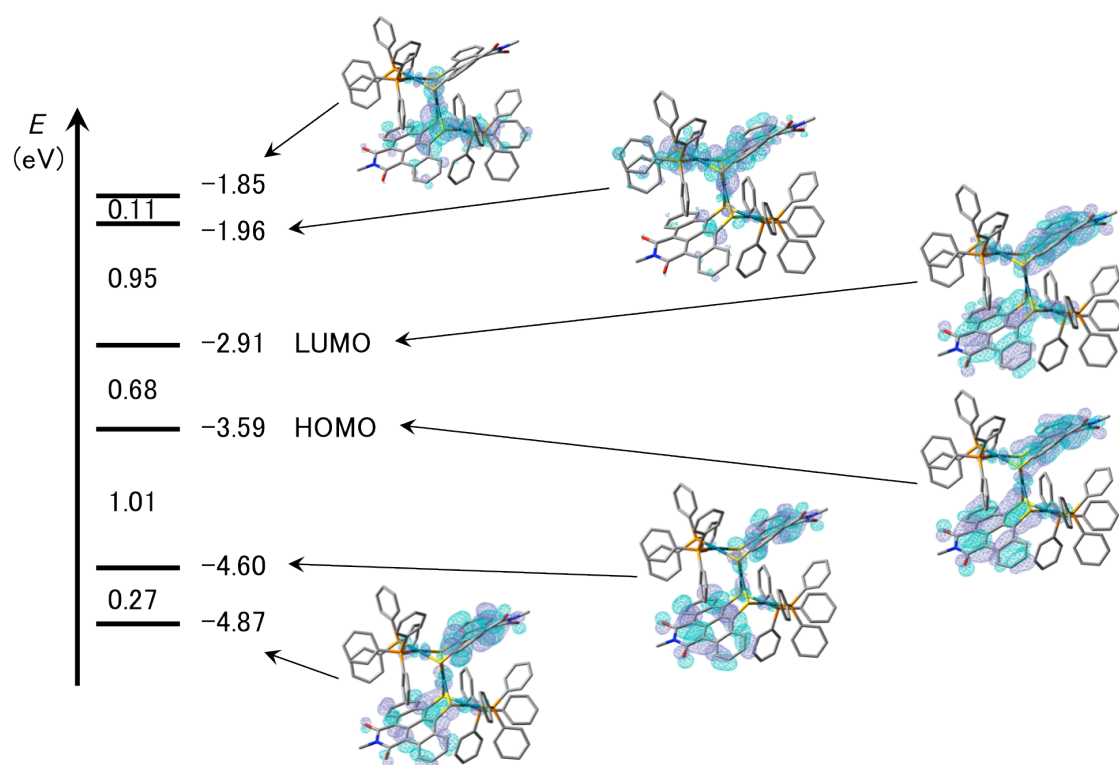
Figure 8. Molecular orbitals of **3** with energy levels.

The excited states are detectable by transient light absorption measurements. The measurement collected light absorption spectra some pico seconds after exciting a sample with a laser. The transient absorption spectra of *tri*-PdTIDS in UV-vis-NIR region were accumulated in THF by irradiating at 800 nm (Figure **9**). First, peaks at 480, 580 and 1080 nm were observed in less than 1 ps. The state readily transferred to the next state in 9 ps with an isosbestic point at around 1200 nm. The state has a peak at 1280 nm with a lifetime of 400 ps. The rate constant was calculated as 1.1×10^{11} s^{-1}. The prompt production and fast transition can be regarded as a singlet excitation state. Remarkably, the second state also has a short lifetime with a high rate constant (2.5×10^9 s^{-1}), which is seemed much shorter than typical triplet state. It would mean the triplet charge transferred (CT) state existed in the excited state. The transient measurements in toluene also demonstrated the similar results. The first excited state with peaks at 480, 580 and 1120 nm corresponded to transition into triplet CT state with a peak at 1300 nm through an isosbestic point at 1200 nm. The rate constant of each state was estimated as 1.2×10^{11} and 3.7×10^9 s^{-1}. The higher rate constant in toluene than THF would imply the stability of excited states depends on dipole of solvent. Notably, it was confirmed that the excited states formed CT structures, which were stabilized by dipole moments to show slower transition in THF.
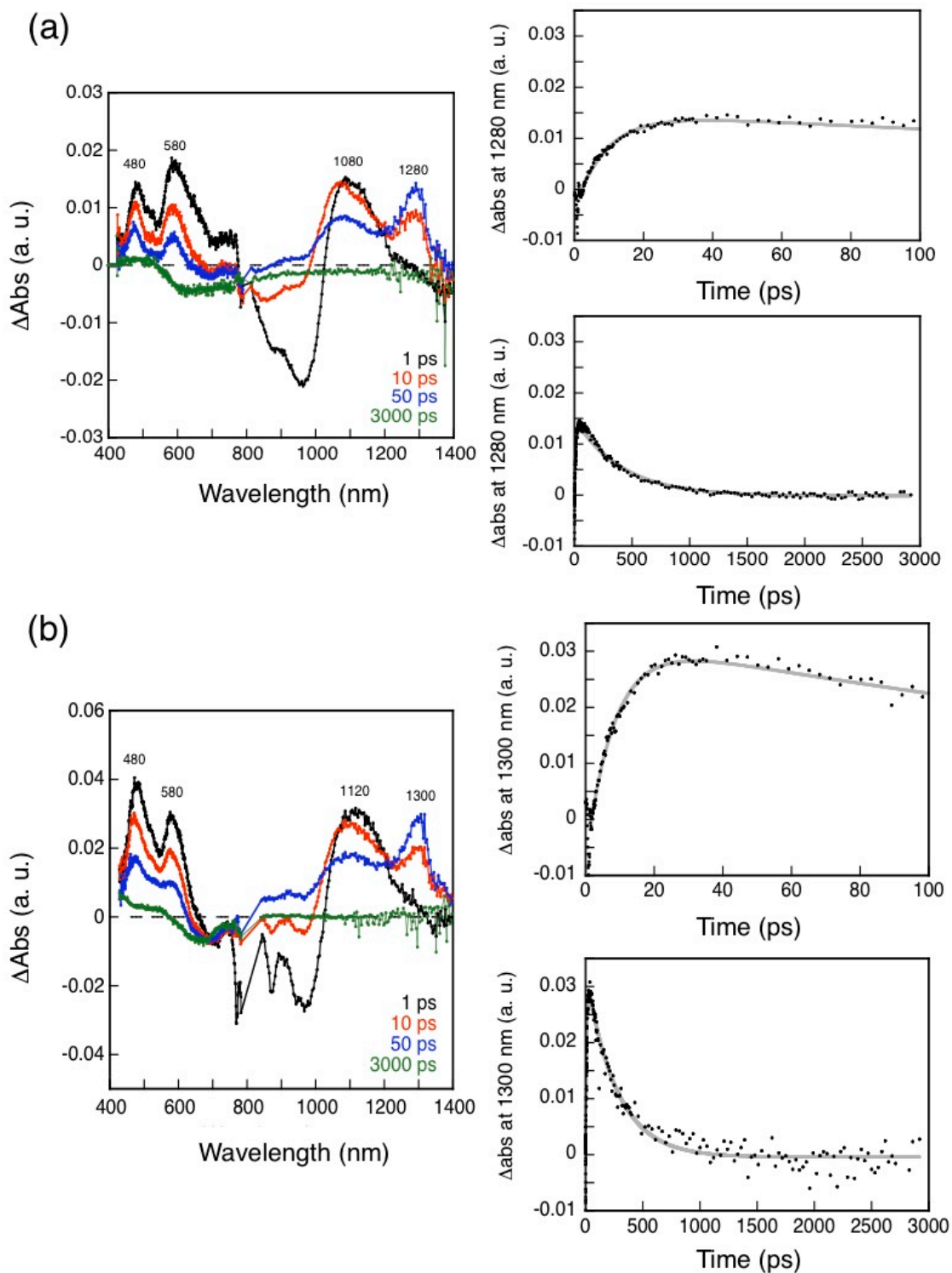
Figure 9. Transient light absorption spectra of *tri*-Pd-TIDS measured in (a) THF and (b) toluene excited at 800 nm.

44

The calculated molecular orbital structures were computationally generated by considering molecular orbital interactions of partial structures (Figure *10*). The phase structures of HOMO and LUMO in **3** were divided into the LUMO of mononuclear TIDS palladium complexes units. By interacting with d_{xy} orbital of one palladium atom with the LUMOs, the HOMO and LUMO of *tri*-Pd-TIDS were reproduced. The exceptionally narrow HOMO–LUMO gap was convinced here that the LUMO of *tri*-Pd-TIDS came from bonding interaction of LUMOs of monomers, but the HOMO of *tri*-Pd-TIDS was brought by the interaction between antibonding interaction of LUMOs of monomers and a palladium d_{xy} orbital. Though antibonding interaction normally has higher energy than bonding interaction, it got slightly lower energy than bonding interaction by interacting with d-orbital of palladium.
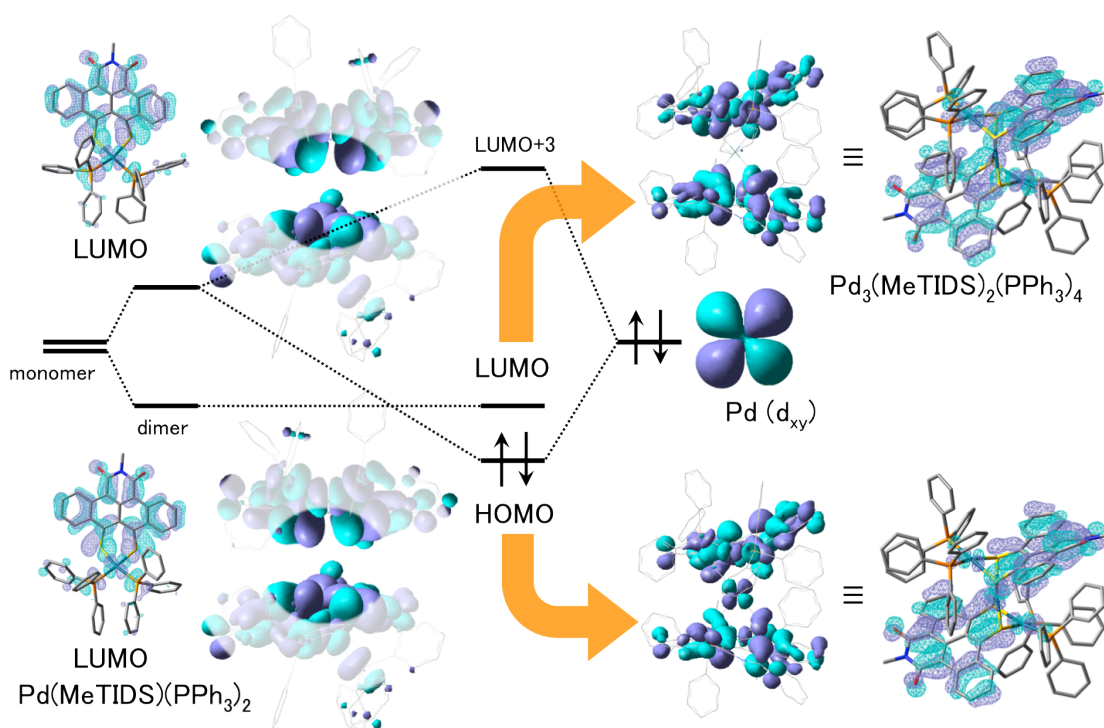
Figure 10. Molecular orbital interaction analysis of **3**. The orbitals were calculated by using B3LYP/SDD/6-31G(d).

The interactions around the palladium atoms were further investigated by calculating Wiberg bond index and natural bonding orbital (NBO) analysis. The Wiberg bond index of **3** is listed in Table *3*. Between carbon and sulfur atom, the values of Wiberg bond index were around 1.1, which reflected single bonds. The values at coordinative bonds were calculated as around 0.3–0.5. It should be noted that this analysis clearly indicated the weak interactions between palladium atoms. The Wiberg bond index showed 0.1325 and 0.1443 at Pd1···Pd2 and Pd2···Pd3, whereas the values at nonbonding positions were less than 0.05. The NBO analysis revealed the interaction

between the atoms more precisely (Table *4*). This analysis also suggested the existence of the clear interaction between the palladium atoms. Furthermore, it was found that the central palladium (Pd2) worked as an electron donor to peripheral atoms. The tendency supported the estimation of oxidation number distribution in the three palladium atoms as Pd(II)–Pd(0)–Pd(II).

Table 3. Wiberg bond index of **3** calculated at B3LYP/SDD/6-31G(d). The atomic labels are described in Figure *5*.

	Pd1	Pd2	Pd3	S4	S5	S6	S7	C30	C32	C50	C52
Pd1	–	**0.1443**	0.0119	**0.4958**	**0.4832**	0.0102	0.0141	0.0423	0.0325	0.0051	0.0070
Pd2	–	–	**0.1325**	**0.3597**	**0.3506**	**0.3406**	**0.3438**	0.0347	0.0359	0.0336	0.0347
Pd3	–	–	–	0.0097	0.0121	**0.4957**	**0.5078**	0.0038	0.0051	0.0286	0.0287
S4	–	–	–	–	0.1004	0.0304	0.1043	**1.1419**	0.0237	0.0064	0.0029
S5	–	–	–	–	–	0.1014	0.0299	0.0244	**1.1335**	0.0044	0.0079
S6	–	–	–	–	–	–	0.1017	0.0074	0.0029	**1.1192**	0.0229
S7	–	–	–	–	–	–	–	0.0039	0.0068	0.0207	**1.1169**
C30	–	–	–	–	–	–	–	–	0.0136	0.0042	0.0044
C32	–	–	–	–	–	–	–	–	–	0.0041	0.0042
C50	–	–	–	–	–	–	–	–	–	–	0.0129
C52	–	–	–	–	–	–	–	–	–	–	–

Table 4. NBO analysis of **3** with the second order perturbation theory analysis of Fock matrix in NBO basis. Stabilization energies derived from the interactions between electron-filled atoms (donor) and electron-empty atoms (acceptor) are listed in kcal/mol. The atomic labels are described in Figure **5**.

		Pd1	Pd2	Pd3	S4	S5	S6	S7	C30	C32	C50	C52
	Acceptor											
Donor	Pd1	–	**110.50**	30.19	23.19	14.05	5.71	6.06	7.38	7.45	0.82	0.71
	Pd2	155.59	–	598.48	118.04	97.92	**308.54**	**176.54**	**611.93**	78.47	**167.96**	**129.37**
	Pd3	28.29	**130.89**	–	4.67	5.20	16.50	16.46	1.52	0.56	7.27	7.15
	S4	16.59	**225.94**	4.79	–	0.96	0.62	1.34	1.29	<0.05	0.22	0.26
	S5	17.30	28.37	5.18	1.39	–	1.15	1.10	<0.05	1.50	0.29	0.18
	S6	5.71	**143.97**	17.93	1.49	1.25	–	1.29	0.30	0.19	1.49	<0.05
	S7	5.17	31.59	16.53	1.58	0.80	0.84	–	0.36	0.10	<0.05	1.43
	C30	<0.05	0.65	<0.05	<0.05	<0.05	<0.05	<0.05	–	<0.05	<0.05	<0.05
	C32	<0.05	0.95	<0.05	<0.05	<0.05	<0.05	<0.05	<0.05	–	<0.05	<0.05
	C50	<0.05	0.69	<0.05	<0.05	<0.05	<0.05	<0.05	<0.05	<0.05	–	<0.05
	C52	<0.05	0.97	<0.05	<0.05	<0.05	<0.05	<0.05	<0.05	<0.05	<0.05	–

[a] Calculations were performed at the B3LYP/SDD/6-31G(d) level. Donations to the own empty levels from themselves are omitted. The highest values among several interactions for each donor-acceptor combination are listed.

The mononuclear palladium TIDS complex, *mono*-Pd-TIDS, was evaluated by X-ray structural analysis and light absorption measurement. A variety of conditions to recrystallize *mono*-Pd-TIDS were tried but those attempts ended in decomposition of the complex. Accordingly, *mono*-Pd-TIDS was stabilized presumably by coordinating the free triphenylphosphine molecules in solution state. A single crystal of *mono*-Pd-TIDS acceptable to preliminary structural analysis was accidentally obtained throughout tremendous trials of recrystallizing *mono*-Pd-TIDS from CH_2Cl_2/hexane, (Figure **11**). The mononuclear structure in solid state was unambiguously determined. Similar to the other TIDS complexes, the structure contains a planar palladium coordination plane, which is tilted against tetracene moiety at 46°. The TIDS ligand and the palladium coordination plains formed envelope structure. The conformation probably evoked to form multi-nuclear cluster, that is *tri*-Pd-TIDS.
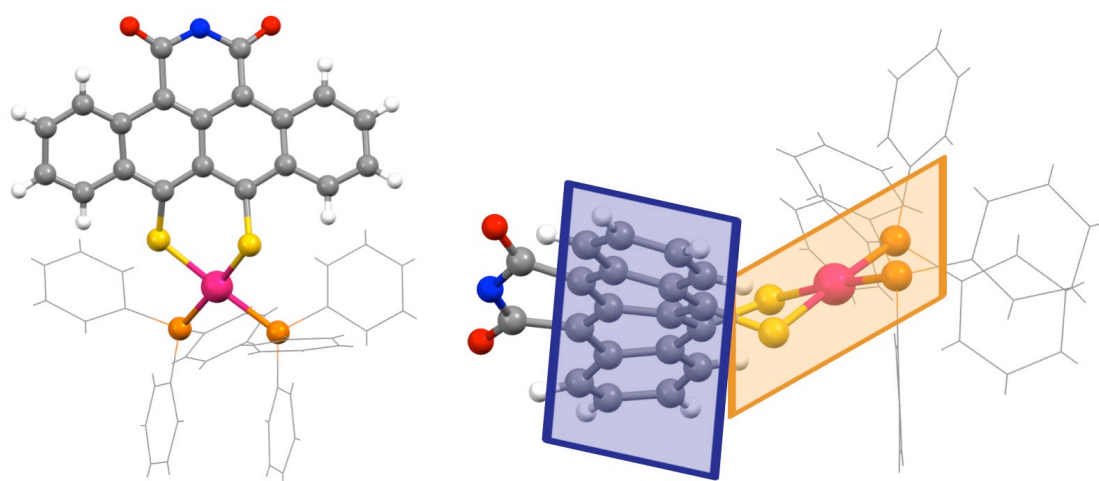
Figure 11. Crystal structure of *mono*-Pd-TIDS.

The light absorption spectrum of *mono*-Pd-TIDS exhibited slightly longer wavelength absorption compared to TIDS ligand (Figure ***12***). The shape of the spectrum was quite similar to that of Pt-TIDS, including vibrational structures. The precise similarity represented the similar structure between *mono*-Pd-TIDS and Pt-TIDS, strongly supporting the mononuclear structure.
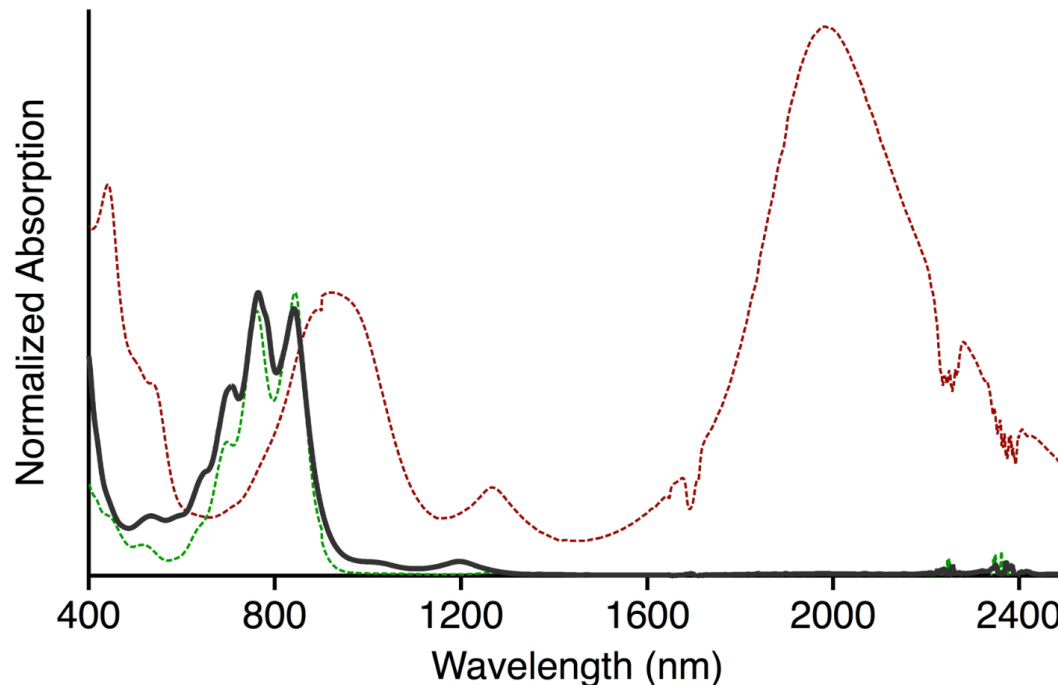
Figure 12. Light absorption spectra of *mono*-Pd-TIDS (black), Pt-TIDS (green), and *tri*-Pd-TIDS (red). The spectra were normalized with the highest peaks around 700–900 nm.

3.3. Summary

The palladium TIDS complexes were successfully obtained as trinuclear and mononuclear structures. The trinuclear palladium TIDS complex showed intense infrared absorption at 1982 nm (4.0 $\times 10^4$ M^{-1} cm^{-1}). The origin of the exceptionally long wavelength absorption was deeply investigated by crystal structural analysis and DFT calculations. The crystal structure depicted parallel ligation of TIDS ligands to effectively conjugate π-orbitals of TIDS through the central palladium atom. The structural similarity between Pt–Ag–Pt complex and the trinuclear palladium TIDS implies the acene disulfide ligand has a potential to form the trimetallic coordination structure. The donor–acceptor structure of TIDS ligand would play an important role to construct wholly π-conjugated system with infrared light absorption. DFT calculations demonstrated that the infrared absorption was assigned as HOMO–LUMO transition. Additionally, the HOMO and LUMO have fully delocalized π-orbitals. Moreover, the absorption around 900 nm was attributed as LMCT by the DFT calculations. It was confirmed by transient absorption measurements, which also gave the lifetime of the excited states. NBO analysis further investigated electronic interactions between the atoms to denote the donative properties of the central palladium atom. This work established the way to elongate light absorption wavelength by extending π-conjugated system with coordinating metal atoms. The important feature is parallel ligation to realize wholly π-delocalization. The achievements would contribute to develop designing new light absorbing materials.

3.4. Experimental Section

General. All NMR spectra were taken at 500 MHz (JEOL ECA-500 spectrometer). NMR spectra were recorded in parts per million (ppm, δ scale) from residual protons of the CD_2Cl_2 for ^1H NMR (δ 5.32 ppm for dichloromethane) and from an external standard for ^{31}P NMR (δ 29.41 ppm of $OPPh_3$ for all solvents). The CD_2Cl_2 was distillated with CaH_2 prior to use and stored under argon with molecular sieves (4 Å). The data were presented as following space: chemical shift, multiplicity (s = singlet, d = doublet, t = triplet, m = multiplet and/or multiplet resonances, br = broad), coupling constant in hertz (Hz), and signal area integration in natural numbers, assignment (italic). Elemental analysis was performed at the University of Tokyo, Department of Chemistry, Organic Elemental Analysis Laboratory. IR absorption was measured on JASCO FT/IR-6100 equipped with an attenuated total reflection (ATR) with ZnSe, and was reported as wavenumber in cm^{-1}.

Synthesis of (Tetraceneimide dithiole)bis(triphenylphosphine)palladium (Pd(TIDS)(PPh₃)₂, *mono*-Pd-TIDS). $Pd(PPh_3)_4$ (127 mg, 0.110 mmol, 1.1 equiv.) in CH_2Cl_2 (6.5 ml) was added dropwise to a solution of TIDS (44.5 mg, 0.100 mmol) in CH_2Cl_2 (20 ml) for 25 min. The appearance of the solution changed from blue

suspension to black solution. It was stirred at room temperature for 1 h. This solution was used for each analysis. ^{1}H NMR (500 MHz, CD$_2$Cl$_2$): δ = 9.81 (d, J = 9.2 Hz, 2H, tetracene), 8.45 (d, J = 9.2 Hz, 2H, tetracene), 7.57–7.54 (m, 2H, tetracene), 7.43 (t, J = 7.5 Hz, 6H, p-Ph), 7.27-7.24 (m, 12H, o-Ph, m-Ph), 7.12–7.08 (m, 2H, tetracene), 4.28 (t, J = 7.7 Hz, 2H, CH$_2$ in hexyl), 1.80–1.74 (m, 2H, CH$_2$CH$_2$ in hexyl), 1.48–1.44 (m, 2H, CH$_2$ in hexyl), 1.40–1.31 (m, 4H, CH$_2$CH$_2$ in hexyl), 0.90 (t, J = 7.2 Hz, 3H, Me in hexyl). ^{31}P NMR (202.4 MHz, CD$_2$Cl$_2$): δ = 27.66 (s, 2P, PPh$_3$).

Synthesis of μ-Bis(tetraceneimide dithiole)-tetrakis(triphenylphosphine)tripalladium (Pd$_3$(TIDS)$_2$(PPh$_3$)$_4$, *tri*-Pd-TIDS). A mixture of TIDS (100 mg, 0.225 mmol) and Pd(PPh$_3$)$_4$ (391 mg, 0.338 mmol, 1.50 equiv.) was stirred in THF (6.6 ml) at room temperature for 3 h. The n-hexane was added to precipitate the crude product, which was purified by crystallization from CH$_2$Cl$_2$/n-hexane to give dark-red crystals in 77% yield (196 mg, 0.0869 mmol). ^{1}H NMR (400 MHz, CD$_2$Cl$_2$): δ = 9.37 (br, tetracene), 7.41 (br, tetracene), 6.99 (t, J = 7.3 Hz, 4H, p-Ph), 6.81–6.73 (m, 16H, o-Ph, m-Ph), 6.11 (br, tetracene), 4.26 (t, J = 6.9 Hz, 4H, CH$_2$ in hexyl), 1.99–1.92 (m, 4H, CH$_2$ in hexyl), 1.62–1.54 (m, 4H, CH$_2$ in hexyl), 1.38–1.51 (m, 8H, CH$_2$CH$_2$ in hexyl), 0.95 (t, J = 7.1 Hz, 6H, Me in hexyl). Anal. calcd for C$_{124}$H$_{102}$N$_2$O$_4$P$_4$Pd$_3$S$_4$: C, 66.03; H, 4.56; N, 1.24. Found: C, 66.13; H, 4.71; N, 1.14.

^{1}H NMR peaks corresponding to the tetracene moiety were broadened at room temperature. This results from thermal dynamic behavior. For the same reason, neither ^{31}P nor ^{13}C NMR were clearly recorded. Low temperature ^{1}H NMR measurements, even at −30 ºC, exhibited broad peaks.

Electrochemical analysis. Cyclic voltammetry (CV) and differential pulse voltammetry (DPV) were performed using HOKUTO DENKO HZ-5000 voltammetric analyzer. All CV measurements were carried out in a one-compartment cell under argon gas, equipped with a glassy-carbon working electrode, a platinum wire counter electrode, and an Ag/Ag$^+$ reference electrode. The supporting electrolyte was a 0.1 mol/L dichloromethane solution of tetrabutylammonium hexafluorophosphate (TBAPF$_6$). Only for the CV measurements of tri-palladium complex **1**, platinum and gold working electrode were additionally used to result in the identical CV charts to that obtained with glassy-carbon electrode. The electrochemical data equipped with a grassy-carbon working electrode are presented in this report.

X-ray crystallographic analysis. X-ray crystallographic analyses for complexes **1** and **2** were performed using a RIGAKU R-AXIS RAPID II (imaging plate detector) with monochromic CuKα (λ = 1.5406 Å) radiation. The positional and thermal parameters were refined by a full-matrix least-squares method using the SHELXL97 program on the Yadokari-software. The CCDC numbers of complexes **1** and **2** were

881159 and 978047, respectively.

Computational studies. All calculations were carried out by Gaussian09 package at the B3LYP level.[15] Palladium atoms were represented by the LANL2DZ or SDD basis set and a 6-31G(d) basis set was used for other atoms (C, H, N, O, S, and P). The calculation levels are described as " B3LYP/LANL2DZ/6-31G(d)" and "B3LYP/SDD/6-31G(d)".

Time-resolved transient absorption mesurements. Femtosecond transient absorption spectroscopy experiments were conducted using an ultrafast Integra-C (Quantronix Corp.), a TOPAS optical parametric amplifier (Light Conversion Ltd.), and a commercially available Helios optical detection system provided by Ultrafast Systems LLC.

Crystal Data Collection Parameters for *tri*-Pd-TIDS.

Formula	$C_{127}H_{108}Cl_6N_2O_4P_4Pd_3S_4$
Formula Weight	2510.17
Crystal System	triclinic
Space Group	$P\bar{1}$
R, R_w ($I > 2\sigma(I)$)	0.0663, 0.2286
$R1$, $wR2$ (all data)	0.0705, 0.2344
GOF on F^2	1.578
a (Å)	17.4188(6)
b (Å)	17.5604(6)
c (Å)	22.7255(4)
α (º)	87.6505(10)
β (º)	71.9113(12)
γ (º)	60.5328(7)
V (Å^3)	5700.3(3)
Z	2
T (K)	173(2)
Crystal Size (mm)	0.60, 0.50, 0.30
D_{calcd} (g·cm^{-3})	1.462
$2\theta_{min}$, $2\theta_{max}$ (º)	2.99, 67.00
no. refl. measured (unique)	19978
no. refl. measured ($I > 2\sigma(I)$)	18233
no. parameters	1327
μ (CuKα)	1.54187

Crystal Data Collection Parameters for *mono*-Pd-TIDS.

Formula	$C_{64}H_{51}Cl_4NO_2P_2PdS_2$
Formula Weight	1240.32
Crystal System	triclinic
Space Group	$P\bar{1}$
R, R_w ($I>2\sigma(I)$)	0.1559, 0.3862
$R1$, $wR2$ (all data)	0.1824, 0.4098
GOF on F^2	1.760
a (Å)	13.8975(3)
b (Å)	16.8234(3)
c (Å)	17.2132(4)
α (º)	99.9912(11)
β (º)	112.2384(11)
γ (º)	111.2751(10)
V (Å^3)	3238.05(12)
Z	2
T (K)	123(2)
Crystal Size (mm)	0.12, 0.22, 0.27
D_{calcd} (g·cm^{-3})	1.272
$2\theta_{min}$, $2\theta_{max}$ (º)	2.97, 67.00
no. refl. measured (unique)	10324
no. refl. measured ($I>2\sigma(I)$)	5864
no. parameters	664
μ (CuKα)	1.54187

3 calculated at B3LYP/LANL2DZ/6-31G(d)

213

Pd	-2.985985	-0.829221	-0.040173
Pd	0.000935	0.001384	-0.060455
Pd	3.006306	0.917540	0.250253
S	-1.277371	-1.174067	-1.743471
S	-1.117206	-1.662225	1.301905
S	1.343195	1.494528	-1.429859
S	1.070153	1.396716	1.610958
P	-4.535798	-1.234824	1.838694
P	-4.391441	0.469053	-1.552008
P	4.651155	0.553010	-1.542500
P	4.347945	0.202342	2.152036
O	3.094612	-6.821868	0.423455
O	1.130778	-7.174636	-3.635966
O	-0.905941	7.964982	-2.012950
O	-2.999183	6.743369	1.800820
C	-0.162516	-3.742062	3.178266
C	0.387106	-4.505100	4.183738
C	1.260406	-5.564625	3.858321
C	1.544884	-5.851887	2.542931
C	0.970401	-5.101808	1.470886
C	1.150364	-5.453600	0.093935
C	0.355471	-4.850471	-0.918258
C	0.296352	-5.413393	-2.224765
C	-0.589865	-4.854331	-3.208992
C	-0.900158	-5.496104	-4.445961
C	-1.740939	-4.917775	-5.371380
C	-2.326795	-3.660829	-5.120777
C	-2.054356	-3.011950	-3.938450
C	-1.194226	-3.575881	-2.952160
C	-0.935731	-2.895293	-1.706665
C	-0.365940	-3.611307	-0.609317
C	-0.420395	-3.175237	0.745850
C	0.115604	-3.999069	1.804183
C	2.150411	-6.448283	-0.291111
C	1.132265	-6.575847	-2.554792
C	0.255553	3.146899	3.819398
C	-0.251340	3.715663	4.964501

C	-1.121989	4.823021	4.869558
C	-1.439074	5.349161	3.640319
C	-0.905853	4.806114	2.428598
C	-1.109768	5.413806	1.153580
C	-0.387495	4.970228	0.011060
C	-0.367331	5.763185	-1.170635
C	0.275556	5.291826	-2.358963
C	0.365717	6.066924	-3.558296
C	0.930054	5.565702	-4.707134
C	1.453571	4.255966	-4.730571
C	1.397855	3.483287	-3.594832
C	0.820021	3.960179	-2.377193
C	0.793732	3.150047	-1.184406
C	0.306237	3.675707	0.052996
C	0.418976	3.014995	1.316948
C	-0.061337	3.648340	2.521112
C	-2.072004	6.513155	1.012276
C	-1.022086	7.083725	-1.155491
C	-5.057393	-3.004697	1.765871
C	-4.297803	-3.902669	0.998690
C	-4.639530	-5.255283	0.941852
C	-5.747853	-5.727810	1.646120
C	-6.513976	-4.843022	2.408594
C	-6.173277	-3.491175	2.469503
C	-6.127819	-0.323547	2.086462
C	-6.228874	0.722783	3.017968
C	-7.422561	1.430335	3.165985
C	-8.535872	1.102333	2.391596
C	-8.445779	0.065010	1.461755
C	-7.251527	-0.638691	1.303505
C	-3.708336	-1.040769	3.478554
C	-2.859733	0.061356	3.672151
C	-2.254359	0.285431	4.909241
C	-2.475486	-0.602751	5.963830
C	-3.301967	-1.712093	5.776418
C	-3.917907	-1.930181	4.542514
C	-4.754672	2.176162	-0.971419
C	-4.351461	2.564531	0.314550
C	-4.530080	3.879187	0.750170
C	-5.125759	4.817695	-0.093074
C	-5.533232	4.442407	-1.376230

C	-5.337285	3.135144	-1.820160
C	-3.700336	0.790636	-3.233499
C	-2.557278	1.602271	-3.335326
C	-1.992562	1.877103	-4.579707
C	-2.556143	1.337370	-5.738909
C	-3.686059	0.524930	-5.647375
C	-4.257434	0.250400	-4.401758
C	-5.992530	-0.371035	-1.911801
C	-5.960463	-1.768073	-2.066079
C	-7.122665	-2.475607	-2.376876
C	-8.334828	-1.796826	-2.526466
C	-8.377071	-0.410386	-2.365566
C	-7.214184	0.300268	-2.059784
C	6.262159	-0.328069	-1.302234
C	6.433651	-1.667829	-1.680786
C	7.660235	-2.306700	-1.489280
C	8.731929	-1.619622	-0.919161
C	8.569094	-0.288049	-0.530894
C	7.344389	0.352196	-0.716321
C	5.199846	2.153202	-2.279345
C	4.551481	3.343817	-1.918009
C	4.951134	4.566141	-2.463980
C	6.004147	4.612943	-3.377095
C	6.660667	3.434158	-3.742156
C	6.265579	2.213252	-3.196403
C	3.832947	-0.394405	-2.892621
C	3.914884	-0.034334	-4.245490
C	3.281259	-0.810670	-5.218321
C	2.568227	-1.954182	-4.854913
C	2.477881	-2.317986	-3.509571
C	3.096542	-1.536330	-2.533551
C	3.481846	0.084447	3.784791
C	2.858654	-1.100709	4.204100
C	2.189732	-1.154190	5.428293
C	2.134135	-0.029331	6.251730
C	2.740020	1.158693	5.837115
C	3.399320	1.219754	4.609056
C	5.725866	1.360714	2.544528
C	6.562668	1.183118	3.661588
C	7.570351	2.104895	3.943997
C	7.745936	3.227303	3.129476

C	6.903999	3.428918	2.035807
C	5.899772	2.500957	1.746940
C	5.057485	-1.481151	1.913847
C	4.193893	-2.485588	1.437187
C	4.635238	-3.804324	1.311056
C	5.956039	-4.126517	1.630610
C	6.829967	-3.131206	2.068260
C	6.385892	-1.815686	2.213538
H	-0.838063	-2.936300	3.437111
H	0.129273	-4.301460	5.220068
H	1.697544	-6.172859	4.646326
H	2.206644	-6.667922	2.295246
H	-0.453283	-6.457219	-4.643988
H	-1.960264	-5.446652	-6.295788
H	-3.000780	-3.209007	-5.843707
H	-2.517630	-2.052556	-3.745150
H	0.928237	2.304930	3.907862
H	0.035645	3.320678	5.935908
H	-1.527396	5.278543	5.769560
H	-2.093994	6.203876	3.570192
H	-0.029557	7.069804	-3.539529
H	0.974669	6.188135	-5.597414
H	1.912725	3.859742	-5.632504
H	1.814075	2.485204	-3.622865
H	-3.434335	-3.544150	0.446172
H	-4.037265	-5.934893	0.345618
H	-6.015431	-6.779998	1.600082
H	-7.379955	-5.203737	2.957336
H	-6.783887	-2.813468	3.058045
H	-5.380519	0.981837	3.642105
H	-7.480166	2.234775	3.894139
H	-9.466513	1.650275	2.511855
H	-9.304387	-0.199857	0.851160
H	-7.203679	-1.441859	0.575798
H	-2.654376	0.742506	2.850513
H	-1.603493	1.145274	5.034831
H	-1.999592	-0.434230	6.926289
H	-3.471266	-2.411781	6.590704
H	-4.555321	-2.798004	4.411296
H	-3.865745	1.840564	0.961360
H	-4.176886	4.187625	1.728866

H	-5.237098	5.842829	0.246685
H	-5.980696	5.174453	-2.043317
H	-5.609993	2.868640	-2.837278
H	-2.107276	2.028081	-2.442517
H	-1.110821	2.508233	-4.638639
H	-2.114460	1.550274	-6.708659
H	-4.133124	0.106044	-6.545251
H	-5.142510	-0.374841	-4.348274
H	-5.022903	-2.303218	-1.938378
H	-7.080087	-3.554890	-2.493945
H	-9.241537	-2.346457	-2.764586
H	-9.317618	0.122927	-2.476249
H	-7.265345	1.374960	-1.922971
H	5.617008	-2.215263	-2.137809
H	7.774440	-3.343349	-1.793486
H	9.687925	-2.116996	-0.778961
H	9.397066	0.258231	-0.086776
H	7.241330	1.390106	-0.418018
H	3.724810	3.315704	-1.215662
H	4.429191	5.475321	-2.180343
H	6.313836	5.563097	-3.803761
H	7.483980	3.464663	-4.450823
H	6.794258	1.307172	-3.476380
H	4.464677	0.851868	-4.544255
H	3.346997	-0.517891	-6.262900
H	2.075642	-2.557448	-5.612004
H	1.917163	-3.200780	-3.219020
H	2.999461	-1.813066	-1.487298
H	2.898030	-1.994559	3.592007
H	1.715959	-2.083690	5.729418
H	1.622641	-0.076551	7.209468
H	2.701014	2.043467	6.467093
H	3.861019	2.152801	4.302005
H	6.414928	0.335096	4.323217
H	8.211803	1.952447	4.807737
H	8.527081	3.947594	3.356962
H	7.019844	4.308316	1.408351
H	5.236817	2.667536	0.903172
H	3.167087	-2.241217	1.174360
H	3.959639	-4.585495	0.975876
H	6.296955	-5.153182	1.530544

H	7.863411	-3.373961	2.301381
H	7.082822	-1.055174	2.545756
C	-2.687585	8.568793	-0.192736
H	-2.018750	9.427898	-0.279681
H	-3.318450	8.542046	-1.086028
H	-3.300187	8.638141	0.702996
C	3.007453	-8.039681	-1.905472
H	4.020517	-7.626752	-1.924787
H	2.978290	-8.823403	-1.145240
H	2.737382	-8.432283	-2.882401
N	-1.897710	7.339539	-0.095807
N	2.042113	-6.991351	-1.566971

3 calculated at B3LYP/SDD/6-31G(d)

213

Pd	-2.992791	-0.797457	-0.040775
Pd	-0.000184	0.006844	-0.064979
Pd	3.010271	0.879699	0.248801
S	-1.289891	-1.134059	-1.731524
S	-1.134476	-1.619857	1.289841
S	1.357324	1.468206	-1.416238
S	1.086759	1.357325	1.602493
P	-4.527856	-1.205195	1.817729
P	-4.378520	0.503917	-1.534595
P	4.626277	0.519854	-1.538961
P	4.338571	0.150242	2.125712
O	2.990314	-6.856427	0.444266
O	1.036724	-7.182170	-3.622593
O	-0.776229	7.982754	-1.971571
O	-2.898554	6.773514	1.831212
C	-0.222928	-3.712856	3.179746
C	0.308851	-4.483619	4.189440
C	1.164663	-5.558852	3.869931
C	1.450168	-5.853429	2.555885
C	0.893793	-5.095754	1.480155
C	1.073196	-5.453072	0.103803
C	0.293567	-4.838177	-0.913467
C	0.231291	-5.400197	-2.220056
C	-0.633688	-4.821089	-3.212635
C	-0.942840	-5.454105	-4.454124
C	-1.757047	-4.855302	-5.390847
C	-2.315675	-3.585063	-5.146614
C	-2.045904	-2.945120	-3.958192
C	-1.213964	-3.530472	-2.960464
C	-0.960018	-2.860553	-1.708347
C	-0.408424	-3.586665	-0.609304
C	-0.461550	-3.149259	0.744924
C	0.056803	-3.977710	1.807822
C	2.056012	-6.466588	-0.274997
C	1.045124	-6.580006	-2.543134
C	0.276878	3.095798	3.829520
C	-0.223106	3.664652	4.978163

60

C	-1.068148	4.791979	4.890160
C	-1.368576	5.336046	3.664073
C	-0.842468	4.792744	2.449817
C	-1.031359	5.415299	1.178917
C	-0.316252	4.967016	0.033892
C	-0.281548	5.765483	-1.143696
C	0.347958	5.286554	-2.336927
C	0.448690	6.064399	-3.533187
C	0.996102	5.555670	-4.687435
C	1.490068	4.234817	-4.719024
C	1.424703	3.459100	-3.585364
C	0.865551	3.944293	-2.362741
C	0.831143	3.133176	-1.171465
C	0.355021	3.660804	0.068425
C	0.455616	2.989581	1.327167
C	-0.021363	3.617374	2.535141
C	-1.973346	6.532370	1.043269
C	-0.910201	7.098074	-1.120083
C	-5.065110	-2.970702	1.734719
C	-4.322440	-3.871395	0.954176
C	-4.679765	-5.219935	0.889935
C	-5.786401	-5.685674	1.601037
C	-6.535322	-4.798284	2.377825
C	-6.179394	-3.450805	2.445444
C	-6.116059	-0.284356	2.063487
C	-6.210196	0.768232	2.988659
C	-7.400565	1.481303	3.136363
C	-8.517943	1.152605	2.367993
C	-8.435315	0.108335	1.445438
C	-7.244163	-0.600894	1.287598
C	-3.710879	-1.026585	3.465709
C	-2.877698	0.083200	3.682279
C	-2.282563	0.295500	4.926341
C	-2.496649	-0.612938	5.965160
C	-3.306218	-1.730378	5.754427
C	-3.913105	-1.936108	4.513744
C	-4.724988	2.211975	-0.943703
C	-4.295954	2.598467	0.334579
C	-4.454387	3.915269	0.772268
C	-5.056138	4.858552	-0.061117
C	-5.489487	4.485537	-1.336680

C	-5.313226	3.176239	-1.782758
C	-3.681132	0.835975	-3.212904
C	-2.548129	1.662285	-3.308804
C	-1.976679	1.939991	-4.549587
C	-2.524339	1.389973	-5.711511
C	-3.645242	0.564410	-5.626101
C	-4.222528	0.286249	-4.384037
C	-5.986440	-0.317464	-1.911146
C	-5.965444	-1.711326	-2.094533
C	-7.133006	-2.403416	-2.420304
C	-8.339557	-1.712275	-2.557396
C	-8.370802	-0.329096	-2.367940
C	-7.202830	0.365853	-2.045975
C	6.236116	-0.369310	-1.312836
C	6.405254	-1.704612	-1.707477
C	7.632869	-2.345758	-1.529981
C	8.707864	-1.665482	-0.957863
C	8.547855	-0.337976	-0.554785
C	7.322428	0.304685	-0.727211
C	5.184754	2.120178	-2.269556
C	4.564914	3.319035	-1.886171
C	4.980073	4.539519	-2.425052
C	6.019159	4.576171	-3.354331
C	6.646314	3.388803	-3.742715
C	6.236768	2.170129	-3.202950
C	3.797882	-0.415523	-2.892364
C	3.850296	-0.029445	-4.239282
C	3.204342	-0.793036	-5.214517
C	2.507738	-1.949304	-4.859535
C	2.446149	-2.338753	-3.519673
C	3.077679	-1.570488	-2.541231
C	3.484100	0.031825	3.765959
C	2.875700	-1.155906	4.199188
C	2.224342	-1.208670	5.433155
C	2.171240	-0.080238	6.251845
C	2.762487	1.110354	5.823455
C	3.404923	1.170168	4.586560
C	5.726603	1.295638	2.525371
C	6.570727	1.091557	3.632291
C	7.584131	2.002982	3.926997
C	7.758067	3.142510	3.136003

C	6.908429	3.371023	2.053814
C	5.898994	2.452678	1.752074
C	5.035469	-1.538854	1.881614
C	4.159234	-2.541253	1.423572
C	4.591554	-3.862963	1.295696
C	5.915899	-4.190502	1.594444
C	6.802045	-3.197581	2.012499
C	6.367090	-1.879216	2.159957
H	-0.885476	-2.895007	3.434117
H	0.050021	-4.272867	5.224095
H	1.587426	-6.173424	4.660871
H	2.098868	-6.681248	2.312634
H	-0.515377	-6.424942	-4.647578
H	-1.975346	-5.377691	-6.319159
H	-2.966485	-3.114958	-5.879147
H	-2.488553	-1.975067	-3.770394
H	0.929173	2.237462	3.912247
H	0.049681	3.253326	5.946912
H	-1.467280	5.248147	5.792626
H	-2.005253	6.204906	3.599047
H	0.074974	7.075467	-3.508239
H	1.049417	6.180589	-5.575481
H	1.933505	3.831550	-5.625742
H	1.817993	2.451887	-3.619530
H	-3.461086	-3.518976	0.394501
H	-4.090729	-5.901099	0.282375
H	-6.066025	-6.734446	1.549562
H	-7.399852	-5.153679	2.932270
H	-6.776472	-2.771253	3.045597
H	-5.359341	1.027676	3.609070
H	-7.452480	2.290391	3.859780
H	-9.446262	1.704402	2.488586
H	-9.297275	-0.158017	0.840266
H	-7.201670	-1.409618	0.565798
H	-2.675948	0.780877	2.873669
H	-1.644688	1.162281	5.069223
H	-2.028327	-0.453643	6.932855
H	-3.470161	-2.446175	6.555702
H	-4.538004	-2.810101	4.365444
H	-3.804071	1.871938	0.973659
H	-4.080774	4.221167	1.744173

H	-5.151669	5.885013	0.279466
H	-5.941669	5.221017	-1.996755
H	-5.605799	2.912361	-2.794999
H	-2.111093	2.097801	-2.414161
H	-1.101594	2.580617	-4.603212
H	-2.078016	1.605806	-6.678485
H	-4.080724	0.137811	-6.526054
H	-5.099603	-0.350456	-4.336089
H	-5.032523	-2.257431	-1.977800
H	-7.098418	-3.480395	-2.559271
H	-9.250270	-2.249669	-2.807748
H	-9.306874	0.213980	-2.468587
H	-7.246329	1.437588	-1.886167
H	5.586517	-2.246530	-2.167185
H	7.745227	-3.378785	-1.846995
H	9.664493	-2.164648	-0.828782
H	9.378494	0.203489	-0.109754
H	7.221356	1.339956	-0.419088
H	3.748472	3.300776	-1.171537
H	4.480423	5.455409	-2.123359
H	6.340380	5.524791	-3.775785
H	7.458580	3.410934	-4.464314
H	6.743216	1.257197	-3.501227
H	4.385846	0.867449	-4.531799
H	3.248241	-0.480360	-6.254470
H	2.005672	-2.542471	-5.618353
H	1.896388	-3.230111	-3.234383
H	3.001211	-1.867288	-1.498650
H	2.913716	-2.052413	3.591054
H	1.762668	-2.140517	5.745583
H	1.674091	-0.127063	7.217110
H	2.725385	1.997888	6.449605
H	3.856081	2.104960	4.269131
H	6.424556	0.230500	4.277159
H	8.231203	1.829252	4.782494
H	8.543681	3.854759	3.373106
H	7.022348	4.263568	1.444858
H	5.229869	2.641621	0.918000
H	3.129218	-2.293838	1.176446
H	3.905511	-4.642149	0.977021
H	6.249930	-5.219390	1.493920

H	7.838317	-3.444267	2.228278
H	7.074054	-1.120876	2.475056
C	-2.548291	8.607532	-0.148238
H	-1.863466	9.454788	-0.226885
H	-3.177212	8.599386	-1.043262
H	-3.161824	8.681221	0.746513
C	2.887754	-8.079056	-1.881714
H	3.908328	-7.685085	-1.905600
H	2.845173	-8.855999	-1.115282
H	2.609431	-8.473947	-2.855399
N	-1.781535	7.363204	-0.058887
N	1.942210	-7.010732	-1.550018

4 calculated at B3LYP/LANL2DZ/6-31G(d)

106

Pd	-0.642978	0.134417	-0.242662
S	0.930370	-1.369894	-1.174396
P	-2.112391	1.864816	0.627368
S	1.079128	1.726981	-0.275120
P	-2.280915	-1.668787	-0.475749
O	7.250472	-2.321847	1.384893
O	7.704625	1.940169	-0.019558
N	7.405540	-0.207206	0.648685
C	-2.091564	-2.973420	0.816244
C	5.522957	0.990923	-0.335848
C	3.270524	-0.066036	-0.350429
C	4.417920	-2.496123	0.634252
C	3.053103	-2.470043	0.158559
C	4.103795	-4.847600	1.256518
H	4.506290	-5.758858	1.692681
C	-2.545349	0.330920	2.940043
H	-1.899440	-0.396367	2.457959
C	2.494890	-1.256551	-0.339007
C	5.236537	-1.337988	0.483327
C	6.931030	0.983806	0.082390
C	-5.760840	2.668751	-1.208816
H	-6.802679	2.790838	-0.925696
C	4.696712	-0.136205	-0.062227
C	-0.937681	-2.984062	1.614935
H	-0.170770	-2.232712	1.457724
C	-1.366753	3.527970	0.923482
C	-1.682826	4.655720	0.153434
H	-2.397533	4.582686	-0.658888
C	-4.807722	-1.250103	0.746111
H	-4.282278	-1.353109	1.688925
C	2.707097	1.208596	-0.673797
C	-3.466132	2.201236	-0.574261
C	-5.376548	2.808969	-2.542478
H	-6.116404	3.048007	-3.301563
C	3.557050	2.238542	-1.176158
C	3.016942	3.388508	-1.831852
H	1.943207	3.450272	-1.959894

66

C	-2.857284	1.526434	2.277948
C	4.985008	2.121825	-1.022090
C	-3.042721	0.075963	4.220941
H	-2.785409	-0.853329	4.721491
C	-3.856197	1.016022	4.853692
H	-4.242126	0.820558	5.850457
C	-3.089960	2.320929	-1.924529
H	-2.050198	2.176477	-2.208747
C	-4.111010	-1.363010	-0.469414
C	-0.431658	3.653460	1.965644
H	-0.163668	2.787895	2.563996
C	-4.037551	2.632173	-2.899515
H	-3.729548	2.732313	-3.936744
C	-4.812783	2.369165	-0.227675
H	-5.132045	2.253655	0.801899
C	-2.021505	-2.503199	-2.101695
C	-6.205457	-1.002892	-1.651498
H	-6.742682	-0.910108	-2.591372
C	-2.130916	-3.890366	-2.272703
H	-2.334860	-4.532480	-1.422685
C	-6.890019	-0.908838	-0.439523
H	-7.964305	-0.745214	-0.428702
C	4.891574	-3.725595	1.201336
H	5.902115	-3.750604	1.575734
C	2.280240	-3.673784	0.217881
H	1.268113	-3.649050	-0.162398
C	-4.157581	2.220362	4.210705
H	-4.774108	2.964306	4.707801
C	-2.887998	-4.943166	1.999796
H	-3.650944	-5.702944	2.146725
C	6.661540	-1.367106	0.868549
C	-1.959448	-4.460193	-3.535152
H	-2.036970	-5.537751	-3.651743
C	-1.725120	-1.700732	-3.215653
H	-1.598466	-0.628856	-3.090481
C	-3.652742	2.480680	2.937407
H	-3.860876	3.436109	2.464846
C	-6.185156	-1.029737	0.759625
H	-6.706244	-0.959803	1.710774
C	2.781416	-4.831291	0.751776
H	2.163860	-5.724729	0.795143

C	-3.069228	-3.963592	1.023380
H	-3.978764	-3.963647	0.431086
C	-0.759985	-3.965262	2.593348
H	0.145949	-3.963340	3.192252
C	0.161314	4.884576	2.238240
H	0.884934	4.964615	3.044396
C	-1.084251	5.887358	0.429426
H	-1.342157	6.754333	-0.172847
C	-1.564570	-2.272658	-4.478204
H	-1.330182	-1.639380	-5.329222
C	-4.827932	-1.228447	-1.668355
H	-4.317085	-1.315174	-2.621020
C	-1.681479	-3.654016	-4.640350
H	-1.544692	-4.101365	-5.620994
C	5.230397	4.252372	-2.205081
H	5.879596	5.018382	-2.622302
C	-0.163671	6.005205	1.470569
H	0.302754	6.963675	1.680983
C	3.826636	4.369843	-2.341629
H	3.394851	5.217617	-2.866807
C	5.790163	3.171895	-1.568142
H	6.861205	3.095537	-1.468099
C	-1.733155	-4.946030	2.786581
H	-1.594596	-5.709997	3.546857
C	8.807510	-0.263537	1.072212
H	9.264186	0.690770	0.823528
H	8.865100	-0.450957	2.147825
H	9.314553	-1.085134	0.560432

4 calculated at B3LYP/SDD/6-31G(d)

106

Pd	-0.643138	0.128775	-0.225792
S	0.921971	-1.381962	-1.119226
P	-2.114303	1.843387	0.618664
S	1.060267	1.712824	-0.222478
P	-2.263088	-1.663500	-0.478463
O	7.294193	-2.313961	1.300575
O	7.685342	1.977783	-0.030587
N	7.417048	-0.183484	0.605071
C	-2.098625	-2.970748	0.816461
C	5.509782	1.010942	-0.335618
C	3.264991	-0.062043	-0.327202
C	4.440294	-2.486675	0.638334
C	3.066565	-2.466072	0.189358
C	4.143865	-4.835709	1.278411
H	4.556659	-5.743473	1.712200
C	-2.578889	0.313551	2.932089
H	-1.925537	-0.415504	2.463265
C	2.496012	-1.256440	-0.303645
C	5.252048	-1.325863	0.469793
C	6.923141	1.011800	0.065736
C	-5.739059	2.673578	-1.254543
H	-6.784147	2.792677	-0.982322
C	4.695702	-0.124321	-0.058810
C	-0.960701	-2.987140	1.637744
H	-0.188382	-2.237896	1.499379
C	-1.370835	3.504978	0.937849
C	-1.661171	4.634098	0.159915
H	-2.355777	4.564815	-0.669972
C	-4.811076	-1.247192	0.704137
H	-4.300896	-1.351580	1.655074
C	2.688790	1.208517	-0.641540
C	-3.452361	2.195863	-0.597902
C	-5.338636	2.831492	-2.581423
H	-6.068934	3.081431	-3.346216
C	3.524945	2.248481	-1.145737
C	2.969060	3.398632	-1.788046
H	1.893620	3.452783	-1.904276

69

C	-2.884089	1.504909	2.259520
C	4.955422	2.142655	-1.006925
C	-3.093807	0.063516	4.207136
H	-2.841496	-0.862981	4.715465
C	-3.918763	1.004129	4.823815
H	-4.318576	0.812206	5.815779
C	-3.059930	2.333559	-1.941948
H	-2.016992	2.192390	-2.216005
C	-4.094463	-1.356607	-0.500108
C	-0.463905	3.626892	2.005067
H	-0.217278	2.760719	2.611784
C	-3.995491	2.658505	-2.924242
H	-3.674442	2.772754	-3.956092
C	-4.803145	2.360276	-0.266045
H	-5.135384	2.230823	0.757612
C	-1.984542	-2.503758	-2.099940
C	-6.171135	-1.000817	-1.714890
H	-6.693506	-0.908848	-2.663195
C	-2.083540	-3.892279	-2.264982
H	-2.290925	-4.531413	-1.413671
C	-6.875105	-0.908994	-0.513937
H	-7.949780	-0.747684	-0.520103
C	4.927900	-3.712278	1.201630
H	5.945782	-3.733593	1.555736
C	2.297915	-3.671248	0.269668
H	1.278521	-3.651001	-0.090813
C	-4.213694	2.204564	4.170701
H	-4.839037	2.949501	4.655136
C	-2.922568	-4.942465	1.978713
H	-3.690255	-5.700650	2.108088
C	6.686287	-1.353099	0.818839
C	-1.897659	-4.467806	-3.522914
H	-1.967599	-5.546451	-3.634128
C	-1.684282	-1.705521	-3.216166
H	-1.564416	-0.632219	-3.096624
C	-3.691002	2.460064	2.903674
H	-3.893995	3.413337	2.424659
C	-6.189085	-1.029685	0.696041
H	-6.725278	-0.962175	1.638953
C	2.811988	-4.824987	0.799504
H	2.197302	-5.719434	0.859843

C	-3.082257	-3.959311	1.002076
H	-3.980113	-3.955874	0.392215
C	-0.804562	-3.971736	2.616471
H	0.089653	-3.973784	3.232888
C	0.129033	4.854813	2.291885
H	0.831796	4.931438	3.116624
C	-1.063742	5.862868	0.450856
H	-1.302151	6.730968	-0.157800
C	-1.509152	-2.283059	-4.474194
H	-1.271089	-1.652608	-5.326328
C	-4.793051	-1.223636	-1.710031
H	-4.267732	-1.310298	-2.654733
C	-1.615657	-3.665997	-4.630128
H	-1.467551	-4.117624	-5.607153
C	5.171574	4.283557	-2.176826
H	5.810216	5.057976	-2.594802
C	-0.169449	5.976517	1.515110
H	0.296536	6.932618	1.736928
C	3.765549	4.390131	-2.298813
H	3.321613	5.237922	-2.813755
C	5.746489	3.203392	-1.553189
H	6.819061	3.135628	-1.463903
C	-1.783438	-4.950860	2.787906
H	-1.661403	-5.717683	3.548123
C	8.827464	-0.235868	1.000123
H	9.270842	0.727667	0.763198
H	8.907535	-0.445557	2.070154
H	9.331662	-1.041669	0.461150

3.5. References

1. (a) Blake, I. M.; Rees, L. H.; Claridge, T. D. W.; Anderson, H. L. *Angew. Chem. Int. Ed.* **2000**, *39*, 1818–1821. (b) Tsuda, A. Osuka, A. *Science* **2001**, *293*, 79–82. (c) Kurotobi, K.; Kim, K. S.; Noh, S. B.; Kim, D.; Osuka, A. *Angew. Chem. Int. Ed.* **2006**, *45*, 3944–3947. (d) Davis, N. K. S.; Thompson, A. L.; Anderson, H. L. *J. Am. Chem. Soc.* **2011**, *133*, 30–31. (e) Sarma, T.; Panda, P. K. *Chem. Eur. J.* **2011**, *17*, 13987–13991.

2. (a) Avlasevich, Y.; Müllen, K. *Chem. Commun.* **2006**, 4440–4442. (b) Pshirer, N. G.; Kohl, C.; Nolde, F.; Qu, J.; Müllen, K. *Angew. Chem. Int. Ed.* **2006**, *45*, 1401–1404. (c) Lin, M.-J.; Fimmel, B.; Radacki, K.; Würthner, F. *Angew. Chem. Int. Ed.* **2011**, *50*, 10847–10850.

3. (a) Qiu, L.; Yu, C.; Zhao, N.; Chen, W.; Guo, Y.; Wan, X.; Yang, R.; Liu, Y. *Chem. Commun.* **2012**, *48*, 12225–12227. (b) Nakao, M.; Mori, H.; Shinamura, S.; Takimiya, K. *Chem. Mater.* **2012**, *24*, 190–198. (c) Más-Montoya, M.; Ortiz, R. P.; Curiel, D.; Espinosa, A.; Allain, M.; Facchetti, A.; Marks, T. J. *J. Mater. Chem. C* **2013**, *1*, 1959–1969 (d) Mori, T.; Nishimura, T.; Yamamoto, T.; Doi, I.; Miyazaki, E.; Osaka, I.; Takimiya, K. *J. Am. Chem. Soc.* **2013**, *135*, 13900–13913.

4. (a) Katz, H. E.; Bao, Z.; Gilat, S. L. *Acc. Chem. Res.* **2001**, *34*, 359–369. (b) Bendikov, M.; Wudl, F.; Perepichka, D. F. *Chem. Rev.* **2004**, *104*, 4891–4946. (c) Anthony, J. E. *Chem. Rev.* **2006**, *106*, 5028–5048. (d) Takimiya, K.; Osaka, I.; Nakano, M. *Chem. Mater.* **2014**, *26*, 587–593.

5. (a) Ma, Y.; Wang, Y. *Coord. Chem. Rev.* **2010**, *254*, 972–990. (b) Lo, K. K.-W.; Zhang, K. Y.; Li, S. P.-Y. *Eur. J. Inorg. Chem.* **2011**, 3551–3568. (c) Yao, S.; Belfield, K. D. *Eur. J. Org. Chem.* **2012**, 3199–3217.

6. (a) Gunnlaugsson, T.; Glynn, M.; Tocci, G. M.; Kruger, P. E.; Pfeffer, F. M. *Coord. Chem. Rev.* **2006**, *250*, 3094–3117. (b) Nolan, E. M.; Lippard, S. J. *Chem. Rev.* **2008**, *108*, 3443–3480. (c) Bryant, J. J.; Bunz, U. H. F. *Chem. Asian J.* **2013**, *8*, 1354–1367. (d) Li, X.; Gao, X.; Shi, W.; Ma, H. *Chem. Rev.* **2014**, *114*, 590–659.

7. (a) Mueller-Westerhoff, U. T.; Vance, B.; Yoon, D. I. *Tetrahedron* **1991**, *47*, 909–932. (b) Kobayashi, A.; Sasa, M.; Suzuki, W.; Fujiwara, E.; Tanaka, H.; Tokumoto, M.; Okano, Y.; Fujiwara, H.; Kobayashi, H. *J. Am. Chem. Soc.* **2004**, *126*, 426–427. (c) Madhu, V.; Das, S. K. *Inorg. Chem.* **2008**, *47*, 5055–5070. (d) Dalgleish, S.; Matsushita, M. M.; Hu, L.; Li, B.; Yoshikawa, H.; Awaga, K. *J. Am. Chem. Soc.* **2012**, *134*, 12742–12750.

8. (a) Ishikawa, N.; Okubo, T.; Kaizu, Y. *Inorg. Chem.* **1999**, *38*, 3173–3181. (b) Fukuda, T.; Biyajima, T.; Kobayashi, N. *J. Am. Chem. Soc.* **2010**, *132*, 6278–6279. (c) Fukuda, T.; Kuroda, W.; Ishikawa, N. *Chem. Commun.* **2011**, *47*, 11686–11688. (d) Wang, H.; Qian, K.; Wang, K.; Bian, Y.; Jiang, J.; Gao, S. *Chem. Commun.* **2011**, *47*, 9624–9626. (e) Wang, H.; Kobayashi, N.; Jiang, J. *Chem. Commun.* **2012**, *18*, 1047–1049. (f) Fukuda, T.; Hata, K.; Ishikawa, N. *J. Am. Chem. Soc.* **2012**, *134*, 14698–

14701. (g) Fukuda, T.; Matsumura, K.; Ishikawa, N. *J. Phys. Chem. A* **2013**, *117*, 10447–10454.

9. (a) Watson, M. D.; Fechtenkötter, A.; Müllen, K. *Chem. Rev.* **2001**, *101*, 1267–1300. (b) Kawasumi, K.; Zhang, Q.; Segawa, Y.; Scott, L. T.; Itami, K. *Nat. Chem.* **2013**, *5*, 739–744.

10. (a) Okamoto, T.; Suzuki, T.; Tanaka, H.; Hashizume, D.; Matsuo, Y. *Chem. Asian J.* **2012**, *7*, 105–111. (b) Suzuki, T.; Okamoto, T.; Saeki, A.; Seki, S.; Sato, H.; Matsuo, Y. *ACS Appl. Mater. Interfaces* **2013**, *5*, 1937–1942.

11. (a) Xu, H.; Yip, J. H. K. *Inorg. Chem.* **2003**, *42*, 4492–4494. (b) Aucott, S. M.; Milton, H. L.; Robertson, S. D.; Slawin, A. M. Z.; Woollins, J. D. *Dalton Trans.* **2004**, 3347–3352. (c) Samuel, A. P. S.; Co, D. T.; Stern, C. L.; Wasielewski, M. R. *J. Am. Chem. Soc.* **2010**, *132*, 8813–8815.

12. (a) Murahashi, T.; Higuchi, Y.; Katoh, T.; Kurosawa, H. *J. Am. Chem. Soc.* **2002**, *124*, 14288–14289. (b) Ohashi, M.; Yi, J.; Shimizu, D.; Yamagata, T.; Ohshima, T.; Mashima, K. *J. Organomet. Chem.* **2006**, *691*, 2457–2464. (c) Brunet, L.; Mercier, F.; Ricard, L.; Mathey, F. *Angew. Chem. Int. Ed. Engl.* **1994**, *33*, 742–745. (d) Kannan, S.; James, A. J.; Sharp, P. R. *J. Am. Chem. Soc.* **1998**, *120*, 215–216.

13. Banister, A. J.; Gorrell, I. B.; Howard, J. A. K.; Lawrence, S. E.; Lehman, C. W.; May, I.; Rawson, J. M.; Tanner, B. K.; Gregory, C. I.; Blake, A. J.; Fricker, S. P. *J. Chem. Soc., Dalton Trans.* **1997**, 377–384.

14. Robertson, S. D.; Slawin, A. M. Z.; Woollins, J. D. *Eur. J. Inorg. Chem.* **2007**, 247–253.

15. (a) *Gaussian 09*, Revision A.02, Frisch, M. J.; Trucks, G. W.; Schlegel, H. B.; Scuseria, G. E.; Robb, M. A.; Cheeseman, J. R.; Scalmani, G.; Barone, V.; Mennucci, B.; Petersson, G. A.; Nakatsuji, H.; Caricato, M.; Li, X.; Hratchian, H. P.; Izmaylov, A. F.; Bloino, J.; Zheng, G.; Sonnenberg, J. L.; Hada, M.; Ehara, M.; Toyota, K.; Fukuda, R.; Hasegawa, J.; Ishida, M.; Nakajima, T.; Honda, Y.; Kitao, O.; Nakai, H.; Vreven, T.; Montgomery, Jr., J. A.; Peralta, J. E.; Ogliaro, F.; Bearpark, M.; Heyd, J. J.; Brothers, E.; Kudin, K. N.; Staroverov, V. N.; Kobayashi, R.; Normand, J.; Raghavachari, K.; Rendell, A.; Burant, J. C.; Iyengar, S. S.; Tomasi, J.; Cossi, M.; Rega, N.; Millam, J. M.; Klene, M.; Knox, J. E.; Cross, J. B.; Bakken, V.; Adamo, C.; Jaramillo, J.; Gomperts, R.; Stratmann, R. E.; Yazyev, O.; Austin, A. J.; Cammi, R.; Pomelli, C.; Ochterski, J. W.; Martin, R. L.; Morokuma, K.; Zakrzewski, V. G.; Voth, G. A.; Salvador, P.; Dannenberg, J. J.; Dapprich, S.; Daniels, A. D.; Farkas, O.; Foresman, J. B.; Ortiz, J. V.; Cioslowski, J.; Fox, D. J. Gaussian, Inc., Wallingford CT, **2009**. (b) *Gaussian 09*, Revision C.01, Frisch, M. J.; Trucks, G. W.; Schlegel, H. B.; Scuseria, G. E.; Robb, M. A.; Cheeseman, J. R.; Scalmani, G.; Barone, V.; Mennucci, B.; Petersson, G. A.; Nakatsuji, H.; Caricato, M.; Li, X.; Hratchian, H. P.; Izmaylov, A. F.; Bloino, J.; Zheng, G.; Sonnenberg, J. L.; Hada, M.; Ehara, M.; Toyota, K.; Fukuda, R.; Hasegawa, J.; Ishida, M.; Nakajima, T.; Honda, Y.; Kitao, O.; Nakai, H.; Vreven,

T.; Montgomery, Jr., J. A.; Peralta, J. E.; Ogliaro, F.; Bearpark, M.; Heyd, J. J.; Brothers, E.; Kudin, K. N.; Staroverov, V. N.; Keith, T.; Kobayashi, R.; Normand, J.; Raghavachari, K.; Rendell, A.; Burant, J. C.; Iyengar, S. S.; Tomasi, J.; Cossi, M.; Rega, N.; Millam, J. M.; Klene, M.; Knox, J. E.; Cross, J. B.; Bakken, V.; Adamo, C.; Jaramillo, J.; Gomperts, R.; Stratmann, R. E.; Yazyev, O.; Austin, A. J.; Cammi, R.; Pomelli, C.; Ochterski, J. W.; Martin, R. L.; Morokuma, K.; Zakrzewski, V. G.; Voth, G. A.; Salvador, P.; Dannenberg, J. J.; Dapprich, S.; Daniels, A. D.; Farkas, O.; Foresman, J. B.; Ortiz, J. V.; Cioslowski, J.; Fox, D. J. Gaussian, Inc., Wallingford CT, **2010**. The Gaussian09 package of b) was used for the calculations performed at Research Center for Computational Science, Okazaki, Japan.

Chapter 4.

**Chromic Properties and Conformational Control
of Fluorenylideneacridane Derivatives**

4.1. Introduction

The simplest π-orbital comprises a double bond. Connection of aromatic rings with double bonds has been used to obtain large π-conjugated systems such as *p*-phenylene vinylene derivatives.[1] A variety of synthetic methods to form double bonds have been reported, and hence the π-conjugated derivatives have grown the field of organic electronic devices. Since double bond has simple π-orbitals having no aromaticity, dipole and other functionalities, the method to link aromatic rings with double bond has been widely used. In the field of extended π-systems, there have been several reports on adding distortion to the molecule for control of packing structure.[2] The distortion gives not only dense packing manner, but also high solubility, metastable structures and unique π-conjugated systems. Although those properties are often required for solution-processed organic electronics, the molecular designs are limited because of introduced structural repulsions.

The combination of double bond and distortion is realized in bis-tricyclic aromatic enes (BAEs). The most typical BAE is bianthrone, which shows several chromic properties.[3] This chromism represented the existence of two stable structures exhibiting yellow color and their blue-shifted color. To clarify the origin of color change, other analogs have been investigated. Among these investigations, two stereoisomers of a fluorenylidenexanthone derivative were separately crystallized. The fluorenylidenexanthone derivative composes V- and X-type conformers (Figure *1*).[4] This research identified that the conformational change between V- and X-type conformers induces the color change. Moreover, other fluorenylidenexanthone derivative was reported to demonstrate light absorption property of each conformer.[5] Despite a lot of literatures and achievements on BAE, the mechanism how the molecule transforms into the other conformer has not been clearly figured out. In addition, the literatures had reported no photophysical properties and electrochemical properties, though the BAE structures consisting of fused aromatic rings are seemed applicable to organic electronic devices. On the other hand, bifluorenylidene derivatives and analogs have been investigated in the application to organic solar cells.[6] However, chromic behaviors of bifluorenylidene type BAEs have not yet been reported.


V-type conformation   X-type conformation
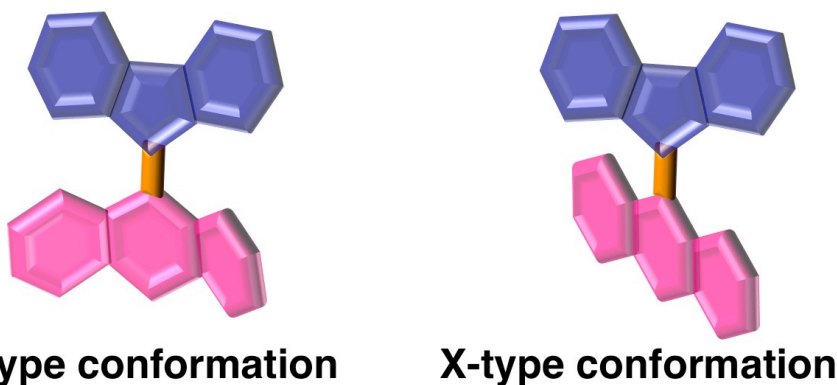
Figure 1. Schematic images of stereoisomers observed in BAEs.

In this work, I focused on the molecule in which a double bond bridges fluorene and acridane backbones, named as fluorenylideneacridane (FA) (Figure *2*). The chromic behaviors observed in BAEs were predicted to appear because of the structural similarity to fluorenylidenexanthone. The molecule would have two canonical structures that neutral one and zwitterionic one. When the molecule has the polarized structure, double bond character of the connecting part changes into single bond one. DFT calculations provided two stable optimized structures that were V-type and X-type conformers. V-type has slightly lower energy than X-type to be a ratio of 10:8.7 in equilibrium (ΔE = 347 J/mol). Furthermore, the calculated electrostatic potential maps of FA displayed larger gradient in X-type conformer having zwitterionic potential surface (Figure *3*). These characteristics induced by V- and X-type stereoisomers are similar to those in BAEs reported previously. Herein, the calculation results also suggested that the two conformers possess different π-orbitals indicating different electrochemical properties. In order to modify the chromic properties, I designed the molecule can contain substituents which do not influence on the electronic structures. The substituents might slightly effect on the conformational stability to change the ratio between V- and X-type conformers. Here, the substituents of FA can be easily changed. This synthetic characteristic is quite effective to smoothly examine the FA derivatives having a variety of substituents. I targeted to construct the organic materials having semiconductive properties and chromic properties at the same time toward sensors for physical stimuli, thin-film devices for charge transport and photovoltaics, and so on.

V−type conformation   X−type conformation
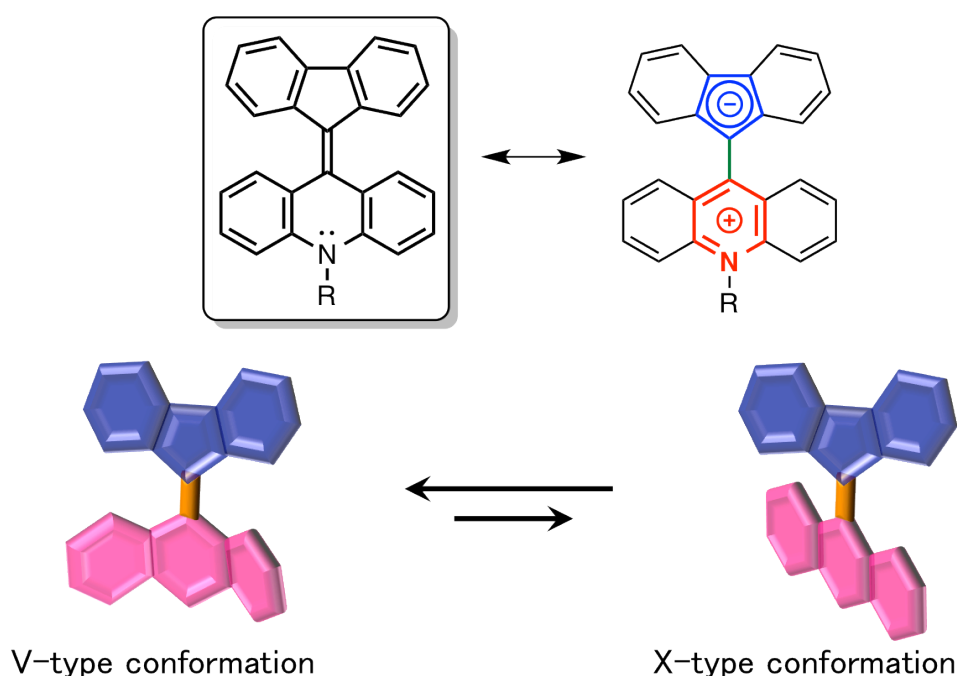
Figure 2. Molecular design of fluorenylideneacridane. The canonical structures and stereoisomers were expected through DFT calculations calculated at B3LYP/ 6-31G(d).
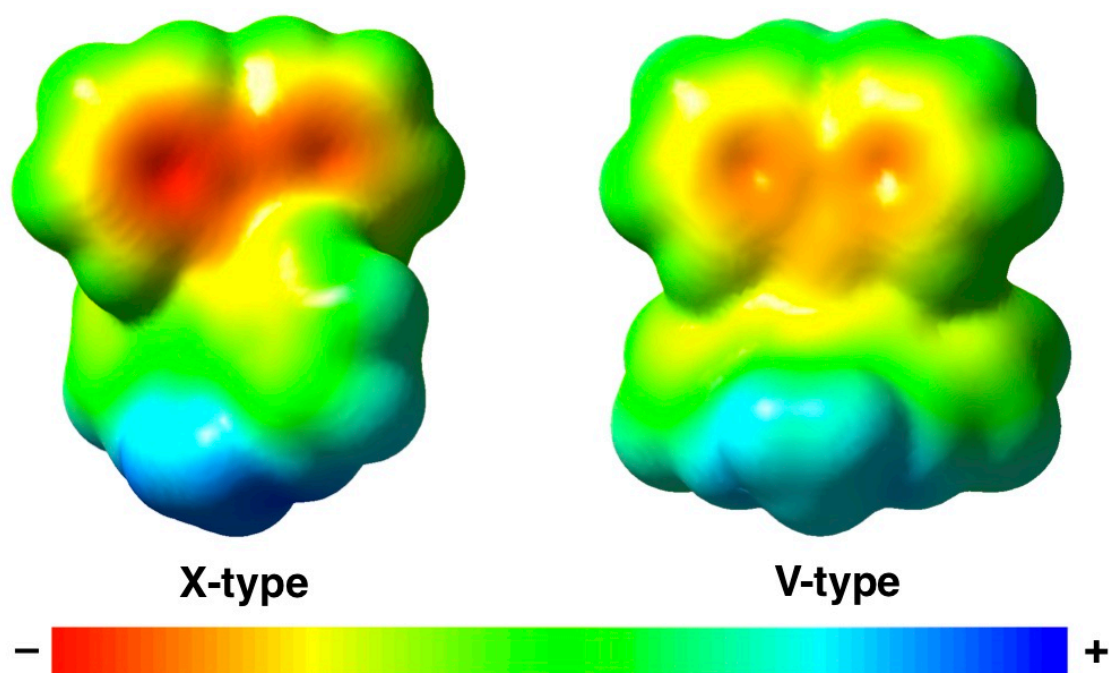
Figure 3. Electrostatic potential maps of FA calculated at B3LYP/6-31G(d).

Unlike thermo- and photo-chromisms, mechanochromism is relatively difficult to evaluate and monitor what happens inside. Nonetheless, a variety of mechanochromic materials have been established recently.[7] Almost all of them were reported that mechanochromic color change occurred by transition between crystalline and amorphous phases. This conclusion was mainly supported by powder XRD measurements that showed sharp peaks in crystalline phase and a wide-range hump in amorphous phase. In those cases, mechanic stimuli did not induce structural changes in the molecular structure. A few literatures provided mechanoresponsive color change accompanying with structural changes.[8]

In this work, I have studied the synthesis of a new BAE series that is FA derivatives having aliphatic substituents. The methyl substituted FA indicated mechanochromic properties like BAEs. Herein, I have tried to accomplish long wavelength light absorption by BAE structure and investigated how the color change occurred during mechanical handling. In addition, I found that the color transition was controlled by modifying the substituents. The photophysical properties and electrochemical properties were deeply investigated to depict the electronic structures.

78

4.2. Results and Discussion

A precursor of fluorenylideneacdidane (FA) derivatives was prepared from fluorenone and acridone (Scheme *1*). Diazofluorene and *tert*-butyl-9-thioxoacridine-10(9H)-carboxylate (*N*-Boc-thioacridone) were synthesized through the reported procedures.[9] Both units were condensed in CH_2Cl_2 at room temperature to give a thiirane compound. In this condition, the substituent on the nitrogen atom of acridone played a quite and important role to proceed the condensation reaction. Methyl or phenyl group on the nitrogen atom never progressed the reaction but remained no reaction (Scheme *2*). Instead of this condition, Knoevenagel condensation condition using fluorene and acridone also resulted in no reaction. In another trial, acridone was reduced to give acridane, which was lithiated to undergo nucleophilic attack to fluorenone. This strategy also ended in no reaction. By considering these failures, it can be said that acridone has considerably low reactivity. An attempt to increase the reactivity and nucleophilicity required an electron-deficient Boc group and an active thioketone group. Introducing diazo group also activated fluorene. After fluorene-acridane condensation succeeded, the sulfur atom of the thiirane ring and the electron-withdrawing Boc group was removed with triphenylphosphine and acid, respectively. The reduction and deprotection reactions were expected to generate fluorenylideneacridane, which has hydrogen on the nitrogen atom. However, NMR data of the product indicated the hydrogen was rearranged to the fluorene unit to give fluorenyl acridine (H-FA). The NMR chart displayed a singlet signal due to the rearranged hydrogen atom at 6.45 ppm and asymmetric peaks pattern for the acridine moiety. X-ray single crystal analysis unambiguously determined this structure (Figure *4*). Some aliphatic substituents were introduced to H-FA by using some leaving groups on the alkyl group. Methyl iodide and methyl tosylate were used to obtain methyl substituted FA (MeFA), but the crude product contained H-FA. MeFA has the methyl group on the nitrogen atom. It was confirmed by ^{1}H NMR showing symmetric peak pattern without a singlet peak around 6.45 ppm as well as by single crystal structural analysis (*vide infra*). In this reaction condition, the yield of MeFA was 68% at the highest through the reaction with 10 equivalent of methyl tosylate. Since the reaction between H-FA and MeFA was seemed to be in equilibrium, the reaction was carried out with base, K_2CO_3. In this condition, all amount of H-FA reacted with smaller amount of methyl tosylate (3.58 equiv.) to achieve higher yield as 88%. Octyl substituted FA (OctylFA) was also synthesized through the similar condition. The octyl group is also placed at the nitrogen atom displaying similar ^{1}H NMR chart to MeFA. Octyl triflate with excess amount of K_2CO_3 smoothly introduced the octyl group to H-FA. OctylFA was sticky solids, which made it difficult to reprecipitate the compound. In the end, solid OctylFA was collected by reprecipitation from CH_2Cl_2/MeOH at low temperature. The yield was low as 35% because OctylFA was soluble even in MeOH at low temperature.

**Scheme 1.** Synthesis of fluorenylideneacridane derivatives.
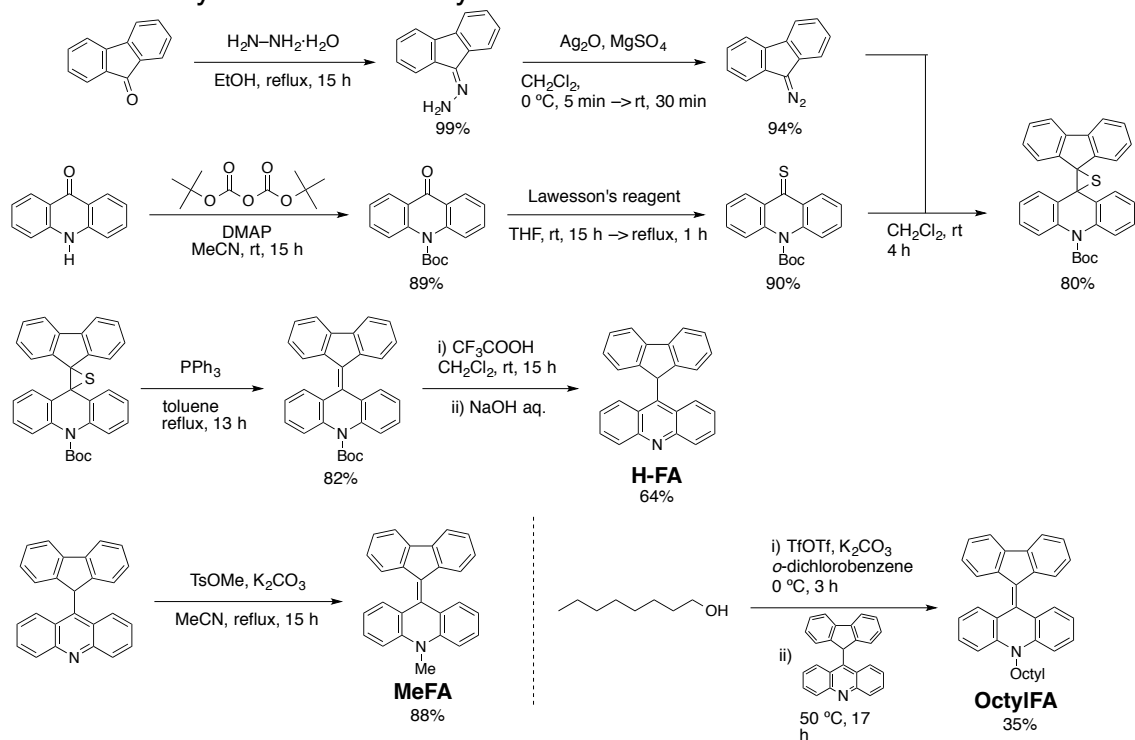
Scheme 2. Trials of synthesis toward fluorene–acridane linked molecules. (a) Barton-Kellogg reaction condition with methyl or phenyl substituent, (b) Knoevenagel reaction condition and (c) nucleophile substitution reaction. Each reaction did not proceed.
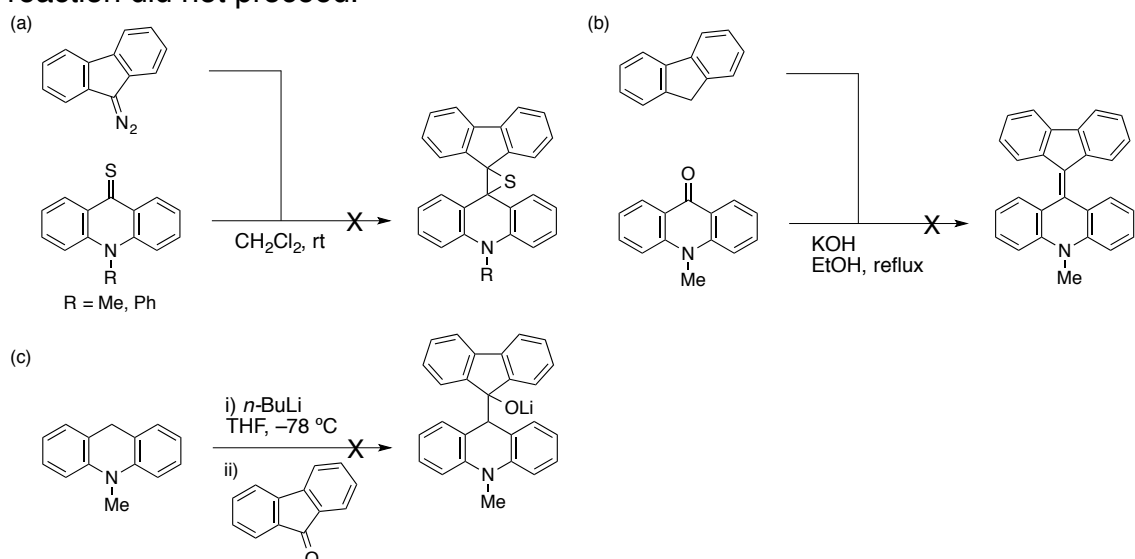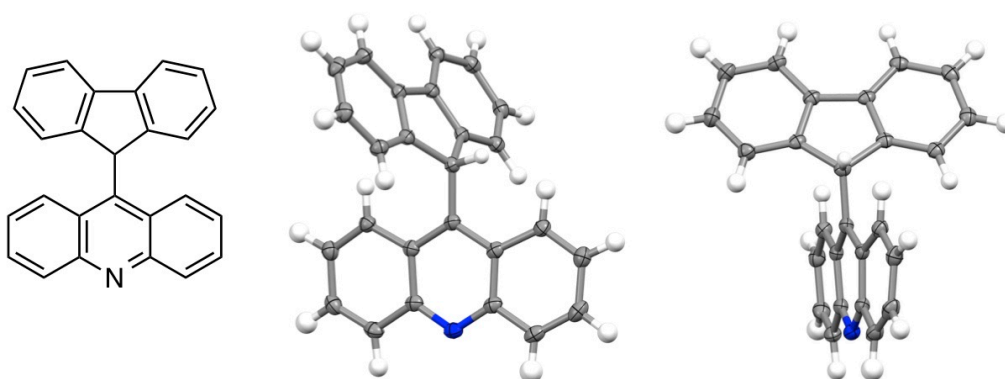
**Figure 4.** Crystal structure of fluorenyl acridine.

Molecular structure of MeFA was confirmed by single crystal X-ray analysis. MeFA showed two crystalline polymorphs. The two kinds of crystals with different space groups were obtained by recrystallization using CH_2Cl_2/hexane, CH_2Cl_2/MeOH, $CHCl_3$/MeOH, toluene/MeOH (Polymorph 1) and benzene/hexane (Polymorph 2) bilayer solvent systems (Figure **5**). Polymorph 1 contained crystallographically independent two MeFA molecules in the single lattice. In both of polymorphs, MeFA formed V-type conformer. The fluorene moiety sustained the planar structure but the acridane moiety is bent at 51.99º and 52.66º in Polymorph 1 and 50.29º in Polymorph 2. The bond lengths of the central double bonds were 1.360(6) and 1.392(6) Å in Polymorph 1 and 1.363(2) Å in Polymorph 2, which are slightly longer than typical C=C distance (1.34 Å). The elongation implies the contribution of zwitterionic structure as a canonical structure.
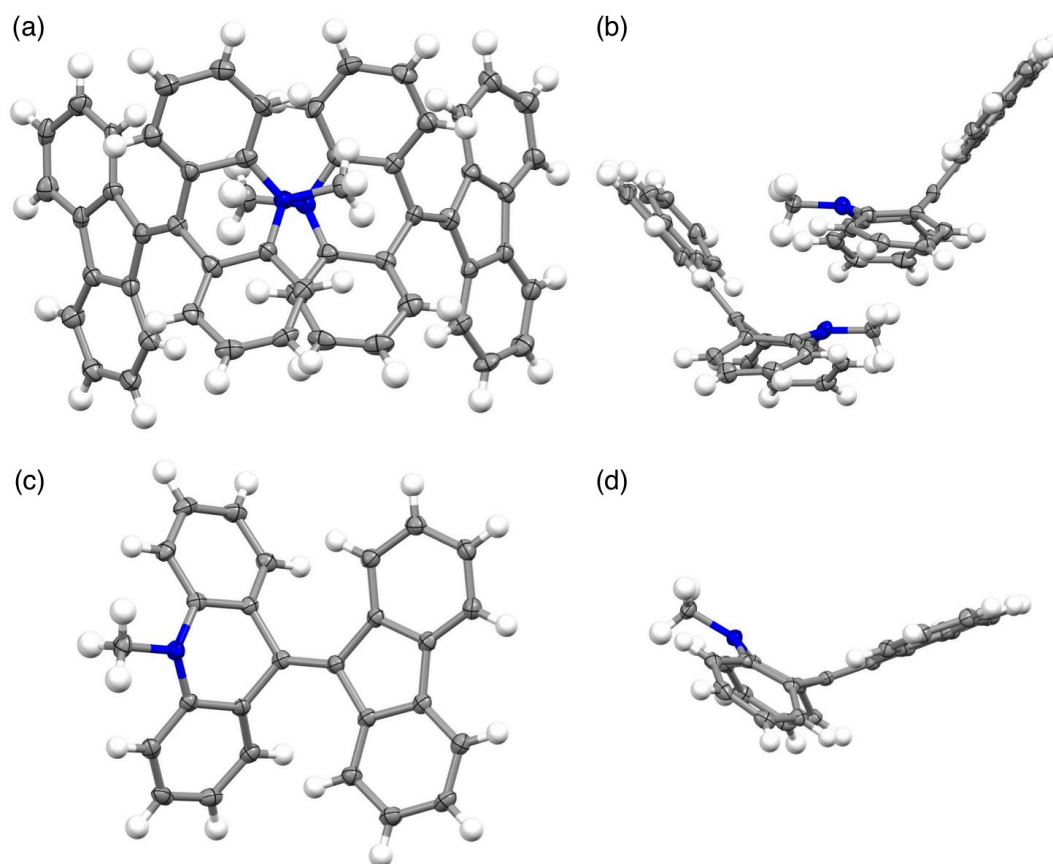
Figure 5. Crystal structure of MeFA. The polymorph is shown: (a), (b) prepared from CH₂Cl₂/hexane (Polymorph 1) and (c), (d) prepared from benzene/hexane (Polymorph 2).

Electrochemical characteristics of FA derivatives were depicted by cyclic voltammetry (CV) and differential pulse voltammetry (DPV) (Figure **6**). MeFA showed two reversible oxidation peaks at –0.17 and 0.74 V (vs Fc/Fc$^+$). The first oxidation potential indicated that MeFA is easily oxidized rather than ferrocene. In contrast to the oxidation process, a reduction process was detected in largely negative region as a reversible wave observed at –1.82 V. DPV data displayed the oxidation and reduction waves at the almost same levels to CV, besides a peak appeared with around half size at –2.29 V, which would indicate decomposition of the two-electron reduced species. HOMO and LUMO levels were estimated from the oxidation and reduction potentials to be –4.63 and –2.98 eV, respectively.[10] The computational calculation with optimized structures gave LUMO and HOMO levels to be –1.823 and –5.197 eV, respectively, for V-type MeFA and –2.313 and –4.571 eV, respectively, for X-type MeFA at B3LYP/6-31G(d) levels. The calculation results provided higher HOMO and lower LUMO for X-type conformer than V-type conformer. Accordingly, the one-electron oxidation potential and one-electron reduction potential would represent those of X-type conformer. The calculation of X-type MeFA anion gave –2.694 eV as SOMO

corresponding to the first reduction potential in CV. This result also supports that the first oxidation and reduction waves in CV denoted the properties of X-type MeFA. In electrochemical measurements, OctylFA also exhibited reversible one-electron oxidation and one-electron reduction waves at the similar positions to MeFA (–0.22 and –1.81 V). On the other hand, the secondary oxidation and reduction waves of OctylFA appeared as irreversible, showing it is electrochemically less stable than MeFA. The DPV chart of OctylFA was also quite similar to MeFA. It was confirmed that influence of aliphatic chains on electrochemical properties is small.
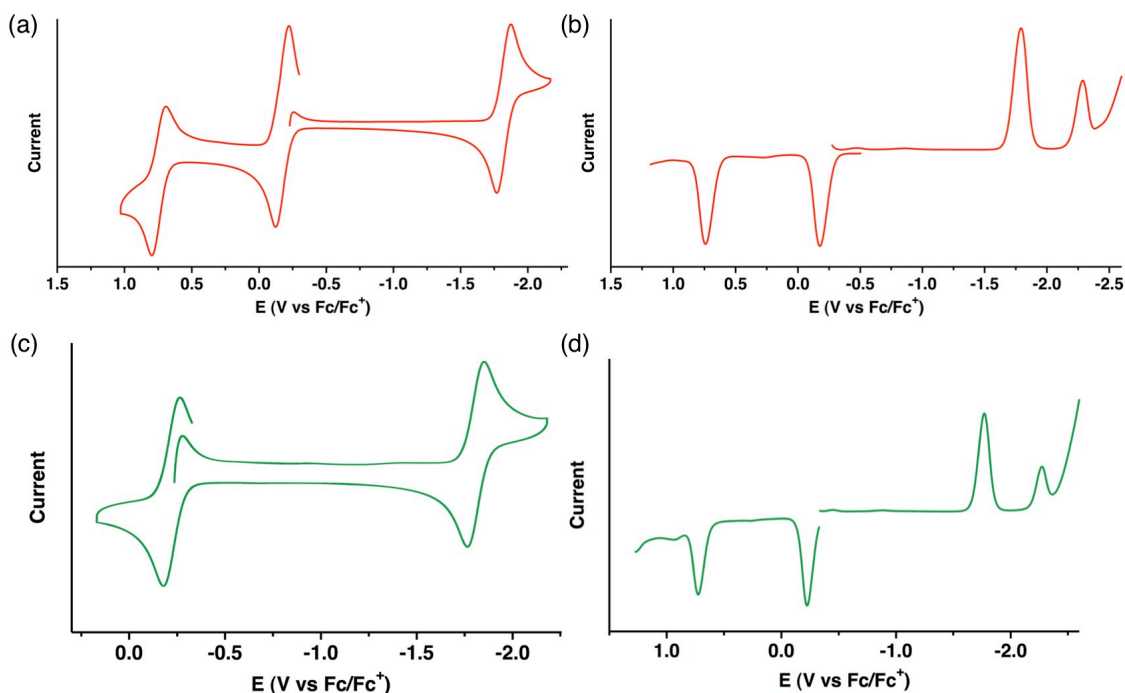
Figure 6. Electrochemical behaviors of MeFA and OctylFA. (a) CV chart and (b) DPV chart of MeFA. (c) CV chart and (d) DPV chart of OctylFA. Detailed experimental conditions are described in experimental section. All measurements started from the rest potentials.

In MeFA and OctylFA solutions, V- and X-type conformers are in equilibrium. I should describe electrochemical reaction by considering the equilibrium. The four-member electrochemical scheme is shown in Figure 7. In a general case, the electrochemical reaction is denoted as:[11]

$$([O] + [Q])/([P] + [R]) = \exp[(F/RT)(E - E_K^{\circ})] \tag{1}$$

$$E_K^{\circ} = E_1^{\circ} - (RT/F) \ln[(1 + K_1^{-1})/(1 + K_2^{-1})] = E_2^{\circ} + (RT/F) \ln[(1 + K_2)/(1 + K_1)] \tag{2}$$

$$K_1 = [Q]/[O], \quad K_2 = [R]/[P] \tag{3}$$

The E_K° value is obtained in CV measurements. When the equation is applied to the case of FA derivatives, the square scheme can be converted as Figure 7b and c. DFT calculations gave the results that the radical anions and radical cations preferentially

form X-type conformer rather than V-type conformer. Accordingly, the electrochemical reduction reactions of FA derivatives are denoted as the following:

$$E_{K\text{red}}{}^{\circ} = E_{X\text{red}}{}^{\circ} - (RT/F) \ln[(1 + K_1^{-1})/(1 + K_2^{-1})] \tag{4}$$

$$K_1 = [\mathbf{X}]/[\mathbf{V}], \; K_2 = [\mathbf{X}^{\bullet-}]/[\mathbf{V}^{\bullet-}] \gg 1 \tag{5}$$

Equation (4), (5) gave ($T = 298$ [K]):

$$E_{K\text{red}}{}^{\circ} \approx E_{X\text{red}}{}^{\circ} - (RT/F) \ln[1 + K_1^{-1}] = E_{X\text{red}}{}^{\circ} - 0.0257 \ln[1 + K_1^{-1}] \tag{6}$$

Here, DFT study estimated the K_1^{-1} value of MeFA as 1.1 ([$\mathbf{V}$]/[$\mathbf{X}$] = 10/8.7) in CH$_2$Cl$_2$ solution. Consequently, $E_{K\text{red}}{}^{\circ} \approx E_{X\text{red}}{}^{\circ}$, suggesting the first reduction wave in CV measurement represented the reduction potential of X-type conformer. As is the same to oxidation step, the electrochemical reaction is described as ($T = 298$ [K]):

$$E_{K\text{ox}}{}^{\circ} = E_{X\text{ox}}{}^{\circ} + (RT/F)\ln[(1 + K_2)/(1 + K_1)] \tag{7}$$

$$K_1 = [\mathbf{V}^{\bullet+}]/[\mathbf{X}^{\bullet+}] \approx 0, \; K_2 = [\mathbf{V}]/[\mathbf{X}] \tag{8}$$

From (7) and (8):

$$E_{K\text{ox}}{}^{\circ} \approx E_{X\text{ox}}{}^{\circ} + (RT/F) \ln[1 + K_2] = E_{X\text{ox}}{}^{\circ} + 0.0257 \ln[1 + K_2] \tag{9}$$

The K_2 value of MeFA is also 1.1, and therefore $E_{K\text{ox}}{}^{\circ} \approx E_{X\text{ox}}{}^{\circ}$. This theoretical investigation clearly demonstrated that the CV charts of FA independently displayed reduction and oxidation of X-type conformer in the first reduction and oxidation waves. The equilibrium between V- and X-type conformers influences to the electrochemical reactions, however the degrees are quite small in this case. This simple picture is derived from the highly energetic difference between radical V- and X-type conformers and coexistence of neutral V- and X-type conformers in the solutions.
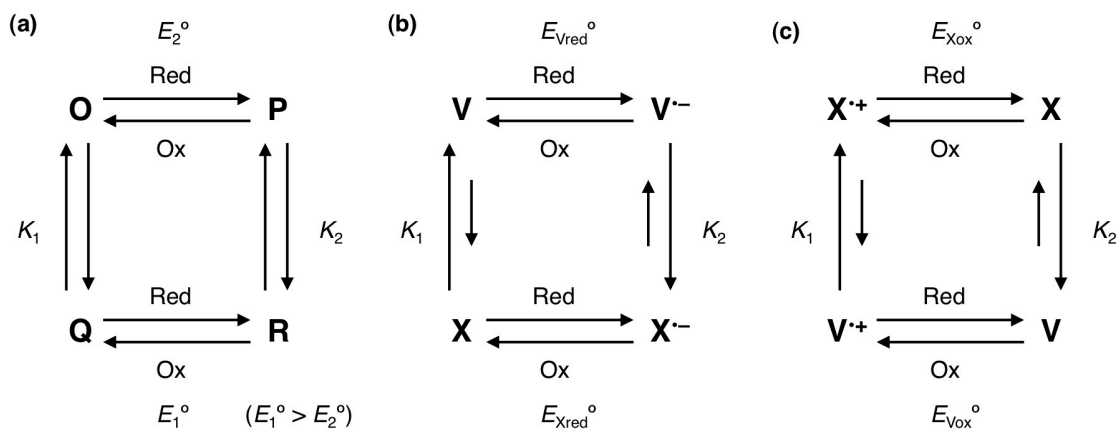
Figure 7. Four-member square scheme of electrochemical reactions. (a) General scheme, (b) the case of FA derivative in a reduction step and (c) an oxidation step of FA derivatives are noted (**V**: V-type conformer, **X**: X-type conformer).

The critical difference between MeFA and OctylFA emerged in color of the solids although the electrochemical properties are almost identical. Both of MeFA and OctylFA showed deep green color in solution states. In any solvents, the FA derivatives

showed deep green color. In the solid states, OctylFA kept the deep green color, while MeFA turned into greenish yellow color in crystalline solid phase (Figure *8*). By grinding the solids with a metal spatula or an agate mortar, the solids color changed into deep green similar to the solution state. Furthermore, greenish yellow was recovered after exposure to chloroform vapor in 5 min. The color change by grinding was in accordance with the well-known color changes of BAEs, but recovery of the color by solvent annealing was firstly reported here among BAEs.


Recrystallized   Ground   Solvent annealing (CHCl$_3$, 5 min)
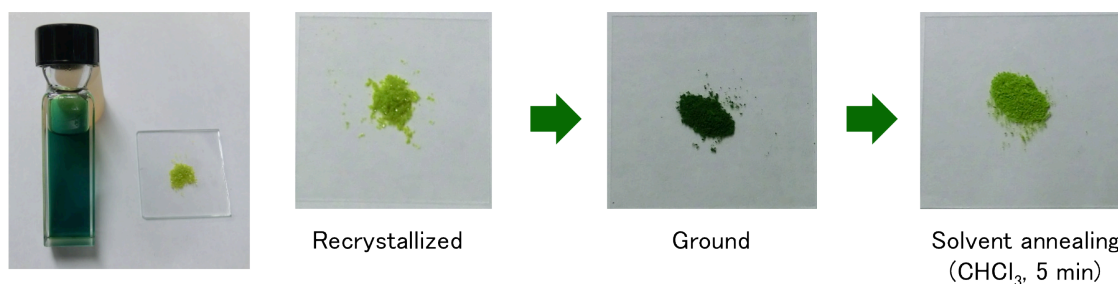
Figure 8. Appearance of MeFA in solid and solution states. It showed mechanochromic behavior by grinding and solvent annealing.

The differences of color were qualitatively and quantitatively evaluated by light absorption measurements (Figure *9*). The FA derivatives have sharp peaks at 423 (MeFA) and 430 nm (OctylFA), and broad peaks at 661 (MeFA) and 671 nm (OctylFA) in dichloromethane. The light absorption at the long wavelength region is assigned to the origin of deep green color in solutions. Although the peaks emerged at the similar wavelength, the ratios of peak intensities were different. MeFA possessed an intense peak at the short wavelength region with a weak broad peak at the long wavelength region. Different from MeFA, OctylFA contained similar intensities for a sharp peak and a broad peak. According to the previous works on BAEs,[5] each peak would correspond to V- and X-type conformer for sharp and broad peaks, respectively. The area of each peak represents the ratio of each conformer. Namely, MeFA solution mainly contains V-type conformer with small ratio of X-type conformer. OctylFA solution was seemed to contain larger amount of X-type conformer rather than V-type unlike MeFA solution. The aliphatic chains on nitrogen would control the distribution ratio.
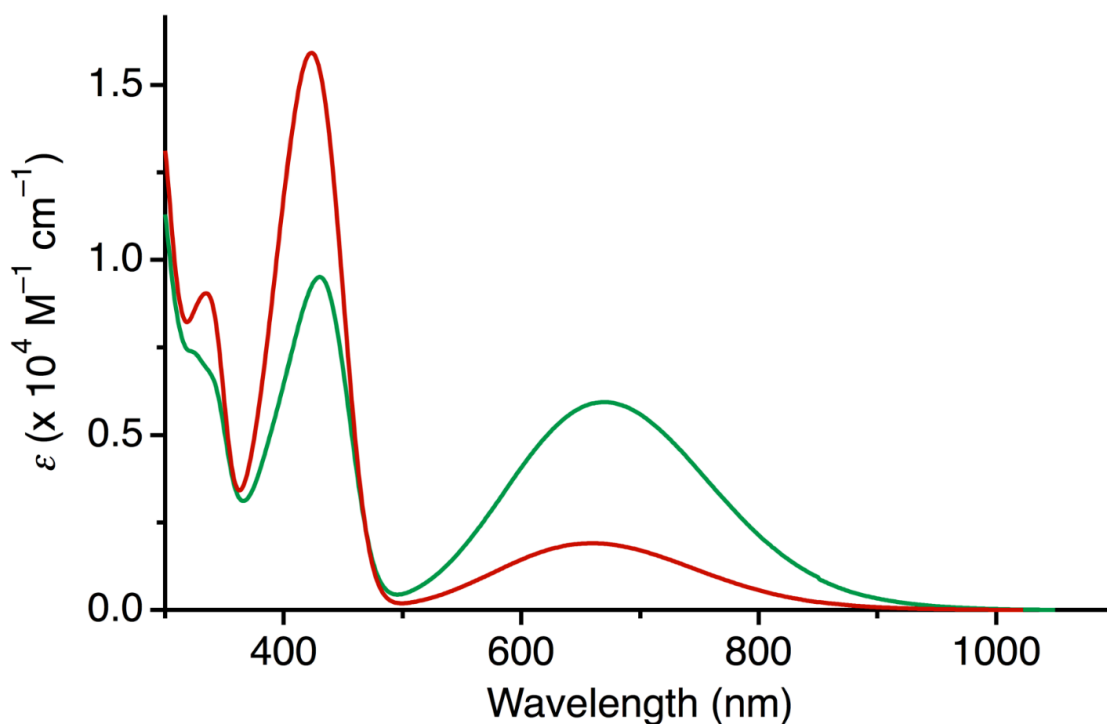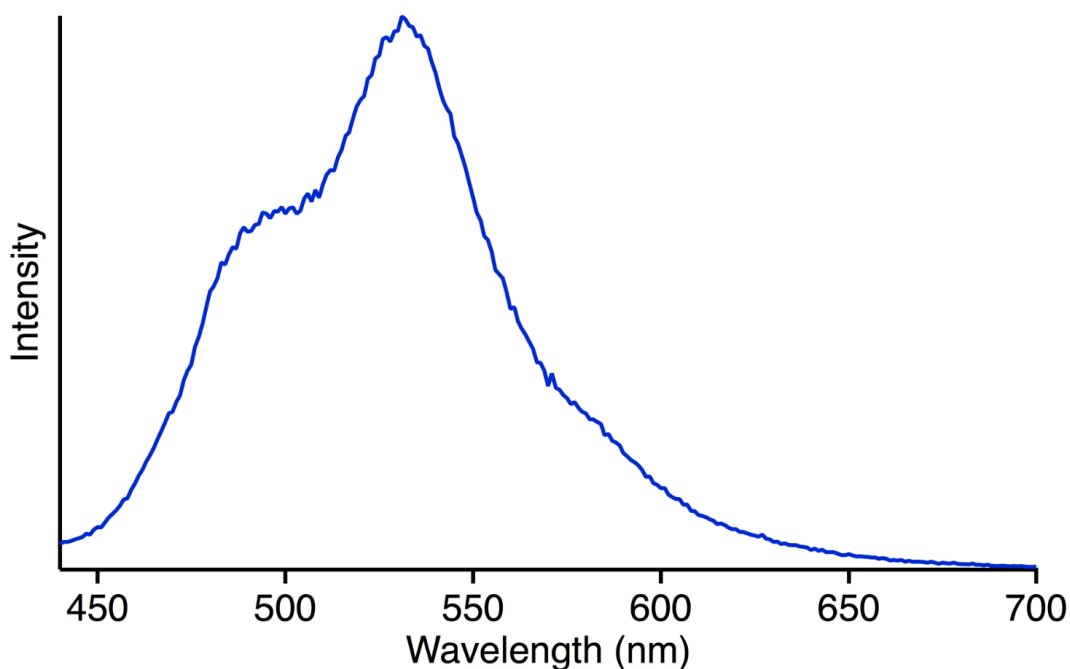

Figure 9. Light absorption spectra of MeFA (red) in CH_2Cl_2 and OctylFA (green) in CH_2Cl_2.

The distribution of V- and X-type conformers was explained with light absorption data indirectly. The evidences to show coexistence of V- and X-types were further supported by TD-DFT simulation for light absorption bands (Figure *10*). The simulation reproduced the experimental spectra of MeFA with characteristic light absorption bands at 624.95 and 430.73 nm. Longer wavelength band is due to X-type confirmation, while shorter one corresponds to V-type one. Observed no confusing band near 624.95 and 430.74 nm supported this assignment and indicated that both absorption bands independently comes from these two conformers.
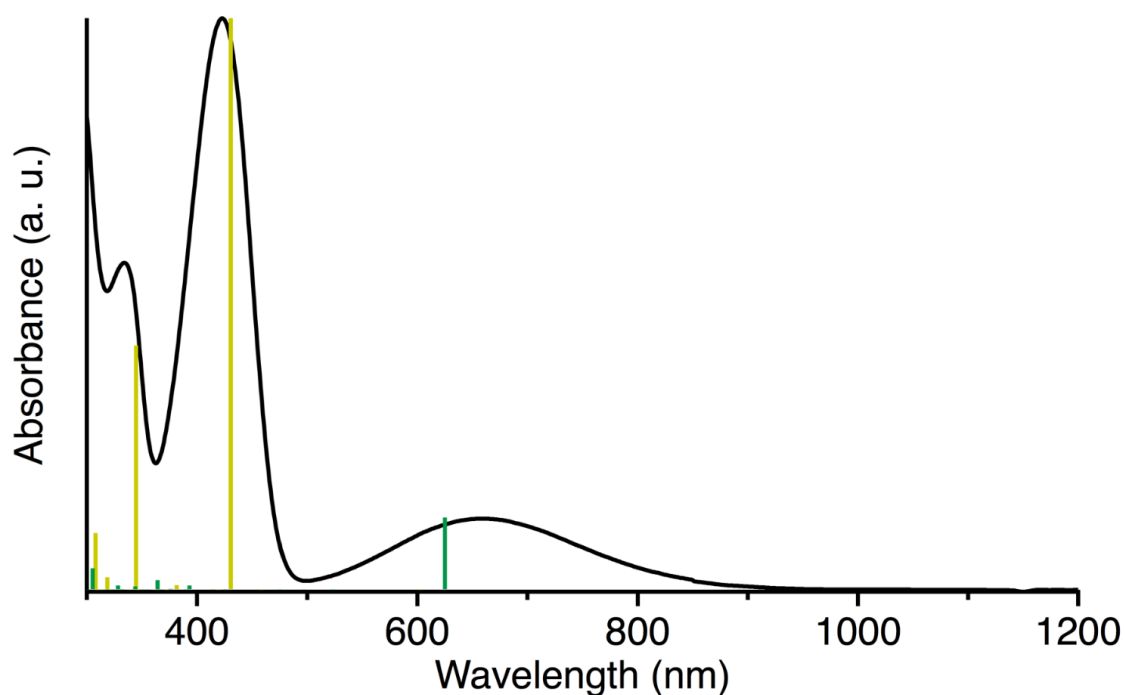
Figure 10. Simulated light absorption bands of MeFA in CH_2Cl_2 calculated at B3LYP/6-31G*. The black solid line is experimental spectra of MeFA in CH_2Cl_2, green line corresponds to X-type conformer and yellow line is V-type.

The MeFA solution showed weak fluorescence in CH_2Cl_2 by exciting at 420 nm (Figure *11*). The fluorescent spectrum exhibits a peak at 530 nm with two shoulders around 500 and 580 nm. Excitation at 680 nm, where the broad light absorption was observed, did not give any fluorescence even when a variety of solvents and concentrations were used in nitrogen atmosphere.


Figure 11. Fluorescence spectrum of MeFA in CH_2Cl_2 by excitation at 420 nm.

The color difference of MeFA in solid and solution states was qualitatively evaluated through light absorption measurements of MeFA's thin films, which was prepared by spin coating methods (Figure *12*). The appearance of an as-cast film was yellow similar to recrystallized solids. Detailed light absorption studies with mechanical stimuli for thin films explained the color difference between solution and film. The spectrum of the as-cast film gave no light absorption peak at long wavelength region. Following grinding process, however, changed the color from yellow into green. The appearance of the color change was identical to what was observed as mechanochromic behavior of the powder. The spectrum of green film was quite similar to that in solution state, accompanying slightly red-shifted light absorption peaks at 440 and 700 nm compared to the light absorption in the solution state. The green color went back to original yellow color after solvent annealing (solvent exposure) by chloroform vapor. The light absorption spectrum also returned with quenching the light absorption peak at the long wavelength region. It was clearly found that mechanical stimuli induced generation of a species for long wavelength absorption, which is attributable to the X-type conformer. Consequently, conformational change was brought after applying

physical stimuli. This mechanochromic generation of long wavelength light absorption resembles to the chromism of bianthrone in the previous paper.[12] The schematic model is shown below. The as-cast solids contain only V-type conformer but grinding the solids partially generates X-type conformer, which can reverse into V-type one by reorientation with exposure to solvent vapor (Figure *13*). Differences in fluorescence between two states were also evaluated (Figure *14*). The as-cast film indicated slightly higher fluorescence intensity at 491 than 528 nm. After grinding the film, the ratio of the peak intensities at 491 and 528 nm changed to give higher intensity at 528 nm. The change of intensity ratio would be derived from ununiformity of film surface. Other films fabricated by several conditions showed different intensity ratios in fluorescence spectra. After solvent annealing, the ratio did not seem changed but the fluorescence intensity increased, implying enhancement of fluorescent quantum yield. The fluorescent quantum yields of ground MeFA powder and solvent annealed MeFA powder as 1% and 3% supported the increase of fluorescence in the film state. The decrease of quantum yield suggested X-type conformer has poorer fluorescent property than V-type.
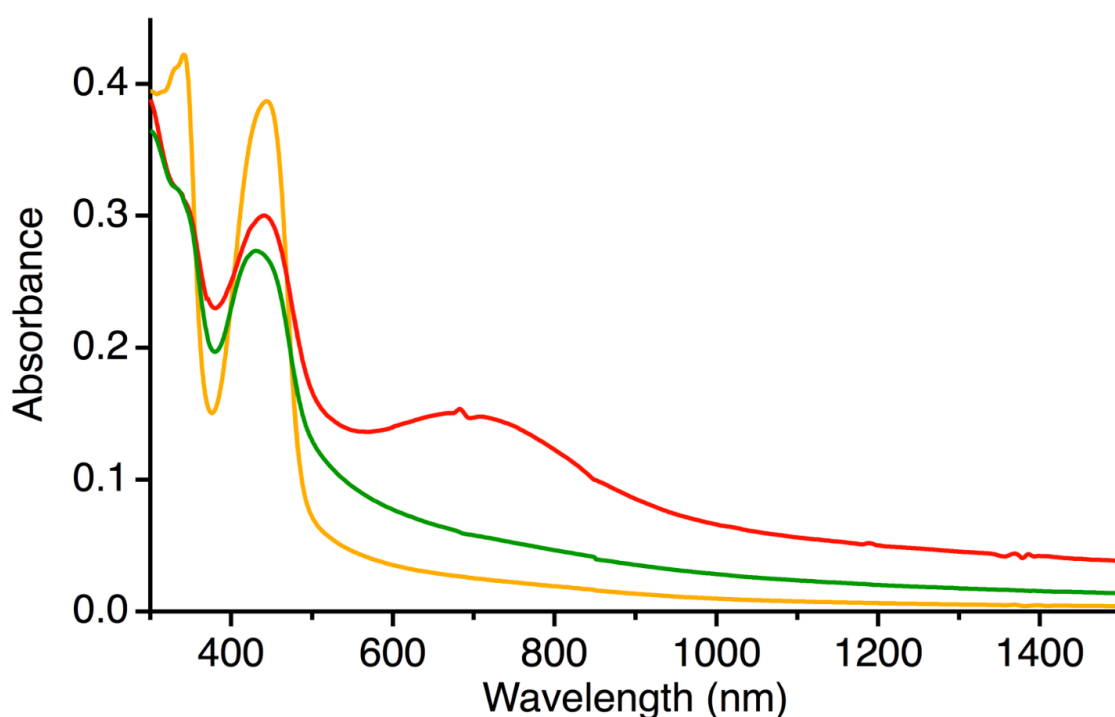
Figure 12. Light absorption spectra of MeFA thin film, which was prepared by spin coating with 500 to 1000 rpm. MeFA solution in PhCl (10 mg/ml) was used. Spectra of as-cast film (yellow), ground (red) and solvent annealed one (green) are shown.
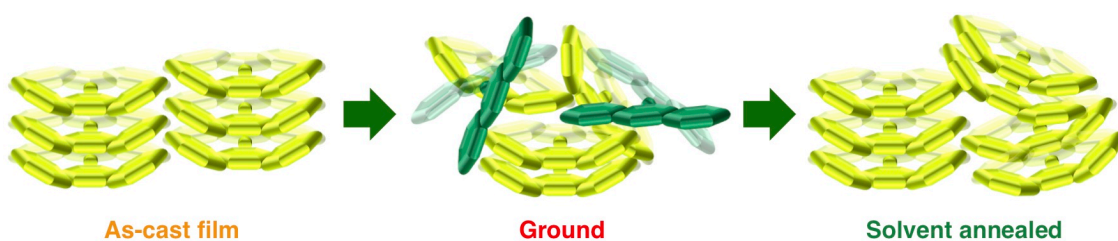
Figure 13. Schematic model of mechanochromic behavior of MeFA.
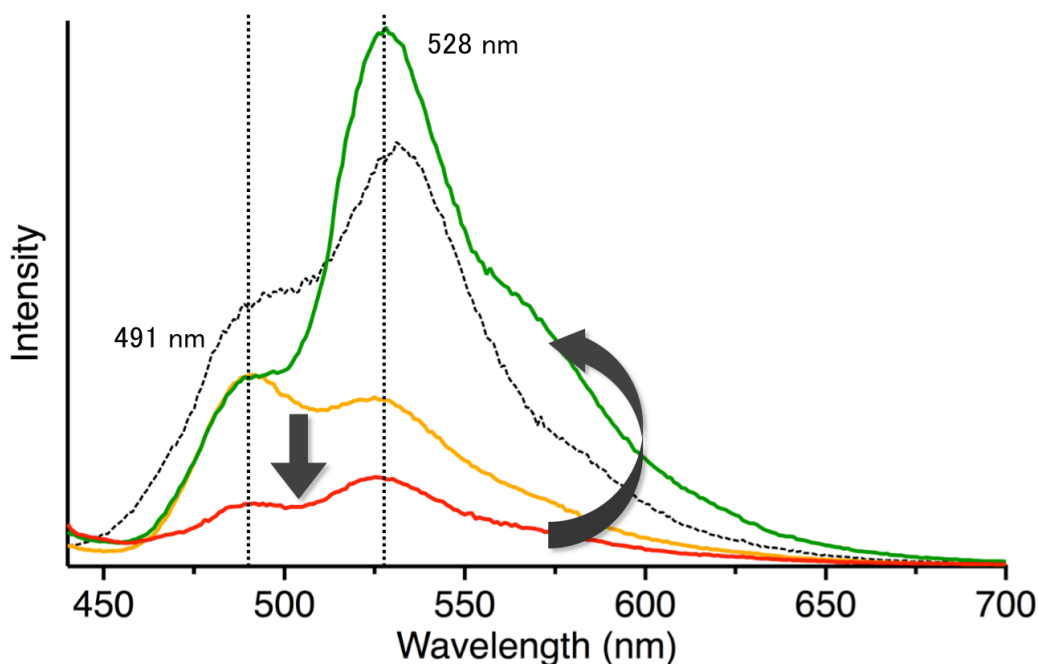
Figure 14. Fluorescent spectra of MeFA as films (colored solid lines) and in solution (black dot). Spectra of as-cast film (yellow), ground (red) and solvent annealed one (green) are shown. Excitation wavelength was 420 nm.

The coexistence of V- and X-type conformers of MeFA in the solution state is regarded as equilibrium, which would be influenced by temperature. The temperature dependence of equilibrium was compared by light absorption spectra (Figure **15**). The spectra at room temperature, 5 and 70 ºC displayed small changes between the temperatures, which is similar to the reported temperature-dependent behavior for dithiolylidenefluorene.[13] Thermochromism of BAEs normally appears at very low temperature around –173 to –70 ºC or very high temperature around 200 ºC.[14] The fractional peak shifting would represent the atmospheric change of solvent molecules at different temperatures. On the other hand, variations of light absorption intensity should account for the alternation of the ratio between V- and X-type conformers. Higher temperature brought higher intensity at the long wavelength region with lower intensity at the short wavelength region. This observation suggests that higher ratio of the X-type

conformer formed at higher temperature. The hypothesis is consistent with the DFT calculation indicating the X-type conformer has higher energy than the V-type one.
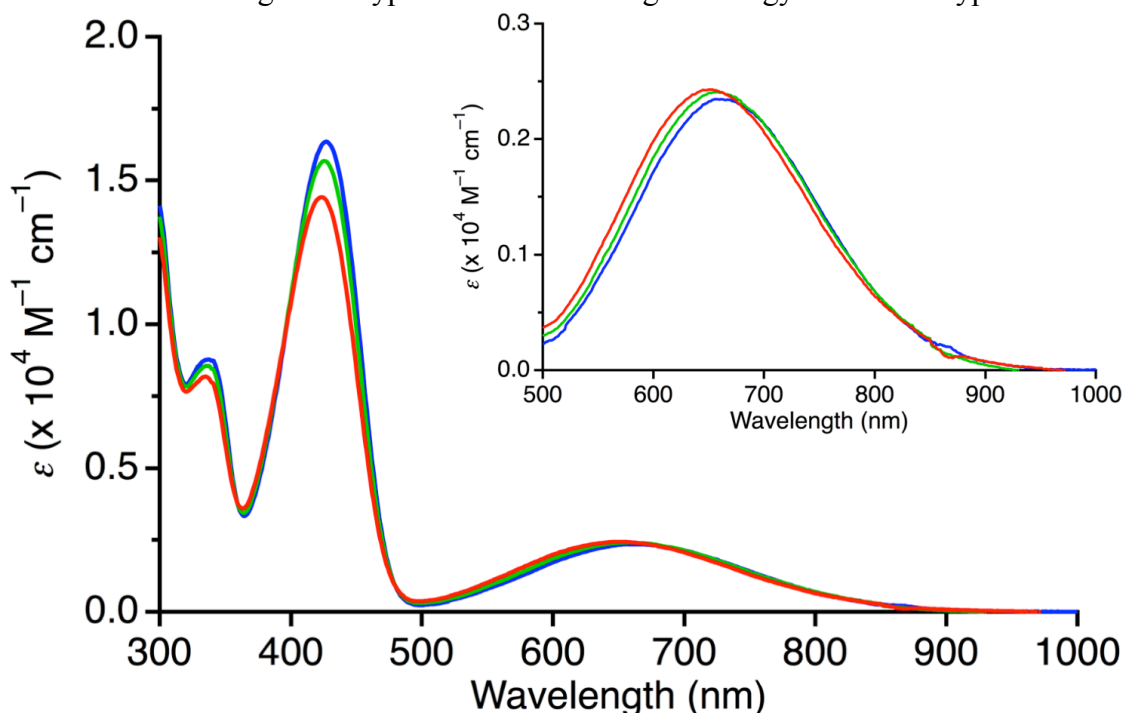

Figure 15. Temperature dependence of light absorption spectra of MeFA in PhCl. Each line corresponds to 5 (blue), 30 (green) or 70 °C (red).

As the molecular design, FA derivatives contain large dipole moment especially in the X-type conformer. The molecules with large dipole moments tend to show solvatochromism in several solvents with various dipole moments. The normalized light absorption spectra of MeFA in several solvents are shown in Figure *16*. The peak shifts of the spectra indicate weak dependence on solvents. With the data normalized at 420 nm, the relative absorption coefficients of peaks at 650–680 nm increased in solvents with higher dipole moment. It suggests the ratio of X-type conformer increases in solvent with larger dipole moment. The phenomena are reasonable with the DFT calculation showing the X-type conformer has larger dipole moment than the V-type one. The molecule with larger dipole is more stabilized than the molecule with lower dipole to change the distribution ratio in equilibrium. Besides the ratios of absorption coefficients, peak shifting was also found. The peaks at 420 nm varied 418–429 nm in various solvents and the peaks at 660 nm were shifted around 650–675 nm. Herein, the energy differences should be noted in wavenumber, and therefore the variations are translated into $2.39 \times 10^5 - 2.33 \times 10^5$ cm^{-1} ($\Delta = 6 \times 10^2$ cm^{-1}) and $1.54 \times 10^5 - 1.48 \times 10^5$ cm^{-1} ($\Delta = 6 \times 10^2$ cm^{-1}). The degrees of peak shifting were almost the same. The wavelengths of peaks at 660 nm and those relative absorptions compared to 420 nm were summarized in a graph against dielectric

91

constants of solvent molecules (Figure *17*). There are clear positive correlations between wavelength, relative absorption and dielectric constant, but plots corresponding to MeOH and EtOH did not correlate with others. Since MeFA are hardly soluble in both of MeOH and EtOH, MeFA would construct aggregated structures in those solvents to show different tendencies.
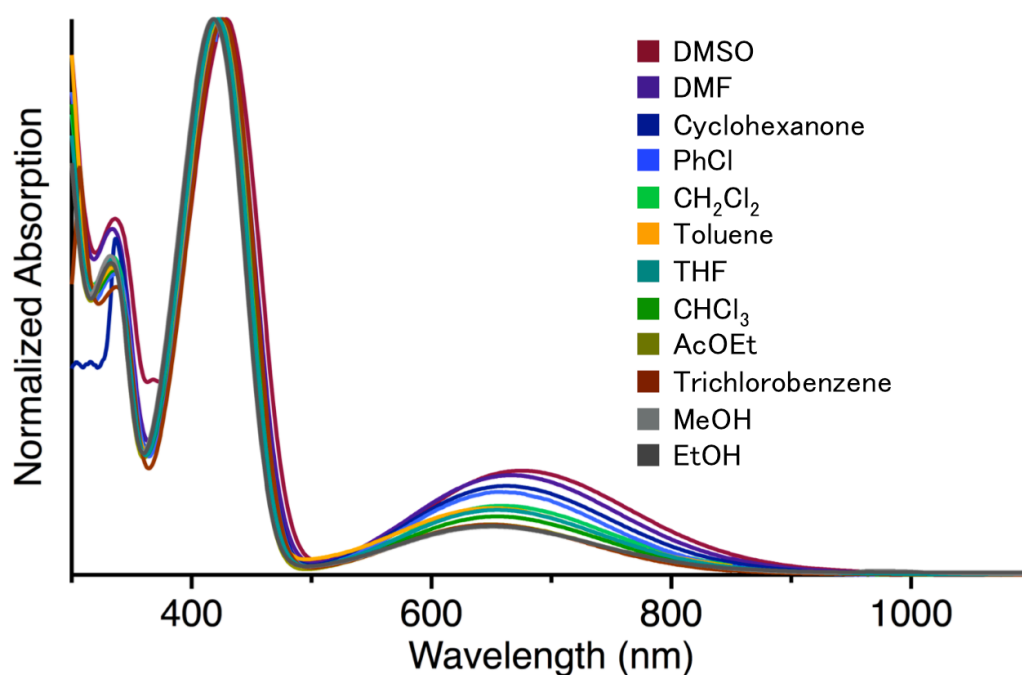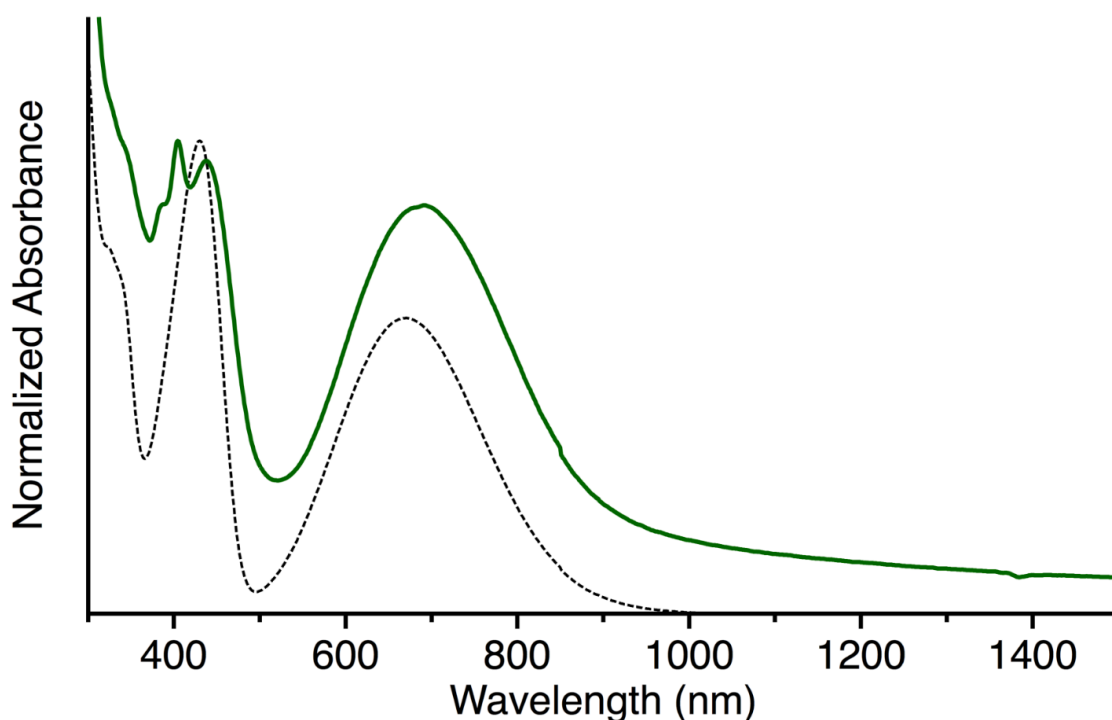

Figure 16. Light absorption spectra of MeFA in solvents. The spectra are normalized with the peaks at 420 nm.
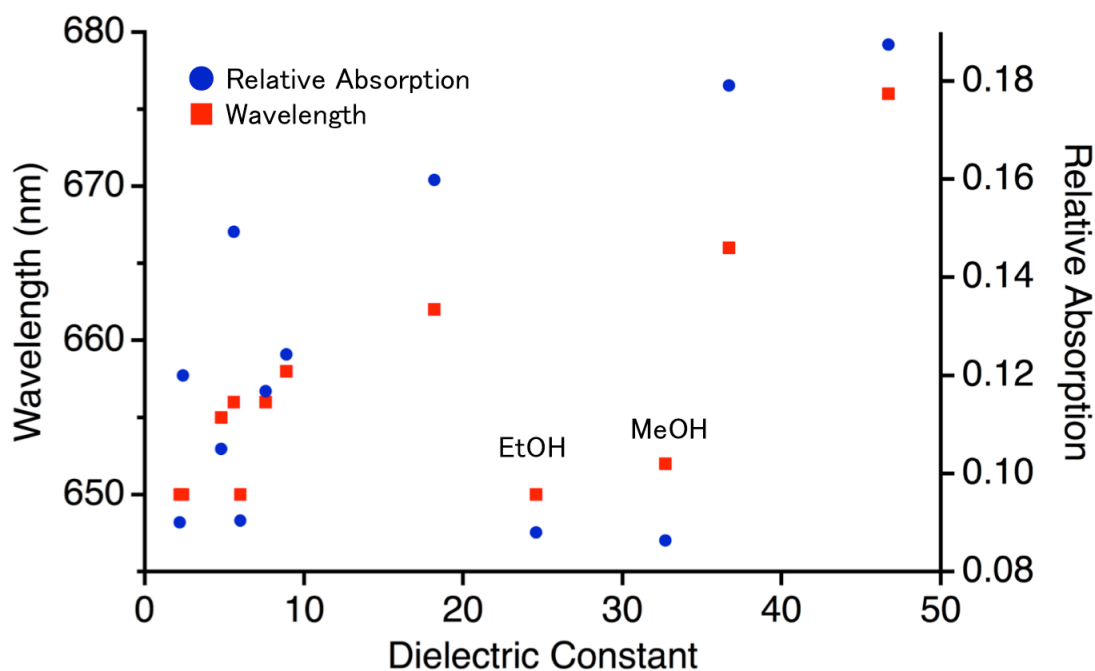
Figure 17. Light absorption wavelength of peaks at 660 nm and those relative absorption compared to 420 nm against dielectric constants of solvent molecules. Those are summarized from the data in Figure **16**.

The color of OctylFA in solution and solid states showed different tendency compared to MeFA. As is MeFA, appearance of the solution was deep green for OctylFA as well. In contrast, thin films of OctylFA prepared by spin coating kept the greenish color (Figure **18**). Light absorption measurements obviously indicated that both of the spectra as solid and solution states contained intense peaks at 671 nm. This data implies the X-type conformer is sustained even in the as-cast film. In other words, the X-type conformer of MeFA is metastable in the film state but introduction of the Octyl chain stabilize the X-type conformer in the film state.

Figure 18. Absorption spectra of OctylFA in solid (green solid line) and solution state in CH₂Cl₂ (black dot).

Solid-state properties of MeFA were deeply investigated by thermal analysis. Differential scanning calorimetry (DSC) revealed some thermal transitions (Figure *19*). Small peaks were observed at 119.6 ℃ at cooling processes and 123.6 ℃ at heating processes. In the first heating process, no sharp peak was detected around 120 ℃. It altered to a low-temperature phase after the first cooling process following the first heating process up to 200 ℃. The thermal properties were slightly changed by mechanochromism (Figure *20*). The first heating process exhibited a grass transition at 60–80 ℃. This transition was observed only at the first heating process, but the same thermal profiles to Figure *19* were detected from the first cooling process around 120 ℃. Ground solids recovered the same solid phase to recrystallized one after the first heating to 200 ℃.
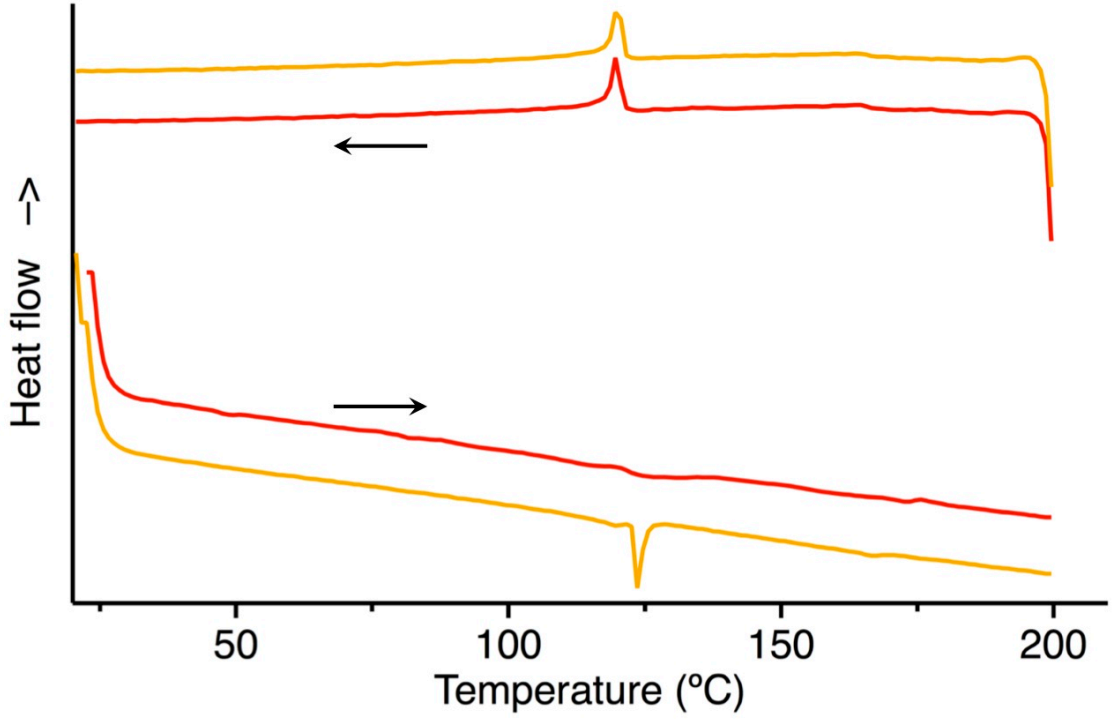
Figure 19. DSC measurement of MeFA. Red line was the first scan and yellow was the second one. The arrows represent the directions of thermal processes.
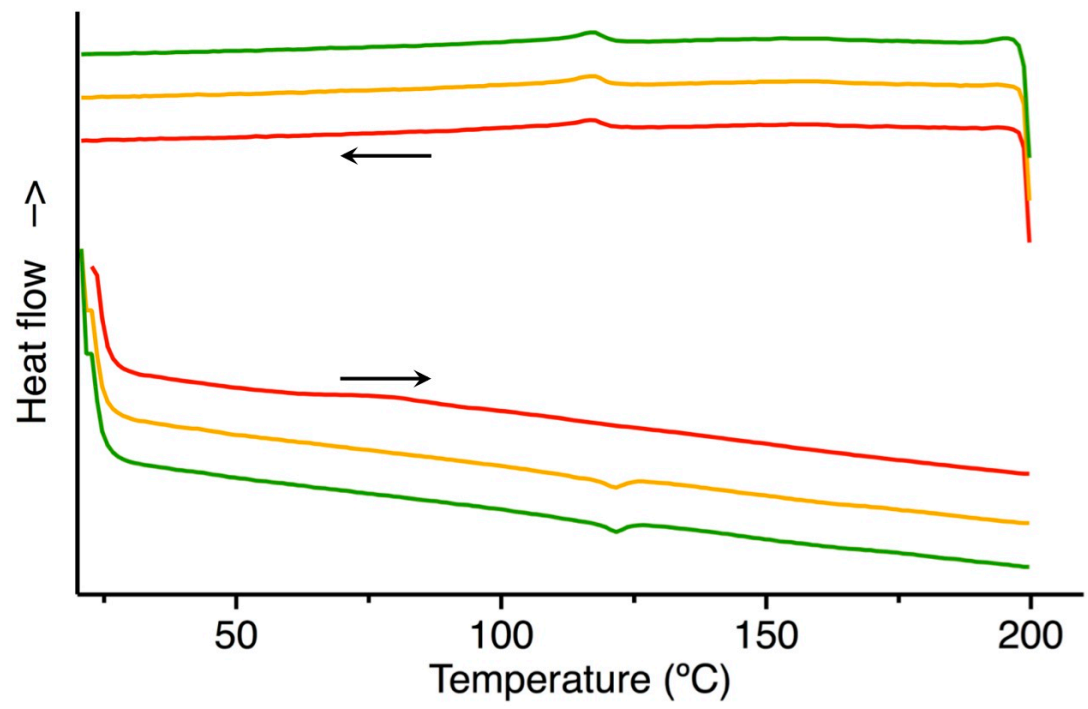

Figure 20. DSC measurement of ground MeFA solids. The first run (red), the second run (yellow) and the third run (green) are shown. The arrows represent the directions of thermal processes.

The crystallinity of MeFA solids during mechanochromic transitions was monitored by XRD analysis. The powder X-ray diffraction pattern of reprecipitated microcrystals was confirmed to be identical to the simulated pattern obtained from the single crystal X-ray structure analysis (Figure *21*). After grinding the microcrystals, the color changed to deep green as mentioned to give broad and weak diffraction pattern in XRD. We consider this pattern is derived from the mixture of crystalline and amorphous phases. The crystalline and amorphous parts are composed of V-type and X-type conformers of MeFA, respectively. As implied as glass transition in DSC measurement, the amorphous phase would be a key to involve the X-type conformer. Exposure of the ground solids to vapor of chloroform recovered the crystallinity to show the same XRD pattern to as-prepared one.
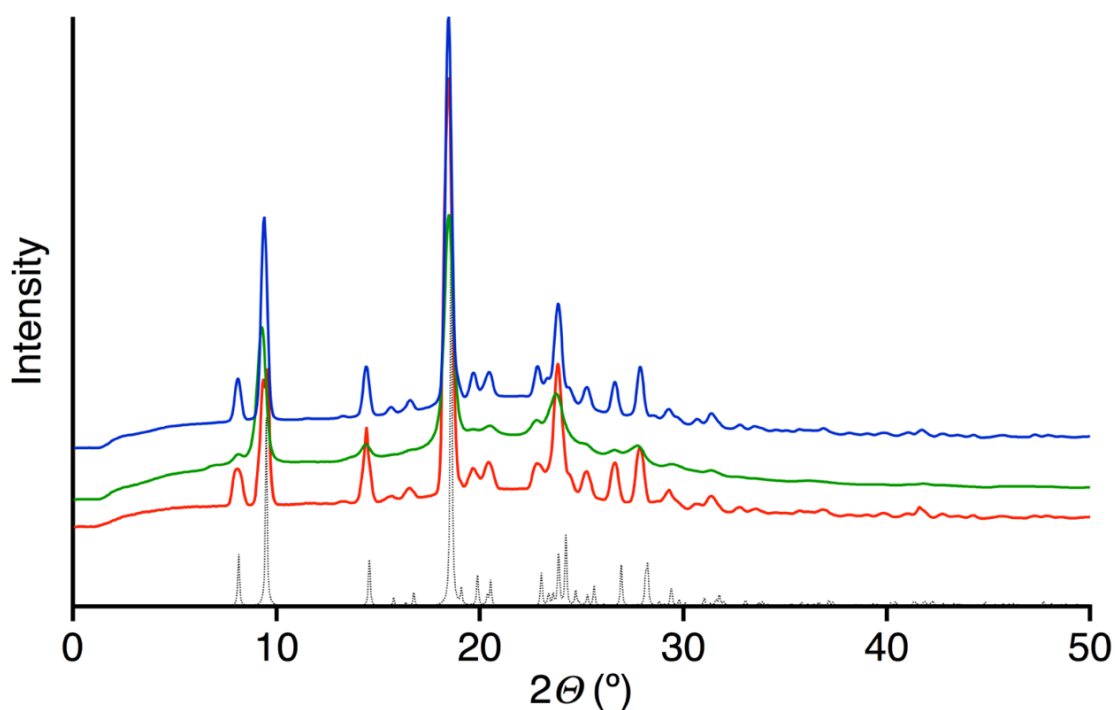

Figure 21. XRD patterns of MeFA powder. Simulation from crystal structure of polymorph 1 (Figure *5*) (black dot), as-prepared microcrystals (red), ground powder (green) and powder after solvent annealing were put in together.

4.3. Summary

The nitrogen-containing BAE, fluorenylideneacridane (FA), was successfully synthesized. FA derivatives possess substituents on the nitrogen atom unlike other BAEs. To form the central double bond by condensing fluorene and acridane, the *tert*-butoxy carbonyl (Boc) group is necessary to proceed the reaction. Here I demonstrated methyl and octyl substituted FA derivatives, which were characterized by NMR, CV, DPV, X-ray, UV and thermal analysis in solution and solid states. As is found in BAEs, MeFA showed mechanochromic properties. DFT calculation successfully assigned light absorption bands observed in light absorption measurement for V- and X-type conformers. The result evidenced that both of V- and X-type conformers existed in the solution state. In contrast to MeFA, OctylFA sustained the deep green color in solid state, which was qualitatively confirmed by light absorption measurements. Herein, I found the amorphous phase plays a critical role to equilibrate V-type with X-type in solid state, resulting in exhibition of green color. By changing the substituents on the nitrogen atom, the octyl chain successfully stabilizes the amorphous phase at room temperature to display deep-green color. This study demonstrated that structural change can occur in amorphous solid state rather than crystalline state. Grinding the crystalline solids and introducing long aliphatic substituent to the molecule controlled the amorphous phase and the equilibrium to have different colors in solid state. The substituent at acridane moiety in BAE structure controls the conformational isomers. Since the substituent is easily changed to different alkyl chains with several lengths, I can smoothly prepare FA derivatives to investigate the dependence of substituents on chromic properties.

4.4. Experimental Section

General. All NMR spectra were taken at 400 MHz (JEOL ECA-500 spectrometer) or 500 MHz (Bruker AVANCE III 500 spectrometer). NMR spectra were recorded in parts per million (ppm, δ scale) from residual protons of the CDCl$_3$ for ^{1}H NMR (δ 7.26 ppm for dichloromethane). The data were presented as following space: chemical shift, multiplicity (s = singlet, d = doublet, t = triplet, m = multiplet and/or multiplet resonances), coupling constant in hertz (Hz), and signal area integration in natural numbers, assignment (italic). Elemental analysis was performed at the University of Tokyo, Department of Chemistry, Organic Elemental Analysis Laboratory. IR absorption was measured on JASCO FT/IR-6100 equipped with an attenuated total reflection (ATR) with diamond, and was reported as wavenumber in cm^{-1}.
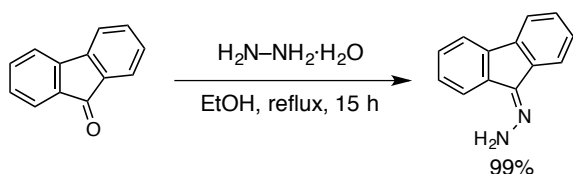
Synthesis of 9-fluorenehydrazone. Fluorene (4.00 g, 22.2 mmol) and hydrazine monohydrate (8.6 ml, *ca.* 8 equiv.) were dissolved in ethanol (220 ml, 0.10 M). The reaction mixture was refluxed and stirred for 15 h. After cooling the solution to room temperature, solvent was evaporated to obtain pale yellow solids (4.27 g, 99%), which was pure enough to use for next reaction. It was identified by ^{1}H NMR reported in the literature.[15]

^{1}H NMR (400 MHz, CDCl$_3$): δ = 7.92 (d, J = 7.3 Hz, 1H), 7.77 (d, J = 7.8 Hz, 1H), 7.74 (d, J = 6.9 Hz, 2H), 7.45 (ddd, J = 8.7, 7.8, 0.9 Hz, 2H), 7.38–7.29 (m, 3H), 6.41 (s, 2H).
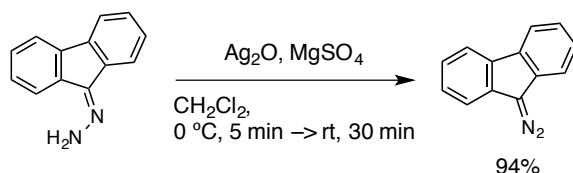

Synthesis of 9-diazofluorene. 9-Fluorenehydrazone (4.27 g, 21.9 mmol) and excess amount of magnesium sulfate (2.86 g) were put in a 500 ml two-neck flask. Dichloromethane (220 ml, 0.10 M) was added to the flask and cooled to 0 ℃ with an ice bath. After silver oxide was added and stirred for 5 min, it was warmed up to room temperature and stirred for 30 min. The filterate was dried to use for next reaction without further purification (3.98 g, 94%). The product gave the identical ^{1}H NMR chart to the literature.[16]

^{1}H NMR (400 MHz, CDCl$_3$): δ = 7.95 (dd, J = 7.4, 0.9 Hz, 2H), 7.52 (dd, J = 7.4, 1.0 Hz, 2H), 7.39 (t, J = 7.4 Hz, 2H), 7.33 (t, J = 7.8 Hz, 2H).
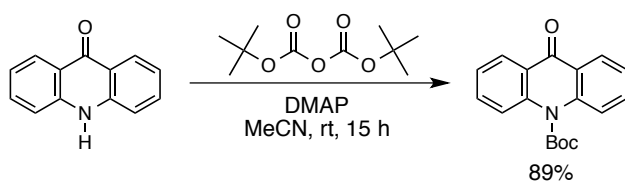
Synthesis of *N*-(*tert*-butoxy carbonyl)-9-acridone. In a 200 ml two-neck flask, 9-acridone (4.00 g, 20.5 mmol), di-tert-butyl dicarbonate (6.71 g, 6.8 ml, 30.7 mmol, 1.5 equiv.), DMAP (3.76 g, 30.7 mmol, 1.5 equiv.) was dissolved in acetonitrile (60 ml, 0.30 M) and stirred for 15 h. The resulted solution was poured into water. The organic component was extracted with ether to get yellow crude solids after drying. It was purified by silica gel column chromatography with chloroform as an eluent to result in yellow solids (5.36 g, 89%). The ^{1}H NMR chart was identical to the literature.[9c]

^{1}H NMR (400 MHz, CDCl$_3$): δ = 8.44 (dd, J = 7.8, 1.8 Hz, 2H), 7.68 (ddd, J = 8.7, 6.9, 1.8 Hz, 2H), 7.58 (d, J = 8.3 Hz, 2H), 7.36 (t, J = 6.9 Hz, 2H), 1.70 (s, 9H).

Synthesis of *N*-(*tert*-butoxy carbonyl)-9-thioacridone. In a 300 ml two-neck flask, *N*-(*tert*-butoxy carbonyl)-9-acridone (5.36 g, 18.1 mmol) and Lawesson's reagent (8.90 g, 22.0 mmol, 1.2 equiv.) were stirred in THF for 15 h at room temperature, and then it was heated up to reflux for 1 h. After drying, sticky brown crude product was obtained to purify silica gel column chromatography with chloroform. The resulted brown solids were reprecipitated from chloroform/methanol to get brown powder (5.10 g, 90%). The product was confirmed by the ^{1}H NMR from the literature.[9c]

^{1}H NMR (400 MHz, CDCl$_3$): δ = 8.91 (dd, J = 8.3, 1.4 Hz, 2H), 7.70 (ddd, J = 8.7, 7.3, 1.8 Hz, 2H), 7.55 (d, J = 7.8 Hz, 2H), 7.36 (ddd, J = 8.3, 6.9, 1.4 Hz, 2H), 1.70 (s, 9H).

Synthesis of dispiro[*N*-(*tert*-butoxy carbonyl)-acridane-9,2'-thiirane-3',9''-fluorene]. *N*-(*tert*-Butoxy carbonyl)-9-acridone (4.92 g, 15.8 mmol) and 9-diazofluorene (3.05 g, 15.9 mmol, 1.1 equiv.) were mixed in dichlorometane (160 ml, 0.10 M) for 4 h. After drying, the crude solids were purified by silica gel column chromatography with chloroform/hexane (1:1) to obtain yellow solids (6.02 g, 80%).

^{1}H NMR (400 MHz, CDCl$_3$): δ = 7.87 (dd, J = 7.6, 1.6 Hz, 2H), 7.52 (d, J = 7.8 Hz, 1H), 7.38 (dd, J = 8.0, 1.1 Hz, 2H), 7.27–7.15 (m, 6H), 6.86 (td, J = 7.6, 0.9 Hz, 2H), 6.78 (d, J = 7.8 Hz, 2H), 1.14 (s, 9H).

^{13}C{^{1}H} NMR (100.53 MHz, CDCl$_3$): δ = 150.6, 141.7, 140.9, 140.8, 134.0, 127.8, 127.1, 127.0, 126.1, 124.3, 124.2, 124.1, 119.4, 81.0, 57.5, 57.0, 27.6.

HR-MS (APCI$^+$): Calcd. for C$_{31}$H$_{25}$NO$_2$S (M)$^+$ = 475.1601, found 475.1597.

Mp 217.2–220.0 ºC (decomposition).

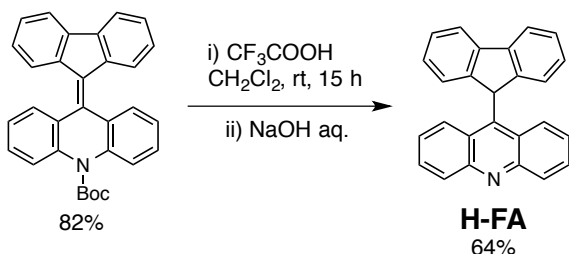**Synthesis of *N*-(*tert*-butoxy carbonyl)-10-(fluoren-9-ylidene)-acridane.**
Dispiro[*N*-(*tert*-butoxy carbonyl)-acridane-9,2'-thiirane-3',9"-fluorene] (5.80 g, 12.2 mmol) and triphenylphosphine (3.20 g, 12.2 mmol, 1.0 equiv.) were refluxed in toluene (61 ml, 0.20 M) for 13 h. The reaction mixture was dried to get yellow crude solids, which was purified by column chromatography and following reprecipitation from chloroform/methanol. The pure compound was obtained as yellow powder (4.41 g, 82%).

^{1}H NMR (400 MHz, CDCl$_3$): δ = 7.87 (d, J = 8.3 Hz, 2H), 7.84 (d, J = 7.8 Hz, 4H), 7.69 (d, J = 7.3 Hz, 2H), 7.34 (td, J = 7.8, 1.5 Hz, 2H), 7.29 (td, J = 7.3, 0.9 Hz, 2H), 7.19 (td, J = 7.6, 1.2 Hz, 2H), 7.03 (t, J = 7.1 Hz, 2H), 1.59 (s, 9H).

^{13}C{^{1}H} NMR (100.53 MHz, CDCl$_3$): δ = 151.7, 140.9, 139.4, 138.2, 133.6, 133.1, 130.8, 128.2, 127.8, 127.6, 125.9, 125.7, 125.1, 124.0, 119.3, 82.4, 28.3.

HR-MS (APCI$^+$): Calcd. for C$_{31}$H$_{25}$NO$_2$ (M)$^+$ = 443.1880, found 443.1880.

Mp 224.0–226.0 ºC (decomposition).

Synthesis of 9-(9-fluorenyl)-acridine (H-FA). *N*-(*tert*-Butoxy carbonyl)-10-(fluoren-9-ylidene)-acridane (4.20 g, 9.47 mmol) was dissolved in dichloromethane (95 ml, 0.10 M) with trifluoroacetic acid (3.24 g, 2.25 ml, 3.0 equiv.) to stir for 15 h. After removing the solvent, methanol and NaOH aq. (0.1 M) were added to neutralize it. The organic compounds were extracted with dichloromethane and dried with magnesium sulfate. Drying the solvent resulted in yellow crude product, which was purified by silica gel column chromatography. By drying it, pale green solids were obtained (2.08 g, 64%).

^{1}H NMR (400 MHz, CDCl$_3$): δ = 8.65 (d, J = 9.2 Hz, 1H), 8.44 (d, J = 8.7 Hz, 1H), 8.22 (d, J = 8.7 Hz, 1H), 7.99 (d, J = 7.3 Hz, 2H), 7.87 (ddd, J = 8.8, 6.5, 1.0 Hz, 1H), 7.63 (ddd, J = 8.8, 6.5, 1.3 Hz, 1H), 7.50 (ddd, J = 8.7, 6.4, 1.4 Hz, 1H), 7.44 (t, J = 7.6 Hz, 2H), 7.16 (td, J = 7.6, 0.9 Hz, 2H), 7.05 (d, J = 7.3 Hz, 2H), 6.88 (ddd, J = 8.8, 6.5, 1.3 Hz, 1H), 6.77 (d, J = 9.2 Hz, 1H), 6.45 (s, 1H).

^{13}C{^{1}H} NMR (100.53 MHz, CDCl$_3$): δ = 148.9, 148.8, 143.4, 140.1, 130.7, 130.0,

129.6, 129.4, 127.5, 127.4, 127.1, 126.4, 125.3, 125.1, 124.3, 124.1, 123.6, 120.5, 48.2. MS (APCI$^+$) 343.1154, Mp 220.2–223.0 ºC (decomposition), Anal. calcd for $C_{26}H_{17}N$: C, 90.93; H, 4.99; N, 4.08. Found: C, 90.90; H, 5.04; N, 3.99.
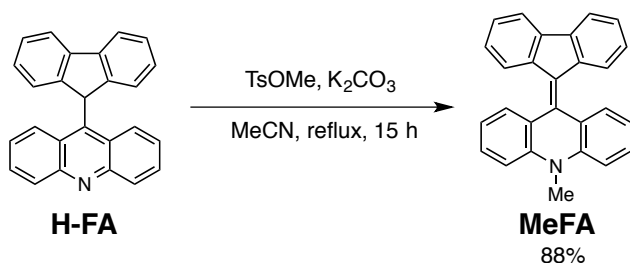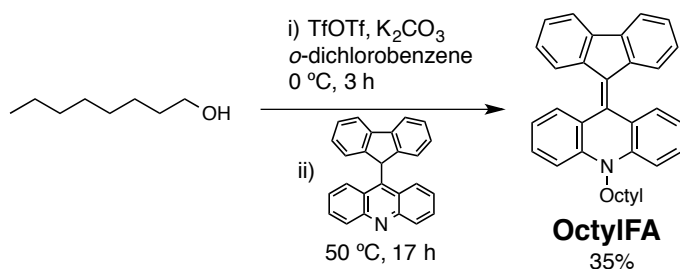

Synthesis of *N*-methyl-10-(fluoren-9-ylidene)-acridane (MeFA). In 30 ml two-neck flask, 9-(9-fluorenyl)-acridine (500 mg, 1.46 mmol), potassium carbonate (2.02 g, 14.6 mmol) and methyl tosylate (971 mg, 5.21 mmol, 3.57 equiv.) were put with acetonitrile (15 ml, 0.10 M). The reaction mixture was refluxed for 15 h. The resulted mixture was poured into water to extract the organic compounds with chloroform. The crude product was further purified by reprecipitation from dichloromethane/methanol. The solids were collected by suction to get greenish yellow solids (459.2 mg, 88%).

^{1}H NMR (400 MHz, CDCl$_3$): δ = 7.95 (dd, *J* = 7.8, 1.4 Hz, 2H), 7.74 (d, *J* = 7.8 Hz, 2H), 7.71 (d, *J* = 7.3 Hz, 2H), 7.41 (t, *J* = 7.1 Hz, 2H), 7.25 (t, *J* = 7.6 Hz, 2H), 7.11 (t, *J* = 7.6 Hz, 2H), 7.02 (t, *J* = 7.1 Hz, 2H), 3.59 (s, 3H).

^{13}C{^{1}H} NMR (100.53 MHz, CDCl$_3$): δ = 143.9, 140.3, 138.8, 133.8, 129.0, 128.8, 128.7, 127.0, 125.6, 124.7, 124.2, 120.3, 119.1, 113.3, 33.4.

MS (APCI$^+$) 357.1325, Mp 261.4–262.6 ºC, Anal. calcd for $C_{27}H_{19}N$: C, 90.72; H, 5.36; N, 3.92. Found: C, 90.64; H, 5.55; N, 3.84.

Synthesis of *N*-octyl-10-(fluoren-9-ylidene)-acridane (OctylFA). In 50 ml two-neck flask, potassium carbonate (10.1 g, 73.0 mmol) and octanol (569 mg, 700 μl, 4.37 mmol, 3.00 equiv.) were dispersed in *o*-dichlorobenzene (22 ml), which was cooled to 0 ºC to slowly add trifluoromethanesulfonic anhydride (1.41 g, 5.01 mmol, 3.44 equiv.). After it was stirred for 3 h, 9-(9-fluorenyl)-acridine (500 mg, 1.46 mmol) was added and heated up to 50 ºC for 17 h. *o*-Dichlorobenzene was distilled to extract the organic compounds with water/chloroform. Evaporation of solvent gave deep green oil, which was passed through alumina column and reprecipitated from ether/methanol at low

temperature. A lump of sticky deep green solids was obtained (230.4 mg, 35%).

^{1}H NMR (500 MHz, CDCl$_3$): δ = 8.08 (dd, J = 7.9, 1.9 Hz, 2H), 7.75 (ddd, J = 7.6, 1.3, 0.6 Hz, 2H), 7.72 (d, J = 7.9 Hz, 2H), 7.40 (ddd, J = 8.2, 6.9, 1.6 Hz, 2H), 7.29 (d, J = 7.6 Hz, 2H), 7.22 (dd, J = 7.6, 1.3 Hz, 2H), 7.04 (dddd, J = 7.9, 6.9, 2.2, 0.9 Hz, 2H), 4.13 (t, J = 7.9 Hz, 2H), 1.94 (q, J = 7.6 Hz, 2H), 1.45 (q, J = 6.9 Hz, 2H), 1.40–1.34 (m, 2H), 1.28–1.19 (m, 6H), 0.83 (t, J = 6.9 Hz, 3H).

^{13}C{^{1}H} NMR (100.53 MHz, CDCl$_3$): δ = 141.7, 139.7, 139.2, 136.2, 130.6, 129.3, 127.0, 129.3, 127.0, 125.9, 125.4, 124.7, 123.4, 120.4, 119.2, 114.1, 46.2, 31.7, 29.22, 29.20, 27.0, 26.9, 22.6, 14.0.

MS (APCI$^+$) 455.2240, Anal. calcd for C$_{34}$H$_{33}$N: C, 89.63; H, 7.30; N, 3.07. Found: C, 89.50; H, 7.35; N, 3.00.

Electrochemical analysis. Cyclic voltammetry (CV) and differential pulse voltammetry (DPV) were performed using HOKUTO DENKO HZ-5000 voltammetric analyzer. All CV measurements were carried out in a one-compartment cell under argon gas, equipped with a glassy-carbon working electrode, a platinum wire counter electrode, and an Ag/Ag$^+$ reference electrode. The supporting electrolyte was a 0.1 mol/L dichloromethane solution of tetrabutylammonium hexafluorophosphate (TBAPF$_6$).

X-ray crystallographic analysis. X-ray crystallographic analyses were performed using a RIGAKU R-AXIS RAPID II (imaging plate detector) with monochromic CuKα (λ = 1.5406 Å) radiation. The positional and thermal parameters were refined by a full-matrix least-squares method using the SHELXL97 program on the Yadokari-software.

Computational studies. All calculations were carried out by using Gaussian09 package at the B3LYP and UB3LYP levels. Solvent effects were estimated by the polarizable continuum model (PCM) method with the dielectric constant for dichloromethane. A 6-31G(d) basis set was used for each level. The calculation levels are described as "B3LYP/ 6-31G(d)" and "UB3LYP/ 6-31G(d)".

Crystal Data Collection Parameters for MeFA (Polymorph 1).

Formula	$C_{27}H_{19}N$
Formula Weight	357.43
Crystal System	Monoclinic
Space Group	$P2_1$
R, R_w ($I>2\sigma(I)$)	0.0829, 0.2095
$R1$, $wR2$ (all data)	0.0655, 0.1717
GOF on F^2	1.465
a (Å)	7.3384(2)
b (Å)	18.5774(6)
c (Å)	13.3299(4)
α (º)	90
β (º)	90.1024(18)
γ (º)	90
V (Å^3)	1817.24(9)
Z	4
T (K)	123(2)
Crystal Size (mm)	0.46, 0.30, 0.16
D_{calcd} (g·cm^{-3})	1.306
$2\theta_{min}$, $2\theta_{max}$ (º)	3.32, 66.99
no. refl. measured (unique)	6277
no. refl. measured ($I>2\sigma(I)$)	5264
no. parameters	507
μ (CuKα)	1.54187

Crystal Data Collection Parameters for MeFA (Polymorph 2).

Formula	$C_{27}H_{19}N$
Formula Weight	357.43
Crystal System	Monoclinic
Space Group	$P2_1/a$
R, R_w ($I>2\sigma(I)$)	0.0416, 0.1383
$R1$, $wR2$ (all data)	0.0372, 0.1320
GOF on F^2	1.175
a (Å)	8.5137(2)
b (Å)	21.9630(6)
c (Å)	9.8776(3)
α (º)	90
β (º)	104.4061(17)
γ (º)	90
V (Å^3)	1788.90(8)
Z	4
T (K)	123(2)
Crystal Size (mm)	0.30, 0.27, 0.24
D_{calcd} (g·cm^{-3})	1.327
$2\theta_{min}$, $2\theta_{max}$ (º)	4.03, 67.00
no. refl. measured (unique)	3190
no. refl. measured ($I>2\sigma(I)$)	2859
no. parameters	255
μ (CuKα)	1.54187

4.5. References

1. (a) Yu, G.; Gao, J.; Hummelen, J. C.; Wudi, F.; Heeger, A. J. *Science* **1995**, *270*, 1789–1791. (b) Kraft, A.; Grimsdale, A. C.; Holmes, A. B. *Angew. Chem. Int. Ed.* **1998**, *37*, 402–428. (c) Cheng, Y.-J.; Yang, S.-H.; Hsu, C.-S. *Chem. Rev.* **2009**, *109*, 5868–5923. (d) Egbe, D. A. M.; Neugebauer, H.; Sariciftci, N. S. *J. Mater. Chem.* **2011**, *21*, 1338–1349. (e) Praveen, V. K.; Ranjith, C.; Bandini, E.; Ajayaghosh, A.; Armaroli, N. *Chem. Soc. Rev.* **2014**, *43*, 4222–4242.

2. (a) Chen, Z.; Debije, M. G.; Debaerdemaeker, T.; Osswald, P.; Würthner, F. *Chem. Phys. Chem.* **2004**, *5*, 137–140. (b) Xiao, S.; Myers, M.; Miao, Q.; Sanaur, S.; Pang, K.; Steigerwald, M. L.; Nuckolls, C. *Angew. Chem. Int. Ed.* **2005**, *44*, 7390–7394. (c) Yoo, B.; Jung, T.; Basu, D.; Dodabalapur, A.; Jones, B. A.; Facchetti, A.; Wasielewski, M. R.; Marks, T. J. *Appl. Phys. Lett.* **2006**, *88*, 08214. (d) Schmidt, R.; Oh, J. H.; Sun, Y.-S.; Deppisch, M.; Krause, A.-M.; Radacki, K.; Braunschweig, H.; Könemann, M.; Erk, P.; Bao, Z.; Würthner, F. *J. Am. Chem. Soc.* **2009**, *131*, 6215–6228. (e) Gsänger, M.; Oh, J. H.; Könemann, M.; Höffken, H. W.; Krause, A.-M.; Bao, Z.; Würthner, F. *Angew. Chem. Int. Ed.* **2010**, *49*, 740–743. (f) Ueda, Y.; Tsuji, H.; Tanaka, H.; Nakamura, E. *Chem. Asian J.* **2014**, *9*, 1623–1628.

3. (a) Meyer, H. *Monatsh. Chem.* **1909**, *30*, 165–177. (b) Harnik, E. *J. Chem. Phys.* **1956**, *24*, 297–299. (c) Wasserman, E.; Davies, R. E. *J. Chem. Phys.* **1959**, *30*, 1367. (d) Korenstein, R.; Muszkat, K. A.; Sharafy-Ozeri, S. *J. Am. Chem. Soc.* **1973**, *95*, 6177–6181.

4. Biedermann, P. U.; Stezowski, J. J.; Agranat, I. *Chem. Eur. J.* **2006**, *12*, 3345–3354.

5. Takezawa, H.; Murase, T.; Fujita, M. *J. Am. Chem. Soc.* **2012**, *134*, 17420–17423.

6. (a) Brunetti, F. G.; Gong, X.; Tong, M.; Heeger, A. J.; Wudl, F.; *Angew. Chem. Int. Ed.* **2010**, *49*, 532–536. (b) Kim, H. U.; Kim, J.-H.; Suh, H.; Kwak, J.; Kim, D.; Grimsdale, A. C.; Yoone, S. C.; Hwang, D.-H. *Chem. Commun.* **2013**, *49*, 10950–10952. (c) Chiu, C.-Y.; Wang, H.; Brunetti, F. G.; Wudl, F.; Hawker, C. J. *Angew. Chem. Int. Ed.* **2014**, *53*, 3996–4000.

7. (a) Chi, Z.; Zhang, X.; Xu, B.; Zhou, X.; Ma, C.; Zhang, Y.; Liua S.; Xu, *J. Chem. Soc. Rev.* **2012**, *41*, 3878–3896. (b) Nagura, K.; Saito, S.; Yusa, H.; Yamawaki, H.; Fujihisa, H.; Sato, H.; Shimoikeda, Y.; Yamaguchi, S. *J. Am. Chem. Soc.* **2013**, *135*, 10322–10325. (c) Lv, Y.; Liu, Y.; Guo, D.; Ye, X.; Liu, G.; Tao. X. *Chem. Asian J.* **2014**, *9*, 2885–2890. (d) Yagai, S.; Okamura, S.; Nakano, Y.; Yamauchi, M.; Kishikawa, K.; Karatsu, T.; Kitamura, A.; Ueno, A.; Kuzuhara, D.; Yamada, H.; Seki, T.; Ito, H. *Nat. Commun.* **2014**, DOI:10.1038/ncomms5013.

8. Davis, D. A.; Hamilton, A.; Yang, J.; Cremar, L. D.; Van Gough, D.; Potisek, S. L.; Ong, M. T.; Braun, P. V.; Martínez, T. J.; White, S. R.; Moore, J. S.; Sottos, N. R. *Nature* **2009**, *459*, 68–72.

9. (a) Chuang, C.; Lapin, S. C.; Schrock, A. K.; Schuster, G. B. *J. Am. Chem. Soc.* **1985**, *107*, 4238–4243. (b) Schroeder, W.; Katz, L. *J. Org. Chem.* **1954**, *19*, 718–720. (c)

Kulago, A. A.; Mes, E. M.; Klok, M.; Meetsma, A.; Brouwer, A. M.; Feringa, B. L. *J. Org. Chem.* **2010**, *75*, 666–679.

10. HOMO and LUMO levels were determined from the first oxidation and reduction potentials in our investigation with the following equation:

HOMO or LUMO level = $-(4.8 + E^{1/2})$ eV.

11. Laviron, E.; Roullier, L. *J. Electroanal. Chem.* **1985**, *186*, 1–15.

12. Fanselow, D. L.; Drickamer, H. G. *J. Chem. Phys.* **1974**, *61*, 4567–4574.

13. Mysyk, D. D.; Perepichka, I. F.; Perepichka, D. F.; Bryce, M. R.; Popov, A. F.; Goldenberg, L. M.; Moore, A. J. *J. Org. Chem.* **1999**, *64*, 6937–6950.

14. (a) Day, J. H. *Chem. Rev.* **1963**, *63*, 65–80. (b) Bouas-Laurent, H.; Dürr, H. *Pure Appl. Chem.* **2001**, *73*, 639–665.

15. Minabe, M.; Takabayashi, Y.; Setta, Y.; Nakamura, H.; Kimura, T.; Tsubota, M. *Bull. Chem. Soc. Jpn.* **1996**, *69*, 3633–3638.

16. Okano, K.; Ogino, S.; Kawamoto, M.; Yamashita, T. *Chem. Commun.* **2011**, *47*, 11891–11893.

Chapter 5.

Overview and Perspective

The achievements of the studies on platinum and palladium complexes with tetraceneimide disulfide ligands demonstrated that polyacene coordinating to metal atoms can extend the π-systems of organic molecules. The dπ orbitals of metal atoms make interaction with organic pπ orbitals. In organometallic chemistry, such orbital interactions are well-known phenomena, but this work established dπ-pπ interactions as a method to expand π-conjugated systems largely. This research provided TIDS complexes with platinum and palladium atoms. Both of the complexes exhibited longer wavelength light absorption to represent containing larger π-system compared to TIDS.

The platinum TIDS complex underwent to triplet excitation state during relaxation from higher excitation states such as S_1 and S_2. High performance light emitting and photovoltaic materials often utilize triplet excitation to include phosphorescence and to enhance lifetime of excitons. Namely, a material with long wavelength absorption and triplet excitation state would be useful for solar cell devices.[1] The applications of triplet excitation state are now under development, and the concept for design of the material with triplet excitation state will accelerates chemistry to utilize long lifetime excitation state.

The palladium case gave amazing results those are formation of trinuclear complex and absorption of infrared light. Palladium and platinum have similar electronic properties, however there is small difference in reactivity. DFT investigation clarified the electronic environments around the three palladium atoms, those are completely delocalized HOMO and LUMO, Pd(II)–Pd(0)–Pd(II) configuration, and donor–acceptor interactions between the central palladium atom and its peripheral atoms. The extensive delocalization within the molecule is attributable to the parallel coordination of two TIDS ligands and linkage of the two ligands with d-orbital of the central palladium atom. These two characteristics play critical roles to give long wavelength absorbing materials. In the tri-palladium TIDS complex, d_{xy} orbital of the central palladium atom links the π-systems of TIDS ligands. By using the mono-palladium TIDS complex, probably I can get tri-metallic complexes containing another metal atom at the center, for example, Pt(0), Ni(0), Ag(I), and so on. The multi-metallic complexes would give different π-conjugation manners with dxy orbitals in different energy levels. In other points of view, the tri-palladium TIDS complex is to be a monomer unit for construction of a one-dimensional chain complex like (Pd–TIDS)n,[2] in which palladium atoms align in one dimension with TIDS ligands bridging two palladium atoms. The complex inherently has charge transferring paths at the palladium chain and between the TIDS ligands. The complex will retain the long wavelength light absorption properties, and hence the one-dimensional complex will be applicable to solar cell devices.

The bridged π-system in fluorenylideneacridane (FA) induced mechanochromism and long wavelength light absorption up to 900 nm. The bridging two π-conjugated aromatic systems with a double bond realized a distorted extended π-conjugated system like bis-tricyclic aromatic ene (BAE) to have these

interesting properties. Moreover, FA showed more red-shifted light absorption compared to oxygen-substituted analogue, fluorenylidenexanthone and other BAEs. I investigated the reason for this mechanochromism by studying equilibrium behaviors in solid state and fundamental properties of conformers contained in this equilibrium. The steric repulsion at bay positions invoked conformational isomers accompanying chromic properties. The FA derivatives underwent equilibrium in solid state between V-type showing yellow color and X-type showing green color. The methyl substituted FA (MeFA) showed deep green color in solution state. The light absorption measurement showed two peaks corresponding to V- and X-type conformers, representing the two conformers are in equilibrium in solution state. When MeFA was precipitated from the deep green solution, only yellow solids were obtained. X-ray crystal structural analysis and powder XRD analysis denoted that only V-type conformer exists in the solid state. By contrast, using a longer aliphatic group, such as the octyl group, kept the X-type conformation even in solid state to exhibit deep green color. Herein, I showed the method to control the equilibrium by changing the aliphatic group, which does not affect the electronic structures. Some DFT calculations about FA derivatives predicted phenyl substituent possesses lower energy for X-type conformer than V-type conformer. This result implies X-type conformer is preferentially obtained in phenyl substituted FA or other aryl substituted derivatives. I expect that the equilibrium between V- and X-type conformers has an essential role in organic electronic devices. The V- and X-type conformers literally construct different structures, which provide different semiconducting properties. In further study, the charge transporting ability of FA derivatives will be improved by fusing aromatic rings to build larger π-conjugation systems and wider π–π overlapping area between peripheral atoms in solid state. The larger compounds will sustain the chromic property, and therefore applying shear stress may transform the compound into the X-type conformer, which may be detectable as an electric signal.

Both of the researches about TIDS complexes and FA derivatives commonly provided the unprecedented methods to extend π-conjugated systems. The concepts would help design for a number of novel organic materials for solar cells, bio imaging, chemical sensing, and dyes of all sorts. In addition, the materials can bear heavy atom effects and chromic properties. These unique characteristics expand the possibilities toward exceptionally long lifetime of excited state, efficient phosphorescence, pressure sensor, and electronic display.

References

1. (a) Guo, F.; Kim, Y.-G.; Reynolds, J. R.; Schanze, K. S. *Chem. Commun.* **2006**, 1887–1889. (b) Guo, F.; Ogawa, K.; Kim, Y.-G.; Danilov, E. O.; Castellano, F. N.; Reynoldsa, J. R.; Schanze, K. S. *Phys. Chem. Chem. Phys.* **2007** ,*9*, 2724–2734.

2. Examples of one-dimensional complex: (a) Little, W. A. *Phys. Rev.* **1964**, *134*, A1416–A1424. (b) Mitsumi, M.; Goto, H.; Umebayashi, S.; Ozawa, Y.; Kobayashi, M.; Yokoyama, T.; Tanaka, H.; Kuroda, S.-i.; Toriumi, K. *Angew. Chem. Int. Ed.* **2005**, *44*, 4164–4168. (c) Uemura, K.; Ebihara, M. *Inorg. Chem.* **2011**, *50*, 7919–7921.

List of Publications

< Publication related to thesis >

1. "Synthesis, photophysical properties, and excited state dynamics of a platinum complex of tetracene imide disulfide"
Takafumi Nakagawa, Tsuyoshi Suzuki, Matthias König, Dirk M. Guldi and Yutaka Matsuo, *Chem. Commun.* **2013**, *49*, 10394–10396. [DOI: 10.1039/C3CC46068A]
2. "Electronic infrared light absorption of a tri-palladium complex containing two π-expanded tetracene ligands"
Tsuyoshi Suzuki, Takafumi Nakagawa, Kei Ohkubo, Shunichi Fukuzumi and Yutaka Matsuo, *Chem. Sci.* **2014**, *5*, 4888–4894. [DOI: 10.1039/C4SC02018A]
3. アクリジン系化合物およびこれを用いた有機薄膜デバイス
特願 2015-008622.

< Publication not related to thesis >

1. "Synthesis, Physical Properties, and Crystal Structure of Acetetracenylene-1,2-dione"
Toshihiro Okamoto, Tsuyoshi Suzuki, Shungo Kojima and Yutaka Matsuo, *Chem. Lett.* **2011**, *40*, 739–741. [DOI: 10.1246/cl.2011.739]
2. "Tetracene Dicarboxylic Imide and Its Disulfide: Synthesis of Ambipolar Organic Semiconductors for Organic Photovoltaic Cells"
Toshihiro Okamoto, Tsuyoshi Suzuki, Hideyuki Tanaka, Daisuke Hashizume and Yutaka Matsuo, *Chem. Asian J.* **2012**, *7*, 105–111. [DOI: 10.1002/asia.201100590]
3. 「長波長領域の光吸収を示す有機薄膜太陽電池材料」鈴木　毅，松尾　豊
有機薄膜太陽電池の研究最前線，シーエムシー出版，2012 年.
4. "Formation of Photoconductive Nanowires of Tetracene Derivative in Composite Thin Film"
Tsuyoshi Suzuki, Toshihiro Okamoto, Akinori Saeki, Shu Seki, Hiroyasu Sato and Yutaka Matsuo, *ACS Appl. Mater. Interfaces* **2013**, *5*, 1937–1942. [DOI: 10.1021/am302914w]
5. "From a Zwitterionic Phosphasilene to Base Stabilized Silyliumylidene-Phosphide and Bis(silylene) Complexes"
Nora C. Breit, Tibor Szilvási, Tsuyoshi Suzuki, Daniel Gallego and Shigeyoshi Inoue, *J. Am. Chem. Soc.* **2013**, *135*, 17958–17968. [DOI: 10.1021/ja409720c]